# Effect of Elevated Temperature on Mechanical Behaviour and Springback of Aluminum Alloy Brazing Sheets

by

Rohit Verma

A thesis

presented to the University of Waterloo

in fulfillment of the

thesis requirement for the degree of

Master of Applied Science

in

Mechanical Engineering

Waterloo, Ontario, Canada, 2016

# Author's Declaration

I hereby declare that I am the sole author of this thesis. This is a true copy of the thesis, including final revisions, as accepted by my examiners.

I understand that my thesis may be made electronically available to the public.

# Abstract

The current work investigates the effect of warm forming process parameters on springback of AA3003 brazing sheets, comprising a modified AA3003 core with a lower melting point AA4045 clad layer used to promote brazing. Three temper conditions were considered including O-, H22- and H24-temper.

Two custom tooling sets were designed to form U-shaped channels, allowing forming temperature, blank holding force and lubricant type to be varied. The forming temperature range considered was from room temperature to 300°C. The formed specimen cross sections were measured and the net shape was evaluated in terms of the measured versus ideal sidewall angle.

Tensile tests were conducted to characterize material behaviour for the range of temperature considered in the forming experiments. The results showed thermal softening and increased strain-rate sensitivity at elevated temperature in the O-, H22-, and H24-tempers, which results in lower forming stresses and thus lower springback. The room temperature strength is recovered after warm forming. Ductility increased significantly at elevated temperature; however, the harder temper conditions exhibited negative strain hardening for high temperatures at strains beyond the ultimate tensile strength.

The experiments revealed that springback reduced steadily for all three tempers as the forming temperature was increased from room temperature to 250°C. The effect of temperature on springback was relatively small for the O-temper condition, but significant for the high-strength tempers. At a forming temperature of 250°C, the H22-and H24-tempers exhibited springback reduction of 95% and 92%, in terms of deviation from the ideal sidewall angle, relative to springback at room temperature, respectively.

The stress-strain data was used to create a numerical model for predicting springback after U-channel forming. One challenge in developing constitutive model parameters for this work was the negative hardening response exhibited by the harder temper conditions at higher temperatures. This caused numerical instabilities, requiring the use of approximate fits to the material response.

The sidewall angle deviation and flange angle were predicted after springback. The numerical models qualitatively captured the reduction in springback with increase in forming temperature, but quantitative differences in the predicted and measured extent of springback exist. Sensitivity analysis using the model showed that friction coefficient and constitutive fit had a large influence on predicted springback. Future studies should address the complex material response data at elevated temperature and develop a more detailed temperature- and strain-rate dependent constitutive model.

# Acknowledgements

I would like to express my gratitude for Prof. Michael Worswick for giving me an opportunity to work on this project. I learned a great deal working on this project and insights from Prof. Worswick were immensely valuable. I would also like to thank Ryan George for guiding me through this project in development of experimental tooling and for helping me with the set-up. I would like to thank Dr. Srihari Kurukuri for his guidance in numerical work and sharing his experience in writing academic articles. I thank Eckhard Budziarek, Jeff Wemp, Tom Gawel, and Andy Barber for providing laboratory support in the High Pressure Lab and helping me deal with specialized equipment.

This project was supported by Dana Canada Corp., CanmetMATERIALS, Automotive Partnerships Canada, the Natural Sciences and Engineering Research Council (NSERC), the Canada Foundation for Innovation, the Ontario Research Fund and the Canada Research Chairs Secretariat. I would like to thank Dr. Sooky Winkler and Dr. Mark Kozdras for providing industrial expertise and guidance throughout the project. I would particularly like to thank Dr. Haiou Jin and Jidong Kang for providing laboratory support at Canmet's facility.

I appreciate the help Laurie Wilfong for providing administrative support during my time here and guiding me through the university procedures. I also had the pleasure of being in the company of extremely talented members in Prof. Worswick's research group. I enjoyed my time with them and appreciate their support.

Lastly, I am extremely grateful for my loving family, who encouraged me and provided endless support during my studies. I couldn't have done it without them.

*To my parents*

# Table of Contents

# List of Figures

# List of Tables

# 1.0 Introduction

## 1.1 Use of Lightweight Metals in the Automotive Industry

In recent years, strict legislative emission regulations have been imposed on auto makers to lower fuel consumption and improve efficiency. This is being done to address growing concerns regarding climate change. Some automakers are developing electric (Chevy Bolt, Tesla Model S) and hybrid-electric vehicles (Toyota Prius, Fisker Karma) to address this concern. The electric energy is stored in battery packs located on the vehicle. The battery packs must operate at uniform temperature. Otherwise, uneven temperature distribution can lead to unbalanced electrical charge in the modules and diminish performance and life span [1]. Automakers overcome this problem by integrating a cooling system inside the battery pack. Regardless of the fuel used to power the vehicle, the overall weight of the vehicle must be optimized for efficient consumption of energy. For each 100 kg reduction in the mass of a car, there is approximately 9 grams less $CO_2$ produced for each kilometer driven in a gasoline car [2]. Most importantly, the manufacturing process for fabricating light weight parts must be cost effective and meet present production volume standards. As a result, government and industry partners are investing heavily in advanced research programs to commercialize lightweight metals for automotive applications.

The primary light-weight materials for future automotive applications are aluminum alloys. Aluminum has one-third the density of steel and offers excellent strength-to-weight ratio relative to steel, when alloyed with other elements. Aluminum is also attractive due to its very good corrosion resistance and brazeability [3]. These alloys have the potential to be used for structural components and sub-components that are part of the vehicle. However, aluminum alloys present unique challenges in production, exhibiting relatively low room temperature formability compared to that of steel and being prone to cracking and wrinkling when using conventional tooling [4]. Other materials that are also being considered for automotive lightweighting applications include fibre-reinforced composites, ultra-high strength steels and multi-material concepts [5]. To meet mass-market vehicle demands and achieve the required efficiency improvements in the current market environment, aluminum is the most attractive alternative to steel among auto-makers [5].

Effective measures are being taken to increase efficiency by implementing the use of aluminum, due to the growing competition among mature auto makers and new participants in the industry (ex. Tesla Motors, Faraday Future). Today, aluminum is used extensively in vehicles and its use is growing steadily.

Figure 1 shows the various applications in a passenger-vehicle, where aluminum is used in the fabrication of the components [2].

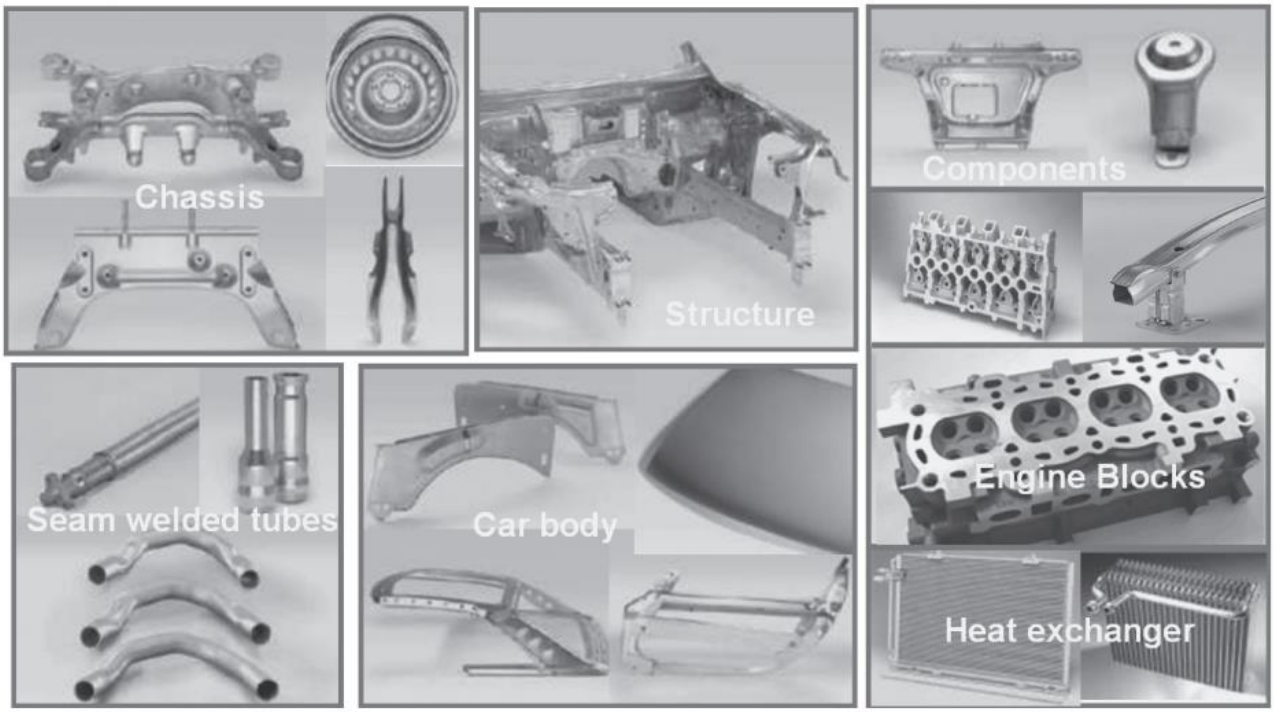


**Figure 1: Applications of Aluminum in a passenger-vehicle. [2]**

One important application of aluminum alloys is in thermal management systems, including heat exchangers for engine and transmission cooling, and more recently, for battery cooling devices used in electric and hybrid vehicles. Aluminum is attractive for the manufacture of automotive heat exchangers due to its high thermal conductivity, good corrosion resistance and good brazeability [3].

Electric/hybrid vehicles need a cooling apparatus specifically for the battery pack in order to prolong life of the battery cells and maintain performance. These battery cooling systems may consist of thin cooling plates stacked between the battery cells. The cooling plates are comprised of brazed stamped thin-gauge aluminum sheets with serpentine channels for coolant flow. Heat is conducted through the battery plates and dissipated by the coolant. The serpentine channels are optimized to maintain a uniform temperature across the face of the cells [6]. A schematic of a battery cooling plate is shown in Figure 2 [7].

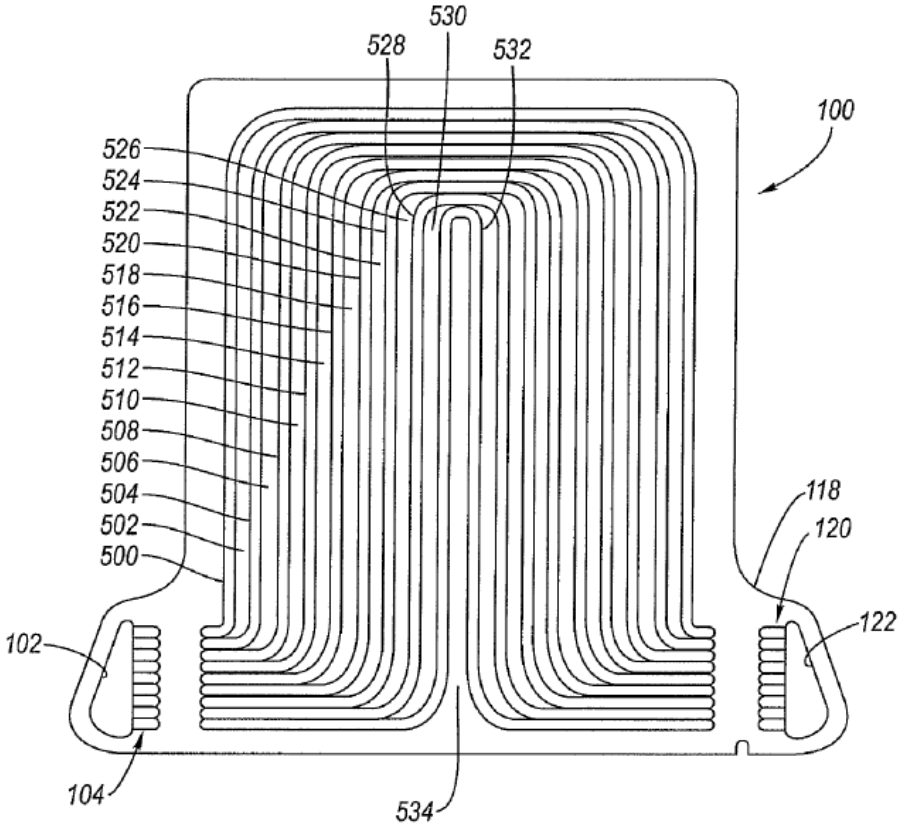


**Figure 2: A schematic of a battery cooling plate [7].**

Aluminum brazing sheets used for the fabrication of battery cooling plates are composite structures that consist of an AA3003-type core alloy laminated with a AA4045-type clad or filler metal. The brazing sheet may be cladded on one or both sides of the AA3003 core, as shown in Figure 3. During the battery cooler manufacturing process, the desired design features such as the cooling channels are stamped into the aluminum braze sheet. The stamped battery cooler component is subsequently assembled and brazed in a furnace. During aluminum brazing, which typically occurs between 575 – 600C, the lower melting point AA4045 clad material melts; and via a process of wetting and capillary action, metallurgically bonds the component assembly to form a brazed heat exchanger [8].

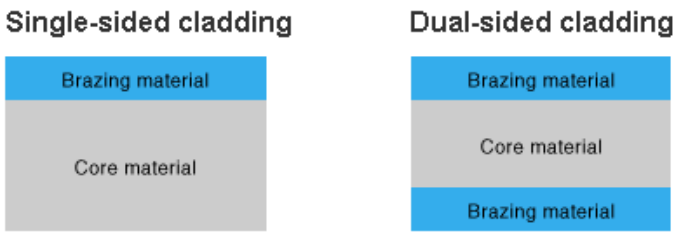


**Figure 3: Different types of brazing sheet material [9].**

The fabrication of thin battery plates made from very thin gauged aluminum braze sheets, posed new manufacturing challenges to the heat-exchanger manufacturer. Production yields are strongly dependent on the flatness between the 2 stamped components in contact to be brazed. Excessive springback in the stamped component results in poor contact between the mating plates, which in turn leads to poor braze joint formation and leaks in the brazed heat exchanger. Furthermore, some design features require higher levels of material forming which limits the use of the more desirable higher-strength and corrosion resistant, but lower formability, H-temper aluminum sheets; and/or may require the use of more expensive multi-stage progressive die systems. Hence, a new forming method that allows for forming of complex geometries while maintaining a consistent degree of flatness in thin gauge aluminum sheets with harder tempers is needed for the development of new battery cooling technologies [10].

This work is focused on aluminum alloy brazing sheet used to fabricate battery cooling plates for electric/electric-hybrid vehicles, in particular, the use of elevated temperature (warm) forming to limit springback and improve net shape after forming.

## 1.2 Springback

The formability of sheet metal is influenced by the design geometry (shape, curvature); choice of material (strength, ductility) and manufacturing technology (die alignment, lubricant, loading) [11]. These parameters are closely related and affect the outcome of the finished product [12]. Aluminum being lighter than steel, also has a lower strength and elastic modulus compare to conventional forming steels. Thus, conventional stamping methods used for stamping steels need to be adapted to successfully form aluminum sheets.

Some drawbacks of forming aluminum are galling and springback. For aluminum brazing sheets, severe galling can have a negative impact on brazing performance. As a result, lubrication is a critical process parameter. Springback also plays a significant role in process design. It is a pivotal parameter that can determine the success of the product and process design. Springback is the dimensional deviation from

the ideal shape, which occurs after the forming loads are removed. It is caused by the recovery of elastic stresses present in the sheet material at the end of the forming operation. Figure 4 illustrates anglular deviation from an ideal bend angle to the resulting angle after springback [13].

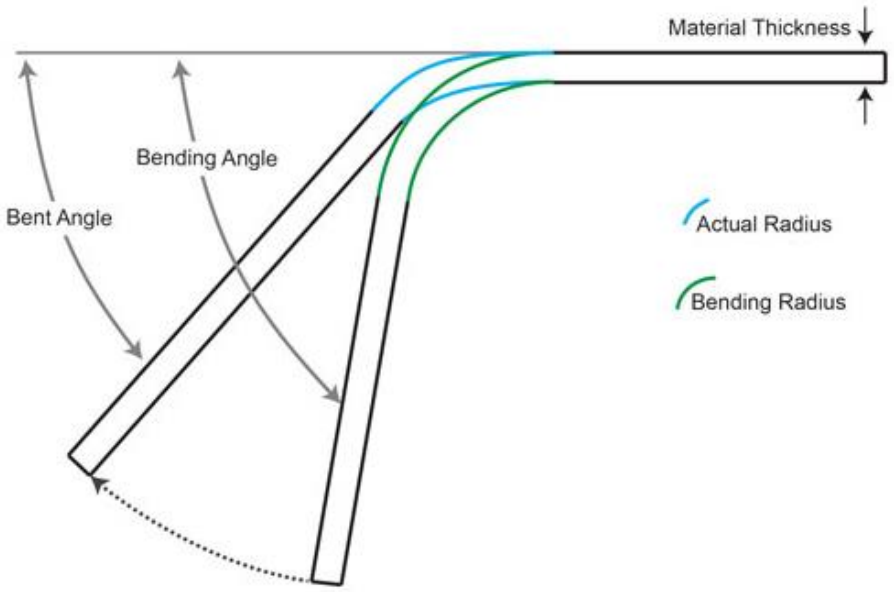


**Figure 4: Angular deviation from the ideal bending angle to the actual angle due to springback [13].**

To compensate for springback, engineers can sometimes specify a bending angle that is greater than the required angle; in doing so the part deforms back to the desired shape. With this method, springback is controlled through tooling design. Another method of influencing springback is to change the material or the material thickness such that lower springback is obtained. Table 1 lists various material and process factors that influence springback [14].

**Table 1: Various geometric, process and material factors that influence springback [14].**

| Geometric Variables | Process Variables | Material Variables |
|---|---|---|
| Curvature<br>Blank Thickness | Clearance (Die and Punch Gap)<br>Binder Force<br>Friction<br>Lubrication | Elastic Modulus<br>Yield Strength<br>Ultimate Tensile Strength<br>Strain Hardening<br>Poisson's Ratio<br>Anisotropy |

The list of factors in Table 1 is by no means exhaustive. Springback behaviour could change for a range of other reasons such as humidity on the shop floor or how the material is stored and transported. Due to the large number of variables, controlling and predicting springback is extremely difficult. In a production environment, springback is compensated for based on the operator's knowledge base or industry standard practice [14]. This involves repeated forming trials with different die geometries and constant tooling re-work.

There are various computer programs that could be used to predict springback [15]. However, the models are extremely sensitive to the parameters specified by the user. In addition to a material model, information about frictional forces between the sheet material and tooling is also needed. Therefore, accurate prediction of springback behaviour is exceptionally challenging. It typically requires a parametric study where the hardening law, yield curve, mesh size, element type and other model parameters are varied and the resulting springback is evaluated [16].

## 1.3 Warm Forming Process

In the current project, warm forming was identified as promising route for limiting springback in aluminum while also improving formability. Warm forming is the process of forming sheet metal parts at elevated temperature but staying below the recrystallization temperature of the material. Figure 5 shows a schematic of a typical warm forming tooling set-up. It should be noted that the circular features in the figures are indicative of cartridge heaters which are commonly used as heating elements in warm forming tooling. For non-isothermal warm forming, the cooling of selected tooling components is done by running chilled water through the body of the part.

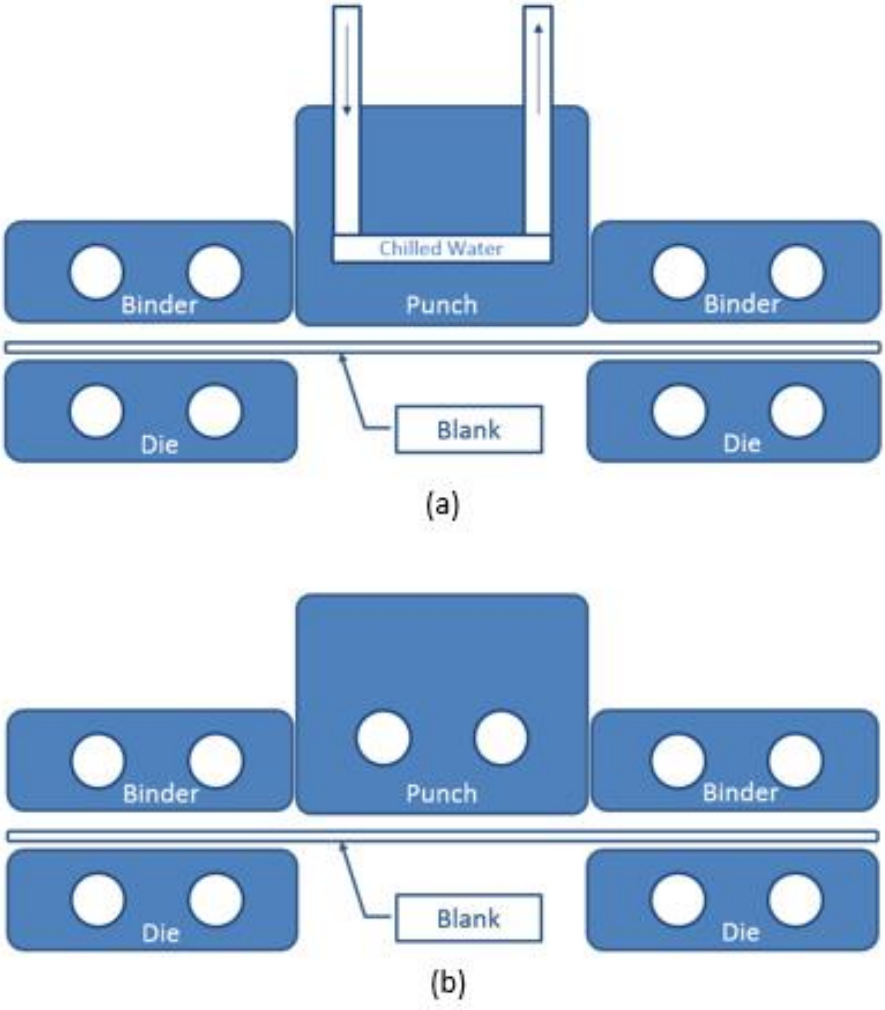


**Figure 5: Typical warm forming tooling set-up. (a) Non-isothermal warm forming, (b) Isothermal warm forming.**

There are two types of warm forming process configurations. In isothermal warm forming process, all the tooling components and the blank are at the same temperature, while for non-isothermal forming, the binder, die are heated and the punch is cooled using running chilled water. Although both variations of warm forming process require special provisions to maintain temperature, non-isothermal forming is technically more challenging compared to isothermal forming. However, non-isothermal processes can potentially achieve deeper draw depths, for example, since the fracture prone region of a part can be cooled to maintain strength in that region pushing deformation away, while forming limit strain is enhanced in the heated, deforming regions. This allows for complex shapes to be formed in single action forming operations rather than having multiple forming stages [17].

Another benefit of forming aluminum at elevated temperature is lower levels of stresses in the material. As a result, forming can be done using lower press tonnage with reduced springback. Figure 6 illustrates the reduction in tensile stress in aluminum sheet and the influence on springback as result of temperature increase [18].

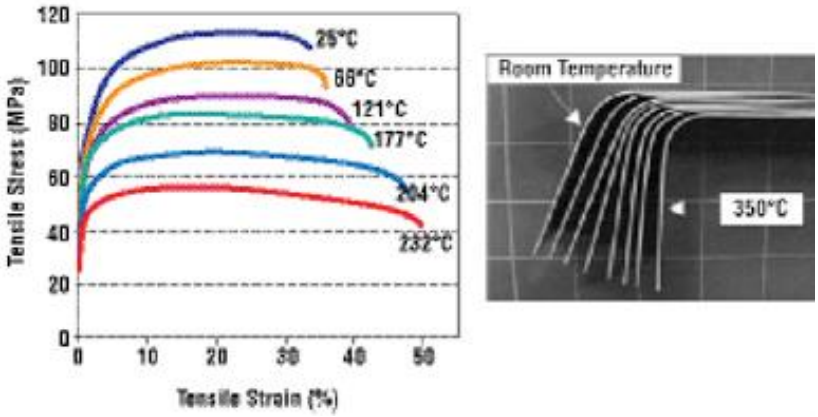


**Figure 6: Influence of temperature on tensile stress and springback in aluminum sheets [18].**

Aluminum alloys show an increase in elongation from 20% at room temperature up to 80% at temperatures near than 300°C [19]. This increase in formability at warm forming temperatures allows for greater part complexity and potentially increased usage of aluminum alloys in the automotive and aerospace market. The challenge with warm forming is the cost incurred to transition from a conventional cold stamping process. More complex tooling is needed and insulation must be added to prevent overheating of the press [20]. Cycle time will be greater for warm forming processes, depending on the blank heating method used, but some improvements may be realized for parts that require progressive die set-ups through reduction in the number of forming stages [21]. With warm forming, it is possible to form parts with a lower number of forming stages. Therefore, the cost per unit for a warm forming process could be comparable to a cold forming process for high production volume [22]. The following section details some of the previous research done on warm forming and springback related studies.

Previous studies with aluminum brazing sheets have shown an increase in formability at elevated temperatures. Bagheriasl (2012) conducted limiting dome height experiment on AA3003-O aluminum alloy brazing sheet and observed a 200% improvement in formability compared to room temperature [23]. Mckinley (2010) performed material characterization studies of aluminum brazing sheets. The flow stress decreased substantially at 250°C compared to room temperature and elongation at failure also increased significantly [24].

An improvement in formability due to warm forming has also been observed in other materials. Shehata et al. (1978) reported a five-fold increase in elongation for aluminum-magnesium alloys in uniaxial tensile tests. Additionally, flow stress was also shown to decrease with increasing temperature. Warm-punch experiments were also conducted where an increase in cup height was evident at elevated test temperatures [25]. Li et al. (2004) measured an increase in forming limit strains of AA5754, AA5182, and AA6111-T4 at a forming temperature of 250°C [26].

Hui et al. (2011) investigated warm forming behaviour of high-strength AA7075 aluminum alloys. Tensile test results showed that for temperatures above 140°C, the yield and ultimate tensile strength decreased with increasing temperature. An important characteristic of this material is the high-strength temper which should be preserved post-forming. Heat treated samples showed permanent loss in strength for temperatures above 220°C [27]. This suggests that temperature for warm forming has an upper limit, if higher-strength temper properties are to be retained in the formed component.

Material behaviour at warm forming conditions has also been captured in numerical models. Kurukuri et al. (2009) developed a temperature and strain-rate sensitive material model that could accurately describe the flow stress of aluminum-magnesium alloys at elevated temperature. This model was used to simulate warm deep drawing of cylinder cups [28].

## 1.4 Springback After Forming at Room and Elevated Temperatures

In recent years, considerable progress has been made in understanding springback at room temperature. Li et al. (2001) simulated draw/bend experiments with high strength low alloy (HSLA) steel and 6022-T4 aluminum to study effects of various process and numerical parameters on the resulting Springback. The magnitude of the tensile force in the sheet during draw bending was found to have a significant effect on springback. The tensile force can be varied through the application of back force or by increasing the friction coefficient between the blank and tooling surfaces. Moreover, the numerical models showed high sensitivity to the number of through-thickness integration points, mesh density, and type of elements. Figure 7 shows the effect of number of integration points through the thickness on simulated springback. The springback model required at minimum 21 integration points for reasonable accuracy [29].

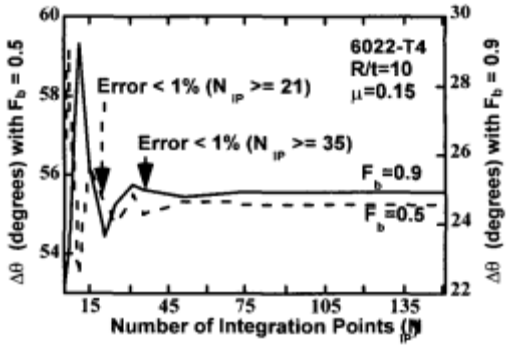


**Figure 7: Measured springback with increasing number of through-thickness integration points [29].**

Livatyali et al. studied springback after flanging operations for steel and aluminum. Aluminum was reported to exhibit higher springback due to its lower elastic modulus [30]. The effect of blank holding force on springback was also considered. The results showed that its effect on springback diminishes after a certain threshold value.

Ling et al. studied the effect of process parameters such as die clearance, die radius, step height, and step distance on springback of AA2024-T3 after an L-bending operation [31]. They report that the die radius and clearance can be optimized to reduce springback. A die radius of 1t (1*thickness of the sheet) and a die clearance of 0.78t will result in the same springback as that of using a die clearance of 1t. The optimal combination depends on the material and sheet thickness.

Very few studies, however, have studied springback under warm forming conditions. Grèze et al. studied springback of AA5754-O split rings cut from cylindrical cups deep drawn at elevated temperatures [32]. The opening of the rings after forming for a range of temperatures is shown in Figure 8 [32]. The opening width for a specimen formed at room temperature was 64mm, whereas the specimen formed at 200°C resulted in an opening of just 21mm. They concluded that forming at higher temperatures results in a decrease of the stress gradient in the cup wall, thereby producing lower springback.

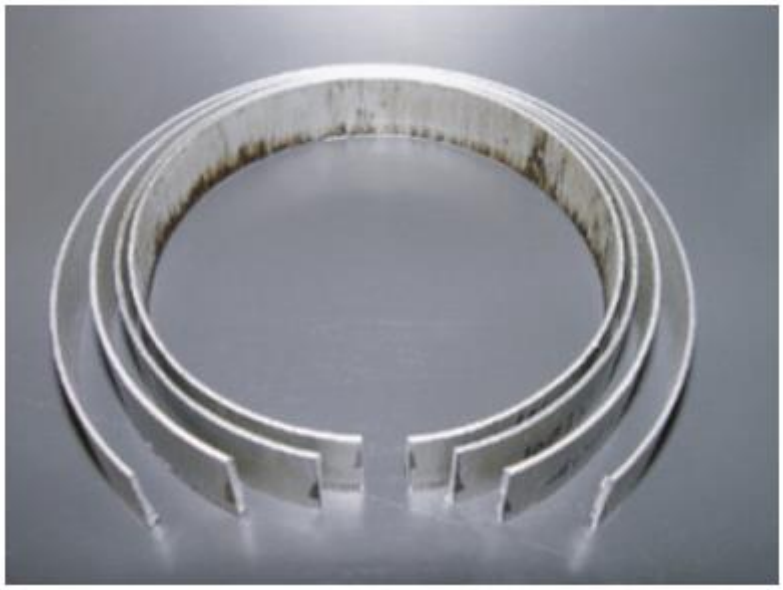

**Figure 8: Opening of the rings for several temperatures in the range 25–250 °C [32].**

Moon et al. investigated the effect of tool temperature on the reduction in springback of AA1050 aluminum sheets [33]. In U-shape bending experiments, the authors measured 20% reduction in springback when using a non-isothermal tooling set-up with a hot die and cold punch, compared to conventional room temperature bending tests. Moreover, tensile tests were performed at temperatures ranging from -10 to 200°C. The results showed that the corresponding yield strength decreased from 135 MPa to 40MPa, accounting for the lower springback observed after forming at warm temperature.

Furthermore, Kim et al. reported a rapid increase in formability and decrease in springback of AZ31B magnesium alloy for temperatures up to 200 °C and very slowly afterwards [34]. For non-isothermal tests, the reduction in springback followed a linear trend with temperature.

Takata applied the non-isothermal warm forming process to a square-punch drawing set-up [21]. The punch temperature was maintained at 25°C using chilled water and die temperature was maintained at 250°C. They compared springback of the formed 5xxx series aluminum alloy samples with mild steel samples. The results are pictured in Figure 9.


**Figure 9: Cold and wam hat-shaped parts of 5xxx series aluminum alloy and cold formed mild steel alloy [21].**

An improvement in shape can be seen for aluminum alloys at higher temperature compared to cold forming. More importantly, the net shape of the aluminum sample after forming at 250°C is comparable to the steel sample that was cold formed [21].

Nguyen et al. created models to predict springback in V-bend samples at room and elevated temperatures using a modified Johnson-Cook hardening law [35]. The simulation results were in good agreement with the measured data. The predicted springback amounts for a range of temperatures are shown in Figure 10 [35]. The models predict a gradual decrease in springback with increasing test temperature.

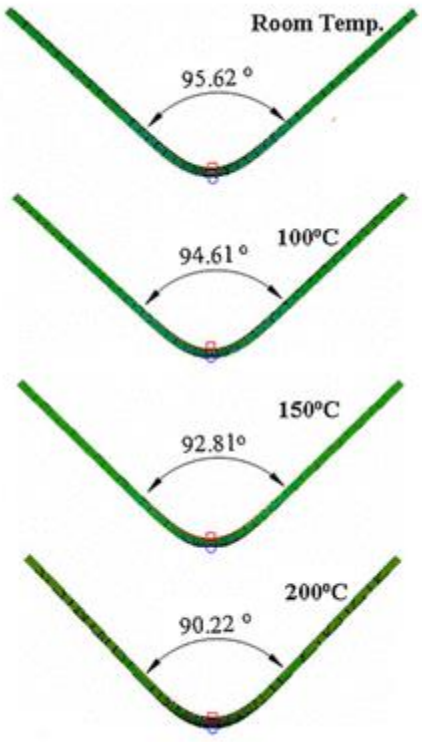


**Figure 10: Deformed shape after springback in V-bend simulations [35].**

## 1.5 Current Work

There has been a considerable amount of prior research conducted on characterizing and predicting springback for room temperature sheet metal forming operations. The number of studies to-date considering springback after warm forming is rather limited. Furthermore, the author is unaware of previous studies on the springback after warm forming of AA3003 brazing sheet, the material commonly used in automotive heat exchanger applications.

To address this shortfall in the literature, the primary objective of the current work was to experimentally evaluate the effect of temperature on the springback behavior of a clad aluminum alloy brazing sheet. The material considered was 0.2mm (0.008in.) thick, comprising of a modified AA3003 core with an AA4045 clad layer on one side. The majority of current heat exchangers are fabricated using fully annealed material; thus, annealed (O-temper) material was considered as a baseline. Strain hardened tempers are also of current interest due to their greater strength and corrosion resistance [3]; however, the higher strength of these materials generally results in higher levels of springback making it difficult to achieve accurate net shapes using such tempers. To examine the effect of material hardness, a range of initial

strain hardened tempers were considered, namely the H24- and H22-tempers, often referred to as “fully-hard” and “half-hard” temper conditions, respectively.

The springback experimental study was divided into two stages. The first stage was a benchmark study which involved a condensed test matrix and relatively simple tooling. Subsequently, a more comprehensive study was conducted which included additional process parameters and more complex tooling. U-channel forming experiments were performed at elevated temperatures after which the final geometry and nominal target geometry were compared to ascertain springback. The U-channel geometry was selected to represent what is seen in cooling channels of various automotive heat exchanger components.

Also, presented herein are results from development of numerical models to predict springback behaviour. The results from a material characterization study were used to create a simplified constitutive model. This model was used to simulate forming and springback of U-bent parts under various process conditions.

This research was performed as part of a larger Automotive Partnership Canada project undertaken by the University of Waterloo and Dana Canada Corporation, addressing the potential benefits of warm forming on aluminum heat exchanger components.

The balance of this thesis is organized as follows. Chapter 2 provides results of tensile tests performed to characterize material behaviour at elevated temperature. Chapter 3 details test results that show the effect of forming temperature on springback, along with the effect of blank holding force and lubricant type. Chapter 4 focuses on development of numerical models to predict springback under various process conditions. Primary conclusions stemming from this research and recommendations for future work are given in Chapter 5.

# 2.0 Material Characterization Study

The brazing sheet material consists of an AA3003 core and AA4045 clad layer on one side, that is coated with Dana Canada's proprietary braze promotor. The nominal thickness of the sheet was 0.2 mm including the clad layers. Three temper conditions were examined in this study which included the O-, H22-, and H24-tempers. The O-temper is the fully annealed condition while the H-tempers are strain hardened and partially annealed, providing increased strength and hardness. Table 2 shows measured nominal sheet thickness and clad thickness of the aluminum brazing sheets at three different temper conditions [36].

**Table 2: Nominal values of overall sheet thickness and clad layer thickness for all three material temper conditions.**

| | **O-Temper** | **H22-Temper** | **H24-Temper** |
|---|---|---|---|
| **Clad Thickness (µm)** | 26.79±1.72 | 21.50±1.63 | 22.10±1.86 |
| **Overall Sheet Thickness (µm)** | 201.17±2.01 | 202.85±1.75 | 203.15±1.69 |

## 2.1 Tensile Experiment Set-up

Tensile tests were conducted to characterize material deformation behaviour at elevated temperatures for the three temper conditions. The tests were conducted on the Instron universal test machine located at the CanmetMATERIAL facility in Hamilton, Ontario. The grips and the specimen were encapsulated in an environmental chamber to regulate temperature of the specimen. The test set-up is shown in Figure 11.


**Figure 11: Experimental set-up for the tensile tests.**

An MTS biaxial video extensometer was used to measure strain in the specimen during testing. An LED light fixture was positioned behind the camera to increase lighting inside the chamber. The extensometer software tracked movement of distinctly marked areas on the specimen. Two points were required for tracking the axial strain and two points for the lateral strain in the specimen. The test geometry used is shown in Figure 12 [37]. Due to the thin nature of the brazing sheet material, the tensile specimens for this study were cut using an electrical discharge machining (EDM) process at the Canmet Facility as opposed to CNC machining. The EDM process produces specimens with a clean edge that did not require any rework or deburring. This is desirable since burrs may initiate edge cracking during the test.

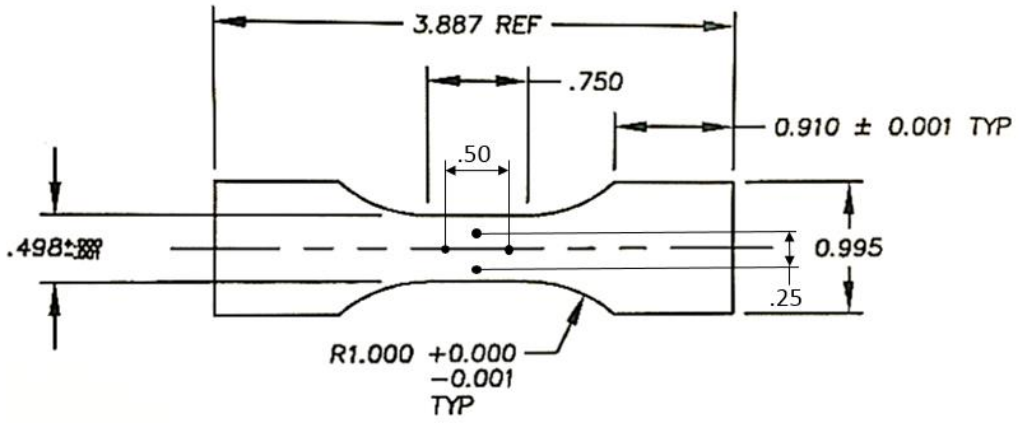


**Figure 12: Tensile Test Geometry. Dimensions shown are in inches.**

The temperature inside the chamber was measured using a thermocouple located near the grip area. Another thermocouple was located at the center of the specimen. The differential between the two was measured using a digital thermometer. It was determined that the grip region temperature was normally 2°C lower than the temperature of the center of the specimen. The second thermocouple was then removed from the remainder of the test and grip area thermocouple was used to monitor the temperature of the sample, manually accounting for the offset. The tests were initiated once the temperature had stabilized to the test temperature. It took 10, 15 and 20 minutes to reach 150, 200, and 250°C, respectively. Figure 13 shows the specimen mounted on the grips with the extensometer markers.

**Figure 13: Tensile test specimen mounted on the test fixture.**

The test parameters considered for this study were temperature (room temperature (RT), 150, 200, and 250°C), strain rate (0.002, 0.02/s) and orientation of the specimen axis relative to the sheet direction (rolling (RD), transverse (TD) and diagonal direction (DD)). The values for each test parameter are listed in Table 3. Three repetitions were done for each test condition. The reported stress-strain response (Section 2.2) is the average of the three measured curves. The transverse and diagonal direction were tested at four temperature conditions and at a strain rate of 0.02/s only.

**Table 3: Test Matrix for the material characterization study.**

| Material Temper Condition | Sheet Orientation | Strain Rate (/s) | Temperature (°C) | | | |
|---|---|---|---|---|---|---|
| | | | Room Temperature | 150 | 200 | 250 |
| O | RD | 0.02 | 3 | 3 | 3 | 3 |
| | | 0.002 | 3 | 3 | 3 | 3 |
| | TD | 0.02 | 3 | 3 | 3 | 3 |
| | DD | 0.02 | 3 | 3 | 3 | 3 |
| H22 | RD | 0.02 | 3 | 3 | 3 | 3 |
| | | 0.002 | 3 | 3 | 3 | 3 |
| | TD | 0.02 | 3 | 3 | 3 | 3 |
| | DD | 0.02 | 3 | 3 | 3 | 3 |
| H24 | RD | 0.02 | 3 | 3 | 3 | 3 |
| | | 0.002 | 3 | 3 | 3 | 3 |
| | TD | 0.02 | 3 | 3 | 3 | 3 |
| | DD | 0.02 | 3 | 3 | 3 | 3 |

## 2.2 Results

Engineering stress-strain values were calculated using the raw data generated by the machine software and video extensometer, at the end of each test. These values were translated into true stress-strain curves using the following formulae. The Young's modulus was estimated from the elastic region of the engineering stress strain curve for each test.

$$True\ Strain\text{:}\ \ \varepsilon = \ln(1+e)$$

$$True\ Stress\text{:}\ \ \sigma = \mathrm{s}\ln(1+\mathrm{e})$$

$$Effective\ Plastic\ Strain\text{:}\ \ \overline{\varepsilon_p} = \varepsilon - \frac{\sigma}{E}$$

where *s* is the engineering stress, *e* is the engineering strain, and E is the measured Young's modulus.

### 2.2.1 Effect of Material Temper

The H-temper material condition is strengthened by strain hardening and subsequently annealed to achieve the desired strength. Figure 14 shows the tensile test results at RT at 0.02/s strain rate in the rolling direction.

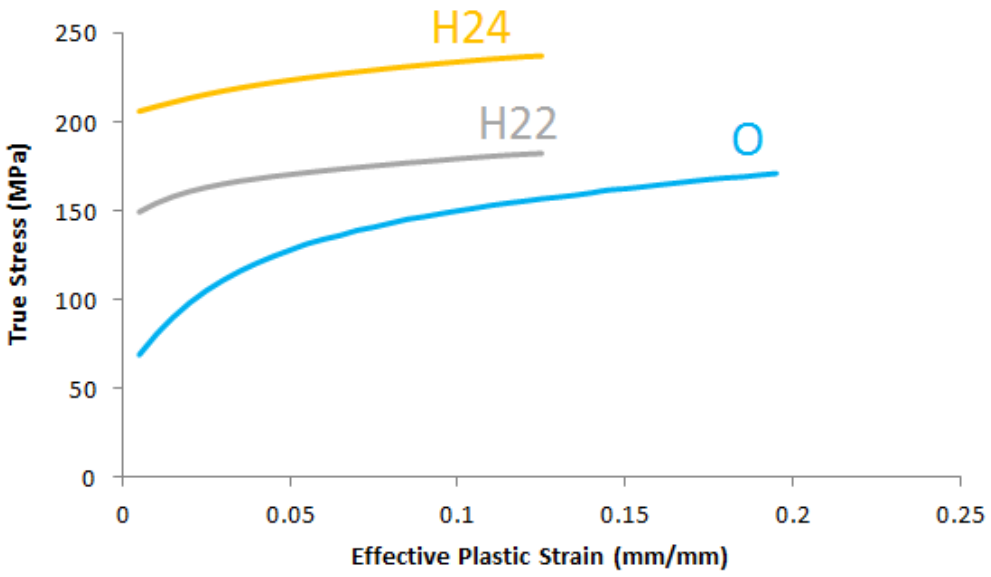


**Figure 14: Flow stress comparison (RD) of O-, H22-, and H24-temper conditions tested at room temperature at 0.02/s.**

There is a noticeable difference in strength between the two H-tempers and the fully annealed conditions. H24-temper resulted in the highest strength relative to the H22- and O-temper conditions. The H-temper conditions also exhibited lower ductility compared to the fully annealed condition. Moreover, the O-temper curves exhibited a greater degree of work hardening than the H22- and H24-tempers.

### 2.2.2 Effect of Thermal Softening

Figure 15, Figure 16 and Figure 17 show the thermal softening effect at elevated temperature test conditions, in the O-, H22- and H24-temper material, and at strain rate of 0.02/s.

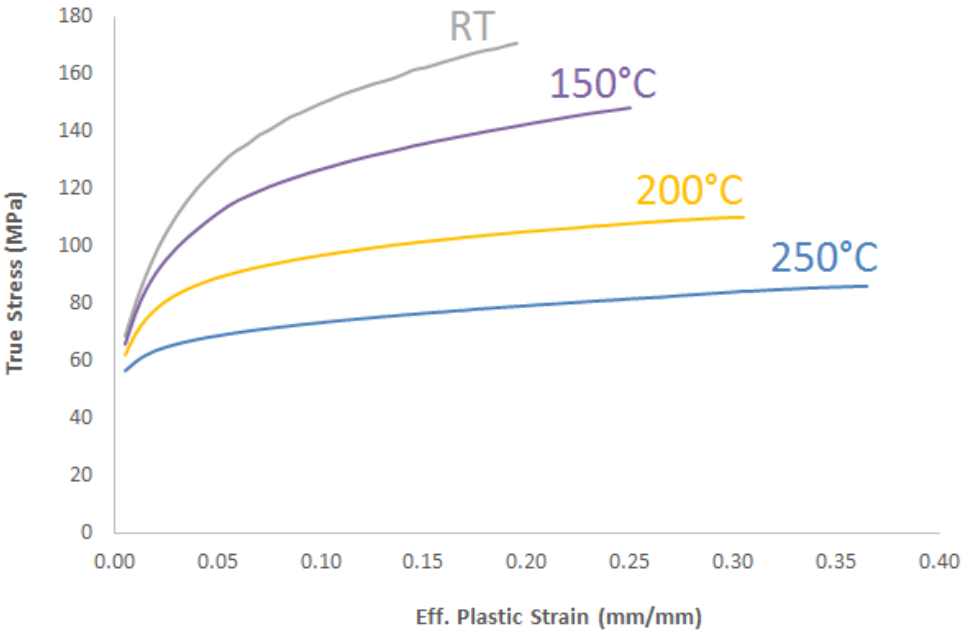


**Figure 15: Flow stress curves for the O-temper at RT, 150, 200, 250°C, at 0.02/s strain rate in RD.**

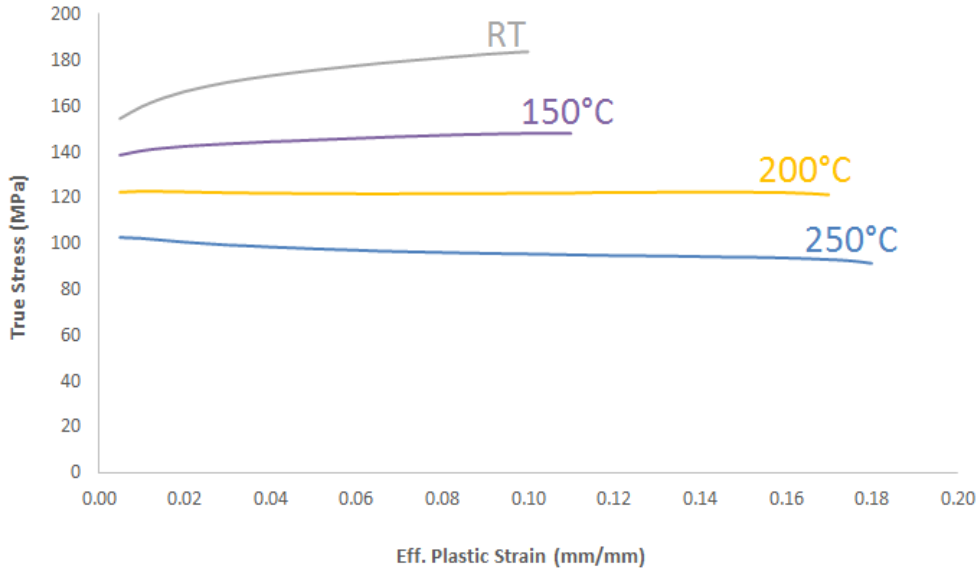


**Figure 16: Flow stress curves for the H22-temper at RT, 150, 200, 250°C, at 0.02/s strain rate in RD.**

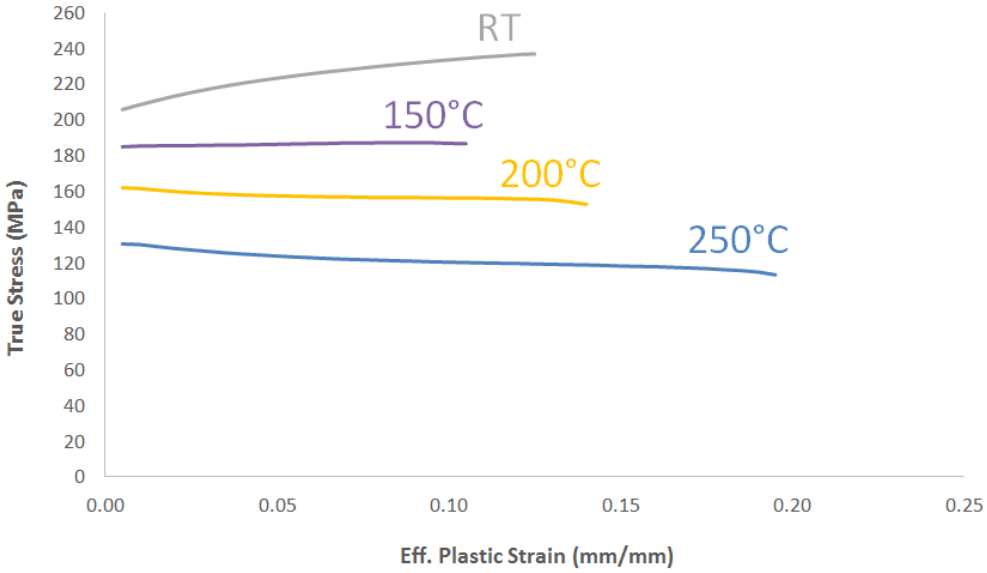


**Figure 17: Flow stress curves for the H24-temper at RT, 150, 200, 250°C, at 0.02/s strain rate in RD.**

All three temper conditions showed a reduction in strength and an increase in ductility, as the test temperature was increased. For the fully annealed condition (O-temper), positive work hardening was observed, whereas the degree of work hardening was lower in strain hardened tempers. The work hardening effect in the H-temper conditions was relatively low to begin with at room temperature and decreased further at higher test temperature. Furthermore, an increase in ductility was observed for all three tempers at higher temperature.

### 2.2.3 Effect of Strain Rate

Another parameter considered in the study was the strain rate at which the experiment was conducted. Two strain rates values were selected, which were 0.002/s and 0.02/s. In general, aluminum exhibits limited strain rate sensitivity at room temperature and shows positive rate sensitivity at elevated temperatures. The test results for O-, H22- and the H24-tempers are shown in Figure 18, Figure 19 and Figure 20, respectively.

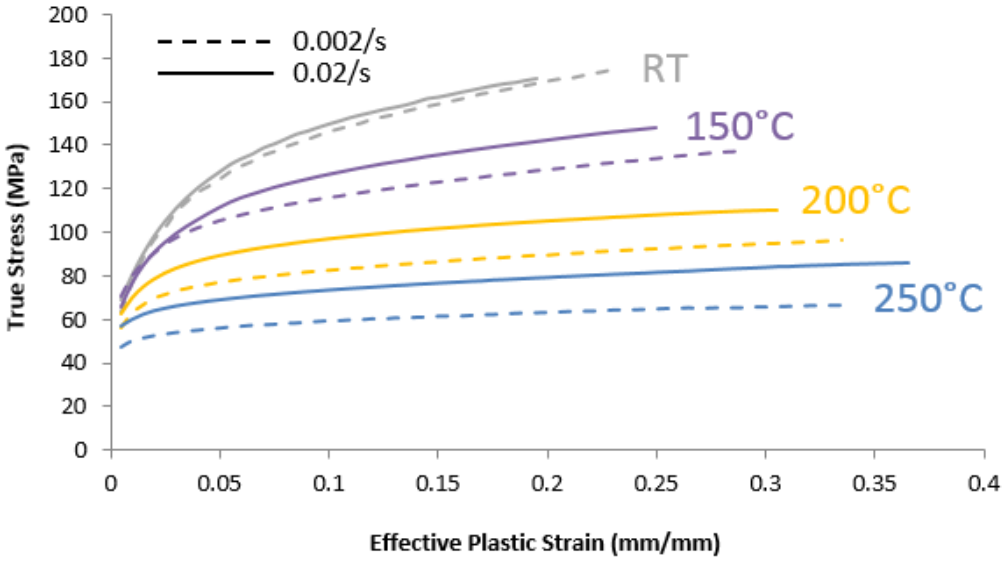


**Figure 18: Flow curves of O-temper at RT, 150, 200 and 250°C, comparing two strain rates (0.002 and 0.02/s) in RD.**

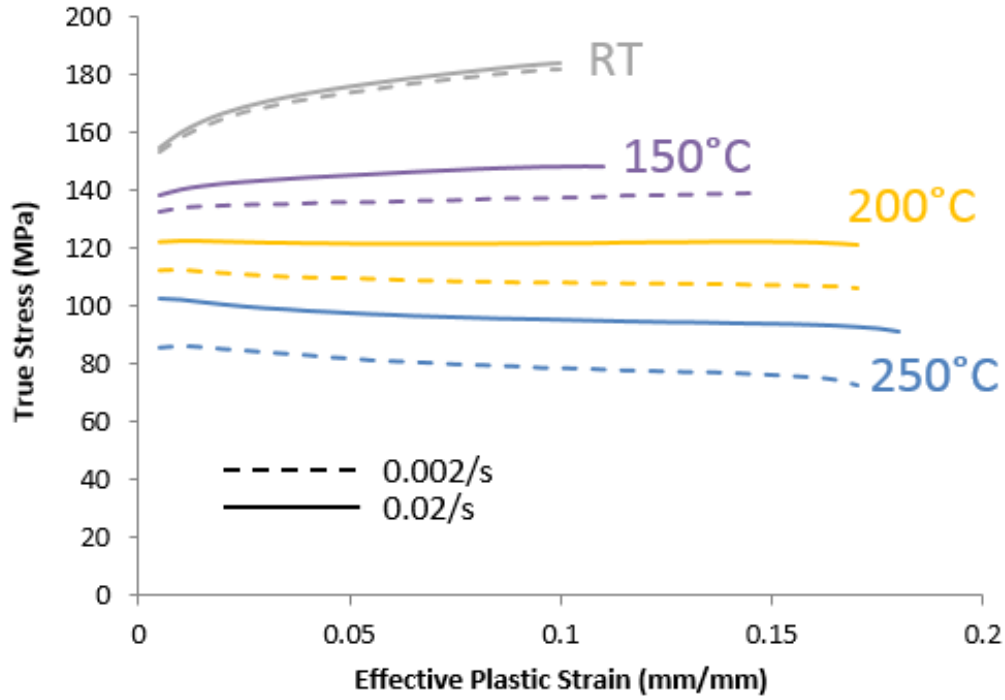


**Figure 19: Flow curves of H22-temper at RT, 150, 200 and 250°C, comparing two strain rates (0.002 and 0.02/s) in RD.**

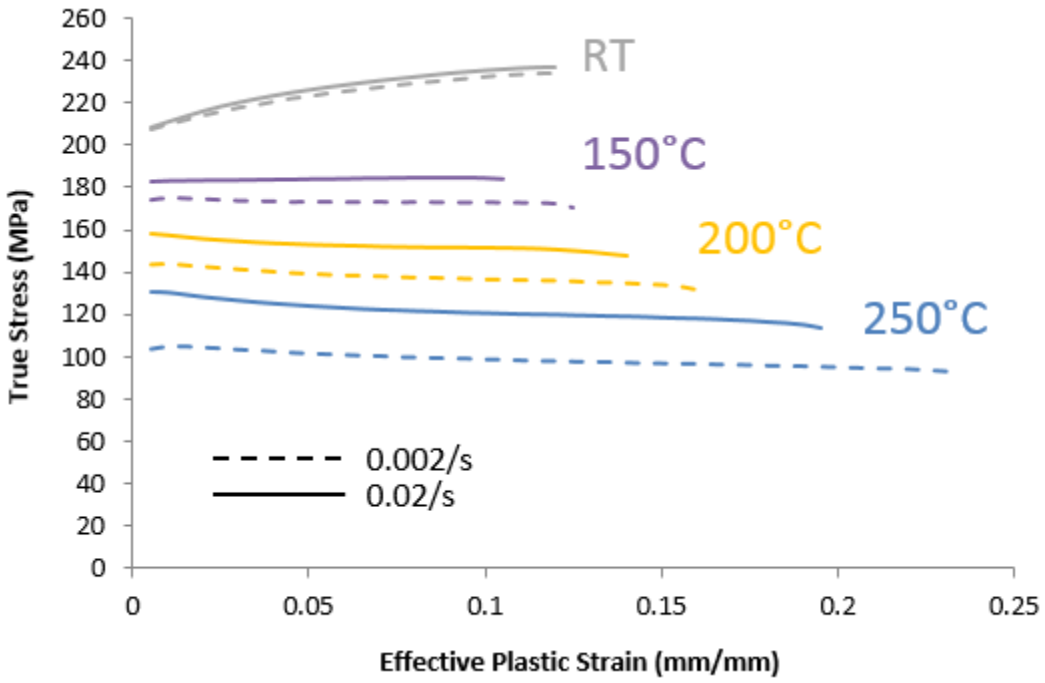


**Figure 20: Flow curves of H24-temper at RT, 150, 200 and 250°C, comparing two strain rates (0.002 and 0.02/s) in RD.**

At room temperature, there was little variation between the flow behaviour at the two strain rates. However, as the temperature was increased, all three material tempers exhibited a strong, positive strain rate sensitivity.

### 2.2.4 Effect of Sheet Orientation

Tensile tests were also conducted to assess the degree of anisotropy in the sheet material. Specimens were machined to orient the axial direction of the specimen in the rolling, transverse and diagonal directions. The corresponding results for the O-, H22- and H24-tempers are shown in Figure 21, Figure 22 and Figure 23.

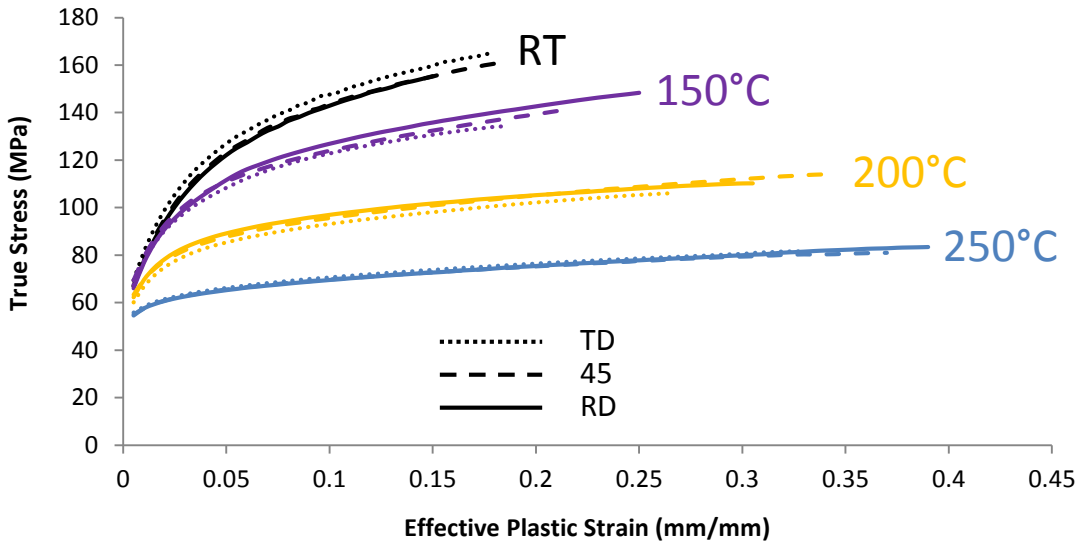


**Figure 21: Flow stress curves of O-temper at RT, 150, 200 and 250°C at 0.02/s in rolling (RD), diagonal (45°), and transverse direction.**

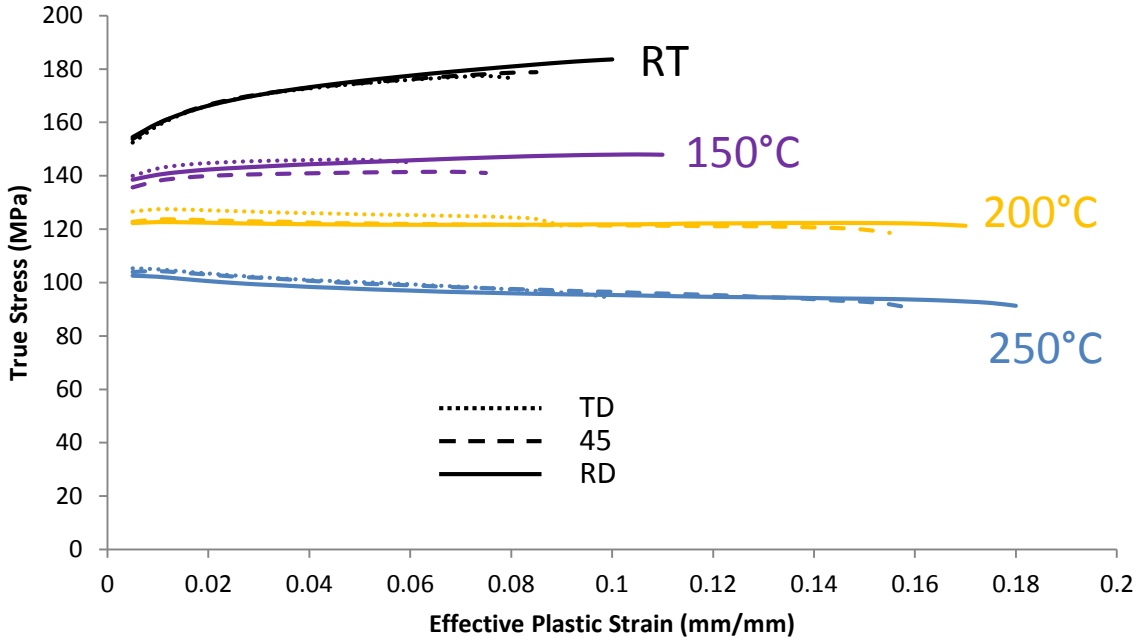


**Figure 22: Flow stress curves of H22-temper at RT, 150, 200 and 250°C at 0.02/s in rolling (RD), diagonal (45°), and transverse direction.**

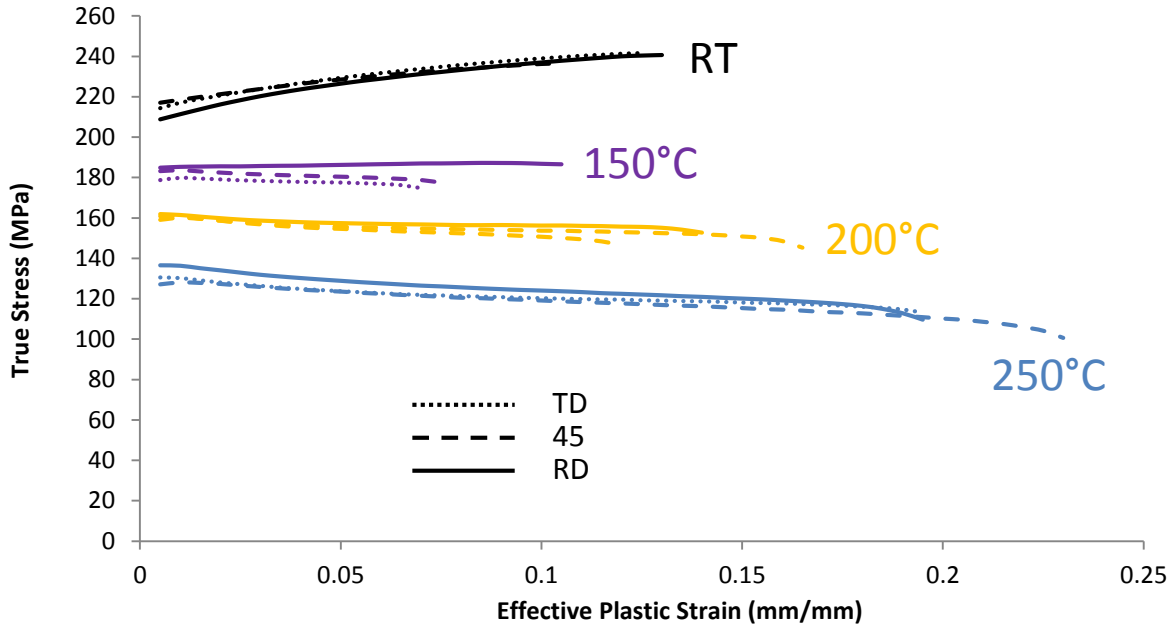


**Figure 23: Flow stress curves of H24-temper at RT, 150, 200 and 250°C at 0.02/s in rolling (RD), diagonal (45°), and transverse direction.**

There was moderate variation in ductility between the three sheet directions. However, the hardening behaviour of diagonal and transverse directions was similar to hardening behaviour in the rolling direction, for all three tempers at RT, 150, 200, 250°C.

Due to the limitations in the current set-up, strain values in the lateral direction could not be measured reliably. Hence, the R-values, which are measure of anisotropy in the sheet, were not determined in this material characterization study. The numerical models shown later assumes the material is isotropic. Nevertheless, future tensile experiments will be conducted using advanced strain measurement systems to obtain the lateral strain data and calculate precise R-values.

## 2.3 Effect of Low Temperature Annealing

One concern with warm forming was whether heating the higher temper material during warm forming temperature could result in permanent thermal softening of the material. In such a case, warm forming in would result in undesirable material properties after stamping.

To study potential annealing effects, a study was conducted in which specimens of H22- and H24-tempers were heated to the required warm forming temperature, then air cooled, and subsequently tensile tested at room temperature. The results were then compared to a specimen that did not see elevated

temperature and was only tested at room temperature. The results of this study are shown in Figure 24 and Figure 25. It should be noted that the curves shown are engineering stress-strain curves.

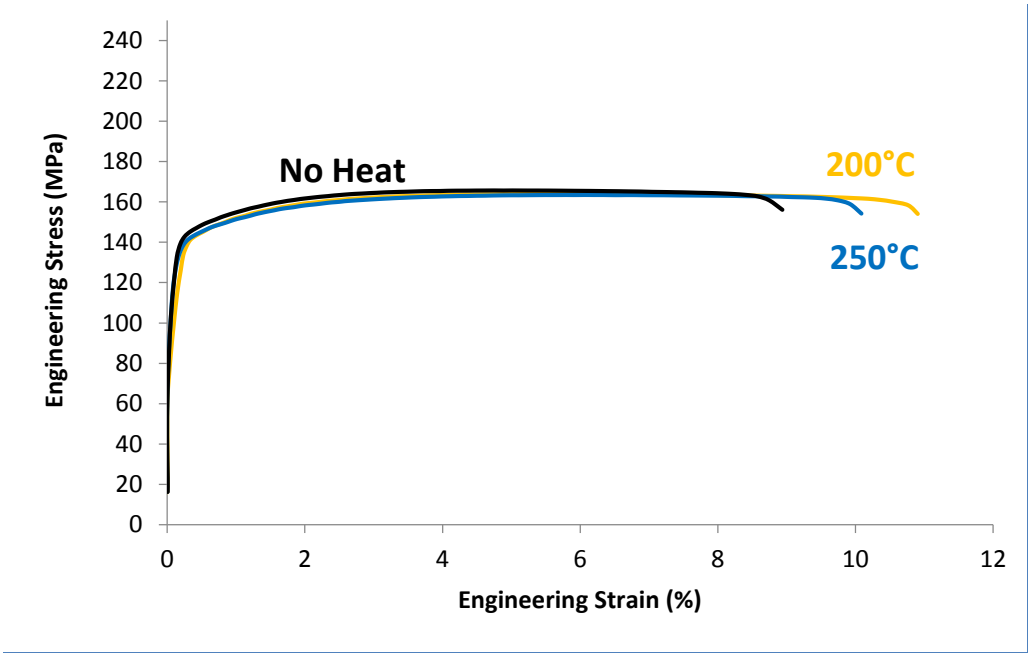


**Figure 24: Flow stress comparison of H22-temper tested at room temperature after heating at 200 and 250°C, 0.02/s strain rate in RD.**

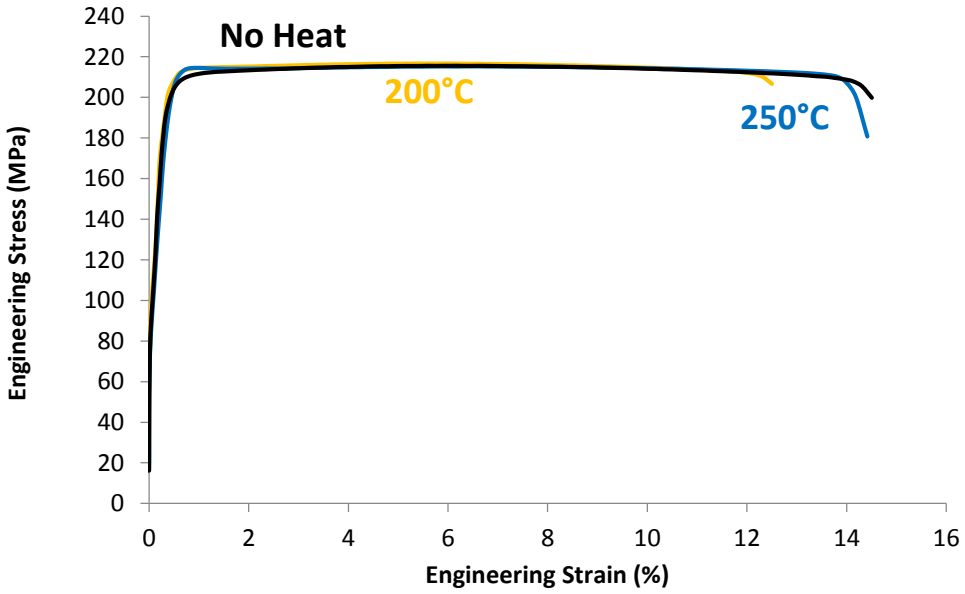


**Figure 25: Flow stress comparison of H24-temper tested at room temperature after heat-treated at 200 and 250°C, 0.02/s strain rate in RD.**

It is apparent from examination of the figures that there was no change in strength characteristics of both H22- and H24 temper specimens between the heat treated (at 200 and 250°C) specimen and the non-

heat treated specimen; although the elongation of the thermally processed samples did increase somewhat. This result indicates that exposure to the warm forming thermal cycle did not permanently alter the inherent strength of the as-received sheet material. The available energy is thought not to be sufficient to promote recrystallization, particularly for such short durations, since the forming temperature is well below the annealing temperature [38].

# 3.0 U-Bend Springback Experiments

## 3.1 Background

Various techniques have been employed to characterize springback behaviour of sheet material. For the current work, a U-shape geometry was selected because it was a close approximation to the battery plate channel geometry. The material experiences sufficient bending strain to produce measurable springback. Moreover, due to the symmetry of the geometry, the samples can be brazed afterwards to assess brazing performance. The biggest advantage of this geometry was that it allows for forming with a wide range of process parameters requiring small-scale tooling.

The focus here is on springback behaviour of the sheet material as a function of forming temperature. Other parameters considered were material temper, lubrication and blank holding force. Two series of experiments were performed. Initially, a benchmark study was conducted using relatively simple tooling to discern whether springback was affected by forming temperature – these results are presented in Section 3.2. Subsequently, additional tooling components were fabricated for a more comprehensive study, which included additional process parameters such as the blank holding force – this second series of experiments is presented in Section 3.3.

The forming of the U-shape parts for both experimental studies was done on the Instron testing machine in the High Pressure Lab at the University of Waterloo. The Instron machine allowed for precise movement of the punch relative to the die cavity. This was needed due to the small draw depth and the excessively thin sheet thickness.

## 3.2 Benchmark Study

### 3.2.1 Experimental Setup

The objective of the benchmark study was to validate whether springback is reduced at elevated temperature using simple tooling components. Custom die components were designed which included forming dies, heating plates and cooling barriers to prevent overheating of the load cell. The die components were mounted on a standard four-post die set procured from Anchor Danly. The CAD assembly of the tooling configuration is shown in Figure 26.

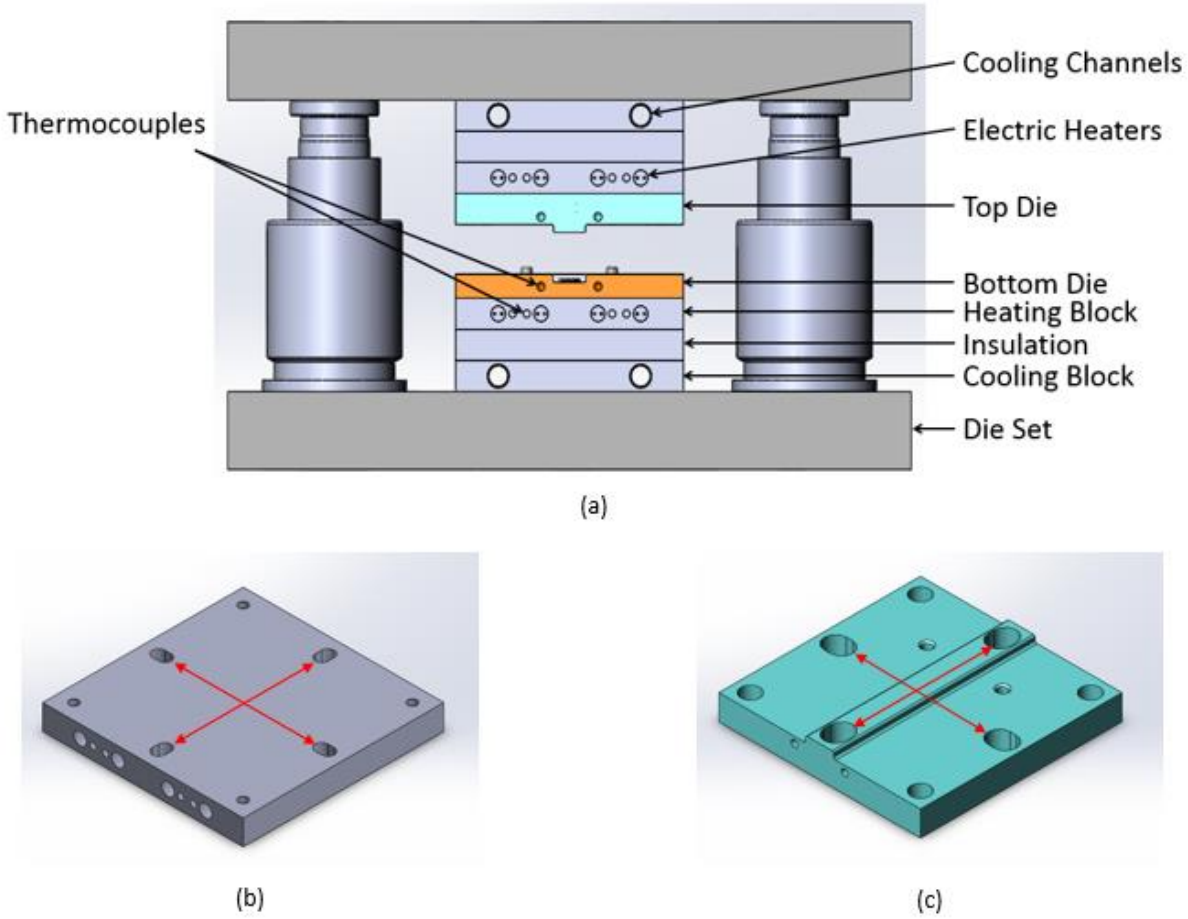


**Figure 26: Tooling set-up used for the benchmark springback study. (a) Assembly view, (b) Slotted holes in the heating block, (c) Slotted holes in the top die.**

The forming dies had slotted holes evenly spaced at the center lines. This was done to prevent misalignment of the two forming dies due to thermal expansion. To provide a source of heat, eight 200W cartridge heaters were inserted into a block located below the forming dies. This allowed for interchangeability of the forming dies while keeping the rest of the components the same. Each heating block had two thermocouples, one to control the temperature and one for sending feedback to the PID controllers.

The test geometry comprised of a single U-shaped channel with a width of 14.3mm (0.56in.) and depth was 3.2mm (0.125in.). The bend radius was 0.8mm (0.03in.) at all bending regions. The test geometry is pictured in Figure 27.

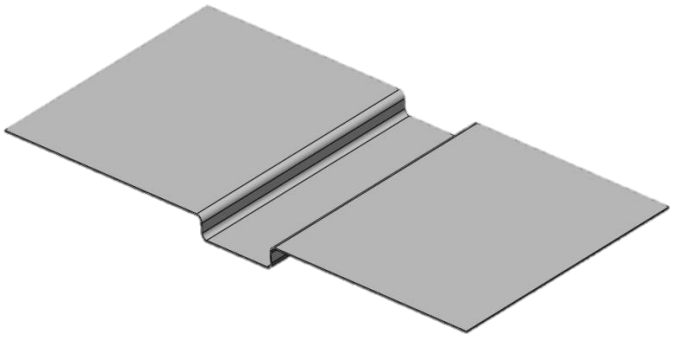

**Figure 27: Test geometry for the benchmark springback study.**

Rectangular blanks 101.6mm x 38.1mm (4in. x 1.5in.) were cut from the coils. A number of cut blanks had slight curvature, which was resolved by bending the blanks around a large radius. This defect was primarily in the O-temper coil. Blanks with excessive curvature were scraped. In the actual production process, the sheet is fed through a straightener to eliminate curvature before forming.

The machine was manually jogged using the fine-motion handheld controller. To heat the blank, the top and bottom die were initially closed such that they were in contact with the blank surface. The dies were held at this position for 30 seconds to allow the blank to reach the test temperature through heating by conduction. Subsequently, the dies were displaced further to draw the sheet into the die cavity. To determine the length of heating period, the temperature of the blank was measured using two thermocouples attached to different locations on the blank, and a data acquisition unit was used to record the temperature over time. The heating curve along with thermocouple location is shown in Figure 28.

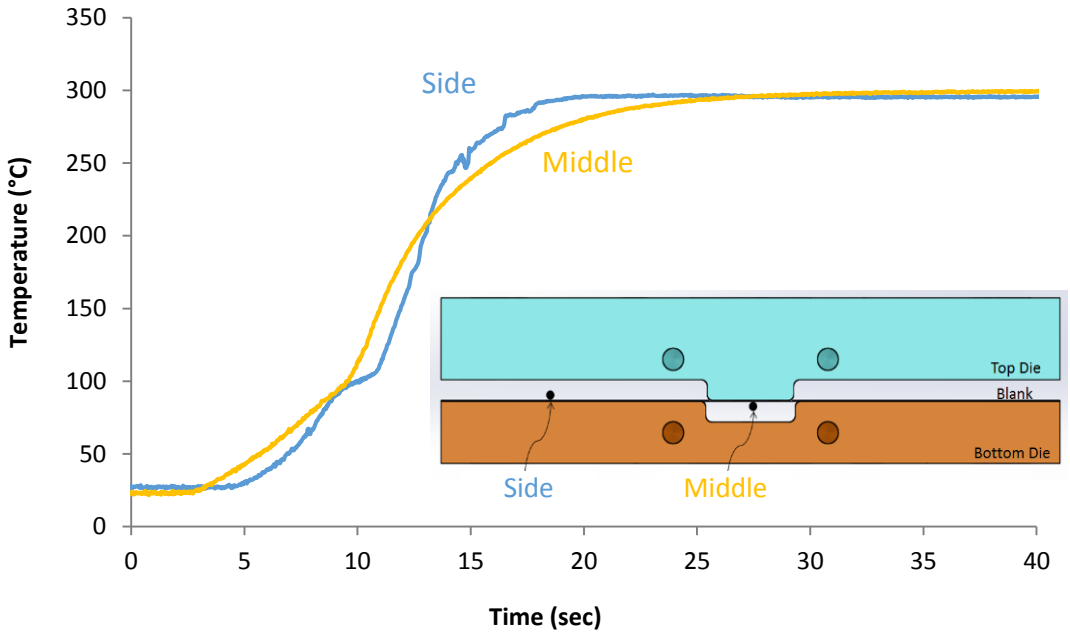


**Figure 28: Temperature vs. time curve showing the heating cycle for pre-heating the blank.**

The test parameters for the benchmark study included temperature and material temper. The test parameters and the values are listed in Table 4. Forge Ease Al278 mixed with alcohol, (hereafter referred to as "Fuchs lubricant"), was applied on all blank samples prior to forming.

**Table 4: Test parameters for the benchmark springback study.**

| Material Temper Condition | Temperature | Lubricant |
|---|---|---|
| O<br>H22<br>H24 | RT<br>100<br>200<br>300 | Fuchs |

### 3.2.2 Results

Springback angle was measured by analyzing images of the formed cross-sectional area, via an orthogonal camera setup. A jig was constructed to locate the formed samples centered beneath of the camera lens for repeatability. These images were imported into CAD software, where the sidewall angle deviation was measured. Figure 29 shows the procedure for measuring the angle.

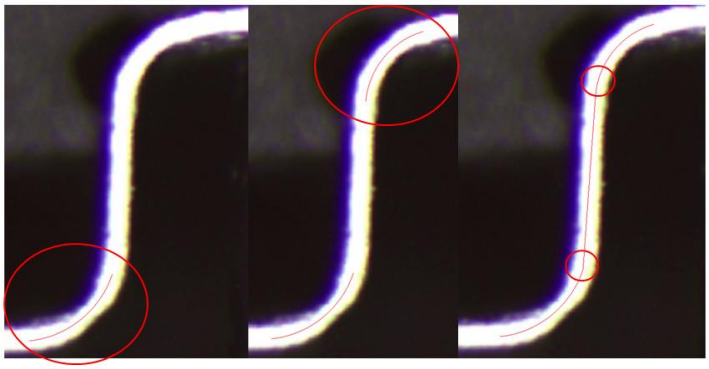

(a)

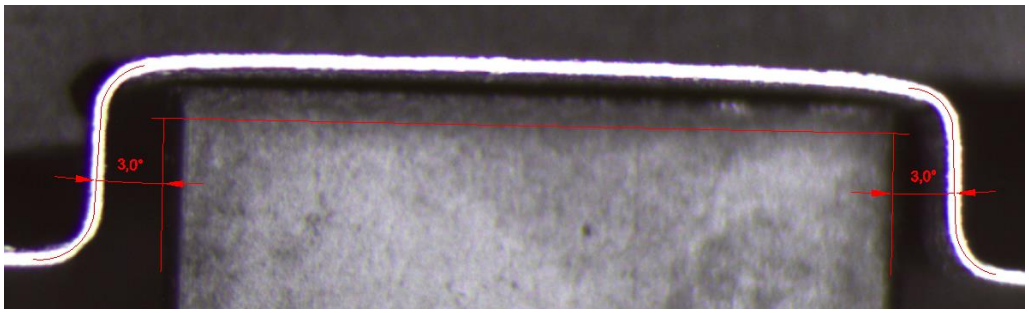


(b)

**Figure 29: Springback angle measurement procedure - O-temper sample formed at RT using Fuchs lubricant. (a) Bend radii and sidewall is outlined. (b) Angle is measured perpendicular to the line parallel the U-channel.**

The cross sectional profile was manually traced and a line as drawn connecting the center point of radii on the either side of the U-channel. Sidewall angle was measured between the sidewall line and the line orthogonal to the line connecting the center points of the two radii. This procedure was repeated for all the tested samples and average springback values for each of the three repetitions for each test condition were calculated.

The springback behaviour of the O-, H22- and H24-temper at room temperature is shown in Figure 30.

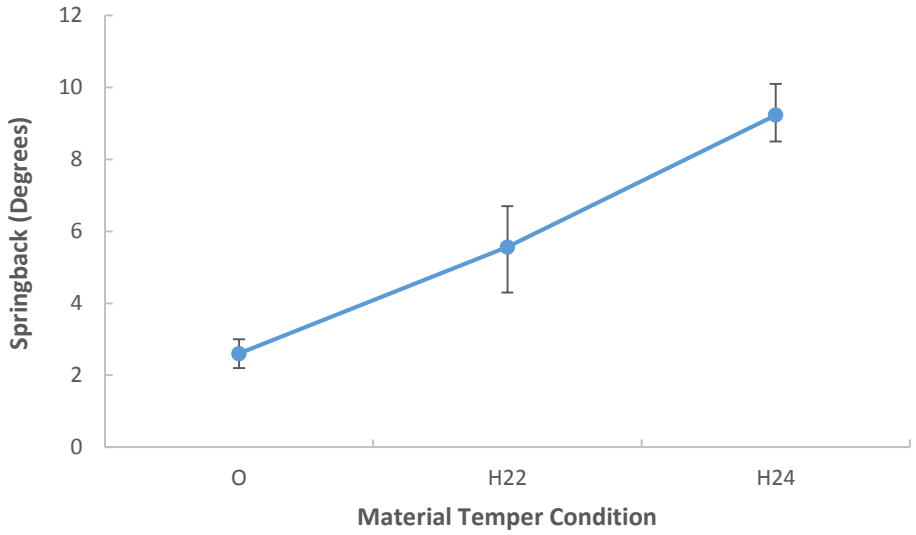


**Figure 30: Material Temper vs. springback angle at room temperature only.**

The H24-temper, the hardest of the three tempers, exhibited the highest springback, followed by the H22- and the O-tempers. As shown by the tensile test results in the previous section, the stresses in the strain hardened tempers are higher, thus resulting in greater springback.

Figure 31 shows the effect of temperature on springback for all three tempers.

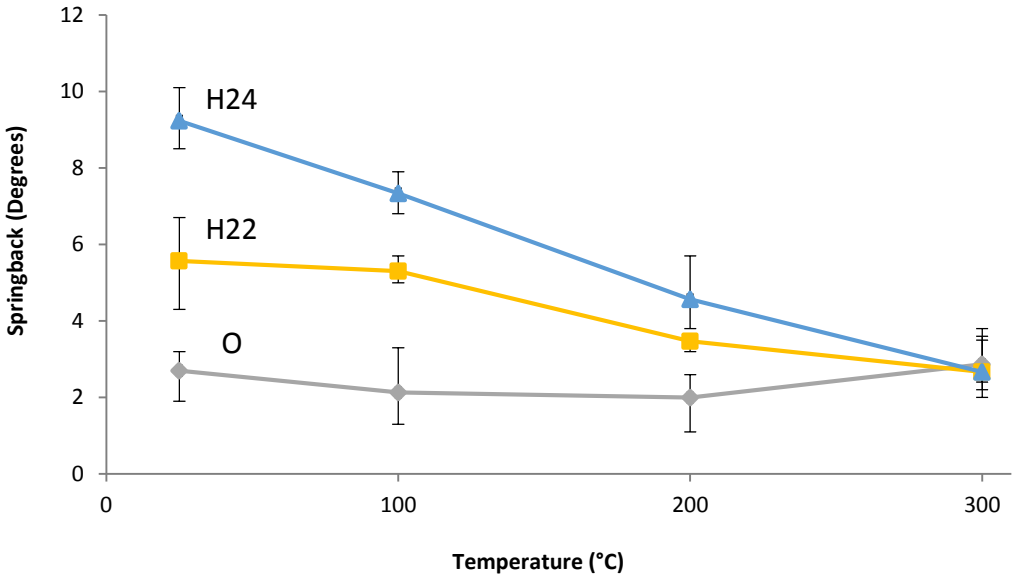


**Figure 31: Springback of three different tempers after forming plotted as function of temperature.**

A significant reduction in springback was observed for the H22- and H24 tempers by forming at elevated temperature. The results for the O-temper were somewhat suspect since there was an increase in

springback at higher temperature. The die geometry for this series of experiments incorporated a sidewall angle of 90°, which resulted in the formed components being wedged into the die cavity. Some force was required to extract these components and, due to the highly soft condition of the O-temper, the applied force may have distorted the shape of the parts. Additionally, there was discoloring on the surface of the formed parts at 300°C due to the lubricant burning off. It was then decided to keep the maximum warm forming temperature at 250°C to avoid burning of the lubricant. The O-temper tests were repeated and similar results were observed, as shown in Figure 32. The resulting springback was higher at elevated temperature compared to the lower temperature.

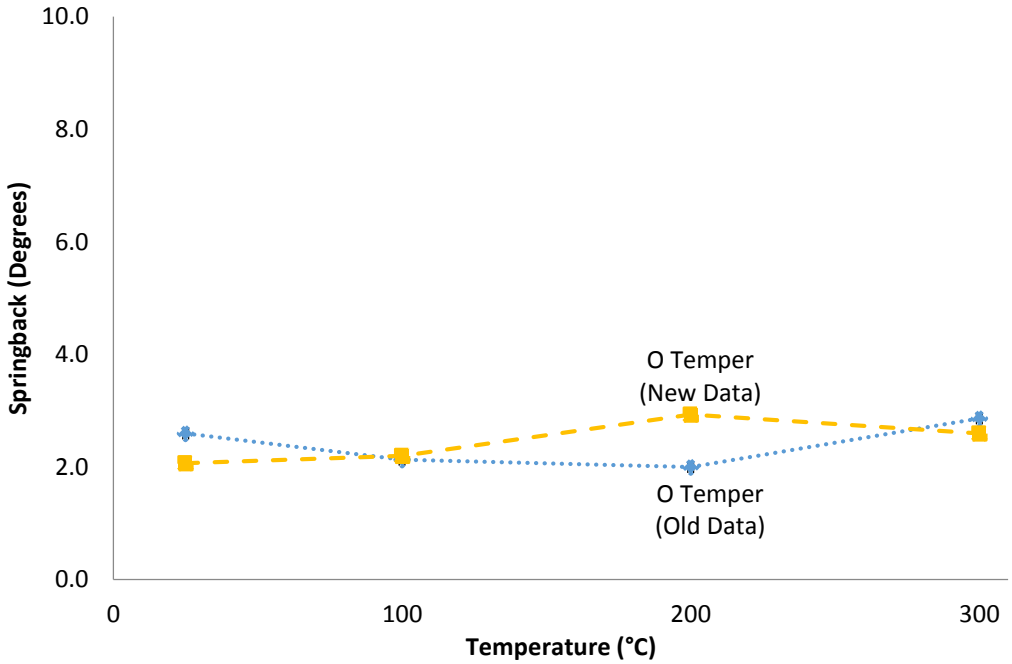


**Figure 32: Comparison of new and old springback data for O temper with respect to temperature, die radius of 0.8mm.**

Similar to the tensile experiments, the effect of annealing prior to forming was also considered. Samples were heated to 300°C, cooled in air and subsequently formed at room temperature. The resulting springback from these heat-treated samples were compared to springback obtained from samples that were cold formed and warm formed. This was done to verify whether there was any permanent strength reduction as a consequence of elevated temperature. The results are shown in Figure 33.

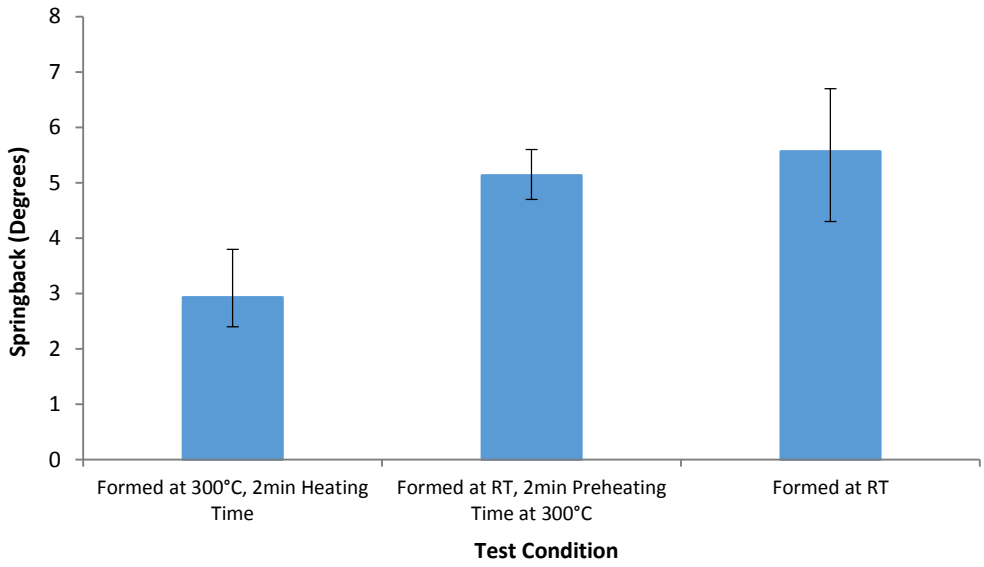


**Figure 33: Results from the annealing study comparing springback for warm formed, cold formed, and heat-treated only samples.**

As seen in the figure, warm forming was effective in reducing springback compared to the samples formed after heating and cooling, as well as the samples that were directly cold formed with no exposure to elevated temperature. Moreover, prior exposure to elevated temperature did not significantly affect the springback after cold forming. In warm forming process, the operative stresses are lower during forming resulting in lower springback.

After noting the results of this benchmark study, a second set of experiments were performed which explored additional process parameters with more sophisticated tooling components. The results of this second study are presented in the following section.

## 3.3 Refined U-shape Springback Study

### 3.3.1 Experimental Set-up

The objective of this study was to expand on the test matrix used in the benchmark study. The experiments were conducted with new custom designed die components that provided the ability to apply and vary binder force on the flanges of the blank during forming. Table 5 shows the test parameters and the corresponding values used in the study.

**Table 5: Test parameters for the comprehensive springback study.**

| Material Temper Condition | Temperature (°C) | Lubricant | Blank Holding Force (N) |
|---|---|---|---|
| O<br>H22<br>H24 | Room Temperature<br>150<br>200<br>230<br>240<br>250<br>260 | Fuchs<br>Teflon (Spray) | 171<br>1174<br>2669 |

Moreover, the test geometry was modified to resolve some of the issues encountered during the first set of experiments. The new test geometry is shown in Figure 34.

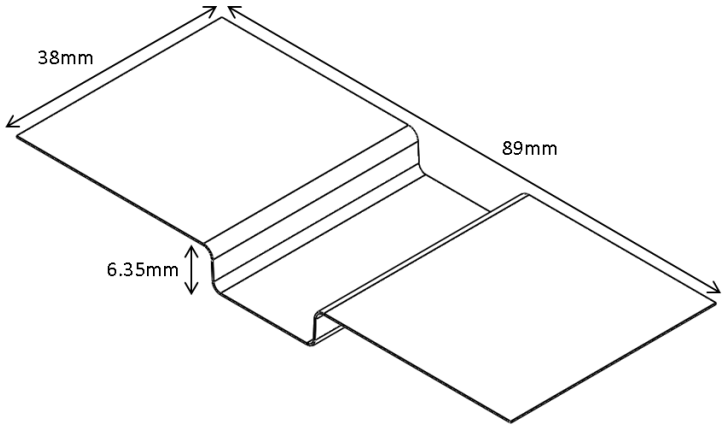


**Figure 34: Test geometry of the U-shape part used for the comprehensive study.**

A draft angle of 2.5° was added to the die sidewall to prevent the formed samples from being wedged into the die cavity. Additionally, the depth of the U-bend geometry was changed from 3.3mm (0.13in.) to 6.35mm (0.25in.). This was done to increase the degree of springback for ease of measurement. The blank size was the same as the one used for the first experimental series.

An alternate lubrication scheme was also considered. Teflon sheets have been widely used in sheet metal forming tests to decrease frictional force between the blank surface and the tooling surfaces. However, the Teflon sheet thickness 0.08mm (0.003in.) was relatively large compared to the sheet thickness of

0.2mm (0.008in.). Teflon in the aerosol spray form, which was rated for use up to 260°C temperature, was procured for this experiment.

The die components were mounted on the same four-pillar die set as used previously. The CAD model of the tooling assembly is shown in Figure 35.

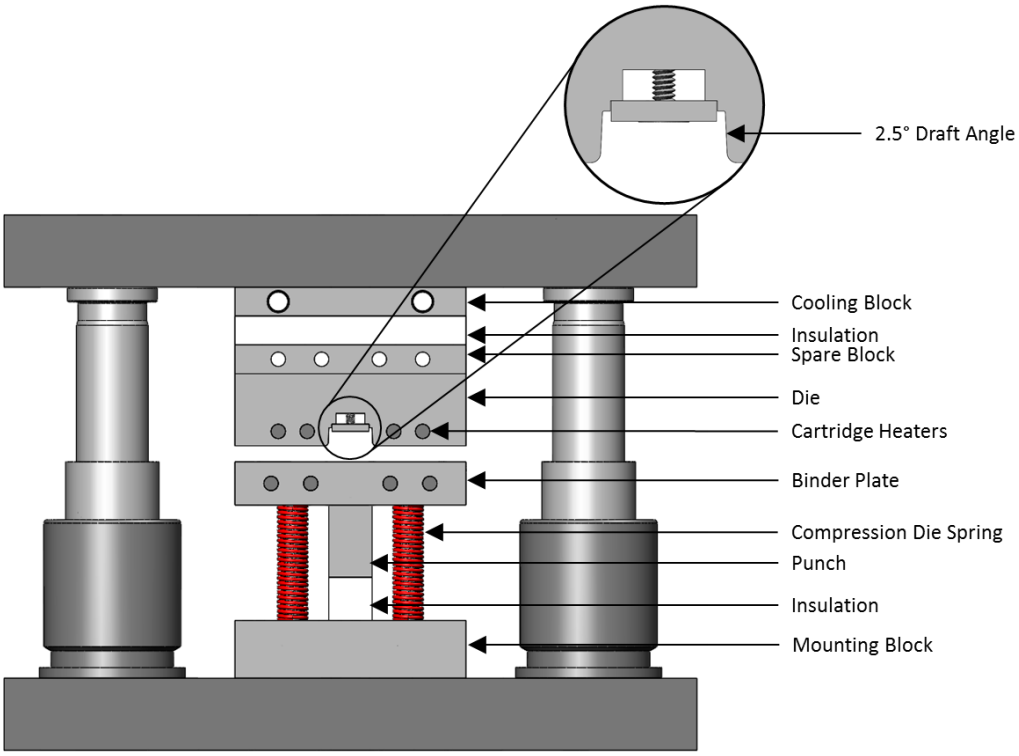


**Figure 35: Tooling set-up used for the comprehensive springback study.**

In stamping processes, the application of a separate binder force is often facilitated by use of double-action forming presses; one for actuating the binder plate and the second for the punch. For this experiment, the binder force was applied using four die compression springs allowing for the use of single-action (Instron) machine. An alternative method considered was using gas springs but these were rejected for this experiment due to the high cost. The binder force was regulated by using springs of different stiffness constants. The stiffness constants selected for this experiment were 6.7, 46.2, and 105 N/mm, providing a low, medium and high blank holding force, respectively. These springs yielded a maximum blank holding force of 171.3, 1174, and 2669 N, respectively.

To provide heat, the cartridge heaters used in the benchmark study were repurposed for this experiment. Four cartridge heaters were inserted into the binder plate and four were inserted into the new forming die. The punch had a separate cartridge heater which was connected to its own PID controller. The surface

temperature of the binder plate, the punch and the forming die was verified using a probe thermocouple and a digital thermometer.

A custom automated program was created in the Instron MAX software which is typically used for cyclic tension-compression testing. The program was modified to run a single forming cycle over a specified time period. Each cycle is divided into four phases, as illustrated in Figure 36.

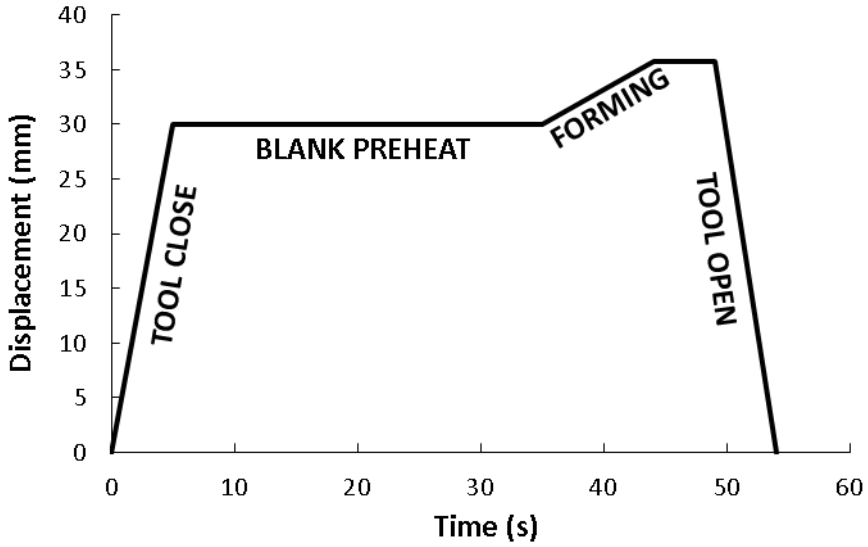


**Figure 36: Punch displacement per forming cycle with 30 seconds heating time, 5 seconds hold time and 0.65 mm/sec punch speed.**

In the first phase, the forming die, the binder and the punch are displaced such that the blank is in contact with the forming die. The dies remain at this height for 30 seconds, during which the blank is heated to the required temperature. The punch is then displaced further into the die cavity to form the U-channel. It is held at the bottom of the draw for one second and then the tools are retracted from the die cavity so the formed part can be removed. An example of a formed component is shown in Figure 37.

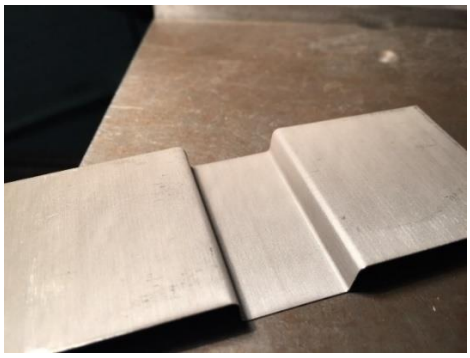

**Figure 37: An example of a formed U-channel from the comprehensive springback study.**

For this study, springback was characterized as the angle measured between the sidewall of the formed sample and the nominal die sidewall angle of 92.5 degrees. The springback measurement technique was the same as for the benchmark study. A typical image of an as-formed sample used for measurement is illustrated in Figure 38.

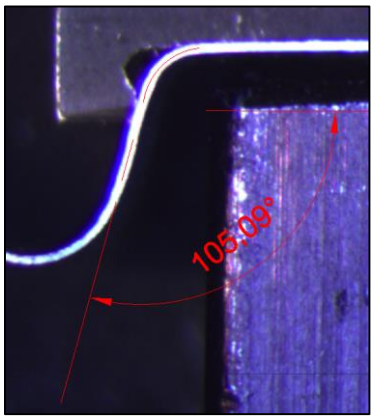


**Figure 38: Sample springback angle measurement of the sidewall angle.**

The reported springback angle in the following presentation of the experimental results was calculated as:

$$Springback\ angle = Measured\ angle - 92.5°$$

### 3.3.2 Results

The springback of the three temper conditions is compared in Figure 39.

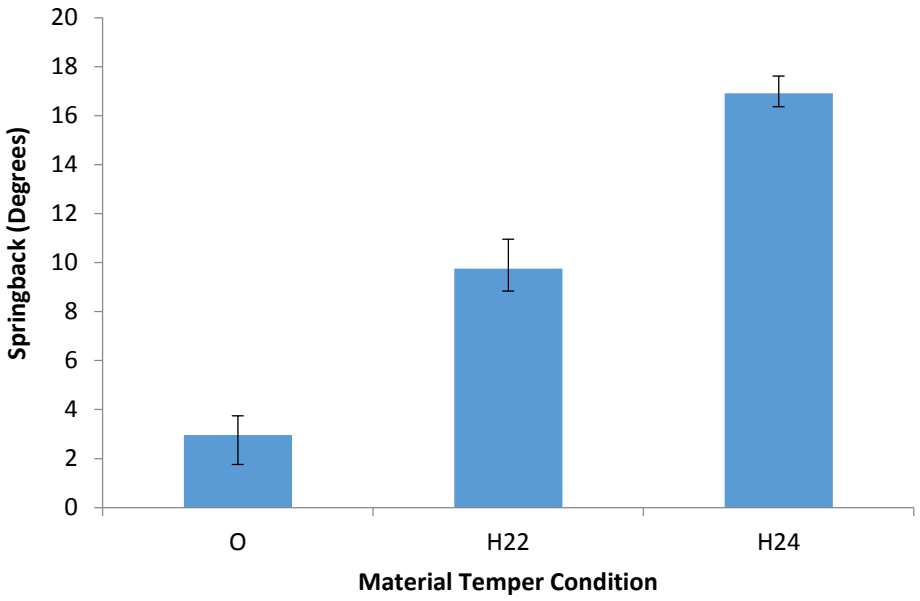


**Figure 39: Springback behaviour of H24-, H22- and O-temper at room temperature with spray Teflon and 171.3 N blank holder force.**

The H24-temper, which has the highest strength of the three tempers, exhibited the greatest springback compared to the intermediate strain-hardened temper (H22) and the fully annealed temper. The effect of temperature on springback of each of these tempers is shown in Figure 40.

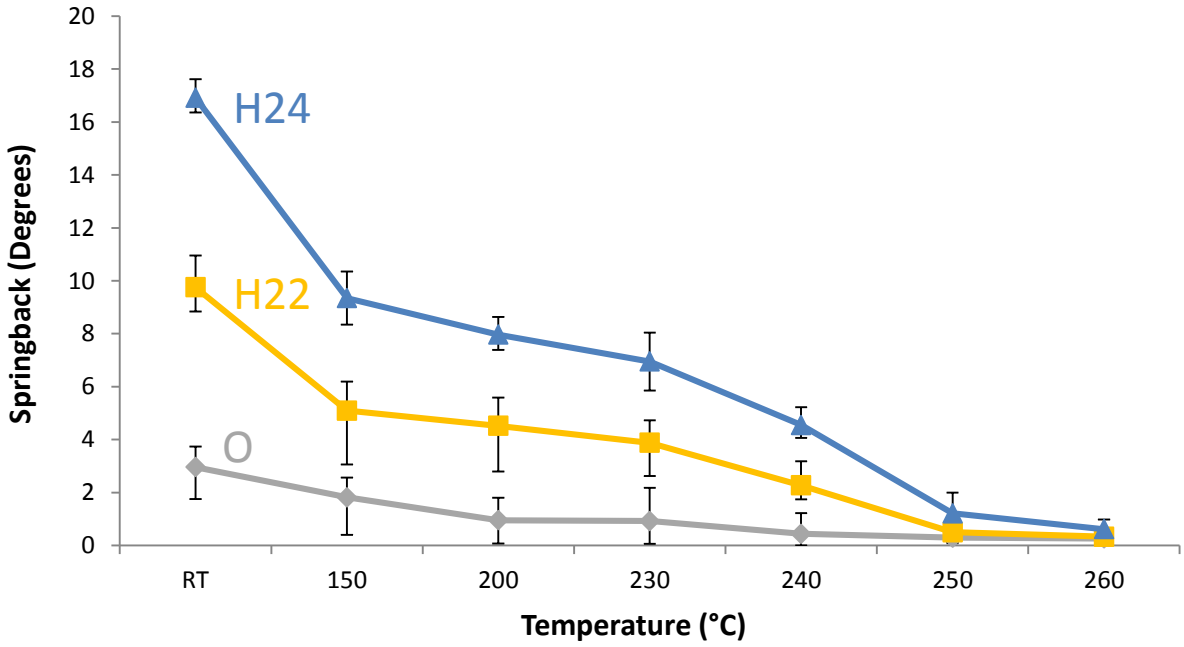


**Figure 40: Springback behaviour of three tempers formed at elevated temperatures with Teflon and 171.3 N blank holder force.**

All three tempers showed a trend in reduction of springback with increasing temperature. At 250°C all three tempers had comparable springback with H24 showing the highest reduction relative to room temperature springback. This reduction can also be seen in the images of H24 as-formed samples shown in Figure 41. The samples shown below were formed at room temperature, 150°C and 250°C using spray Teflon as lubricant and low blank holding force (BHF).

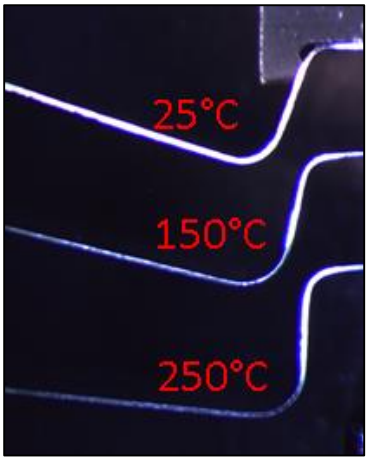


**Figure 41: Springback behaviour of H24 with increasing forming temperature using Teflon and 171.3 N blank holder force.**

In addition to temperature, the effect of blank holding force was also considered. The difference in springback with different blank holding pressure is shown in Figure 42. These values correspond to forming at room temperature with Teflon. A minor decrease in springback with increasing blank holder force was observed for all three tempers.

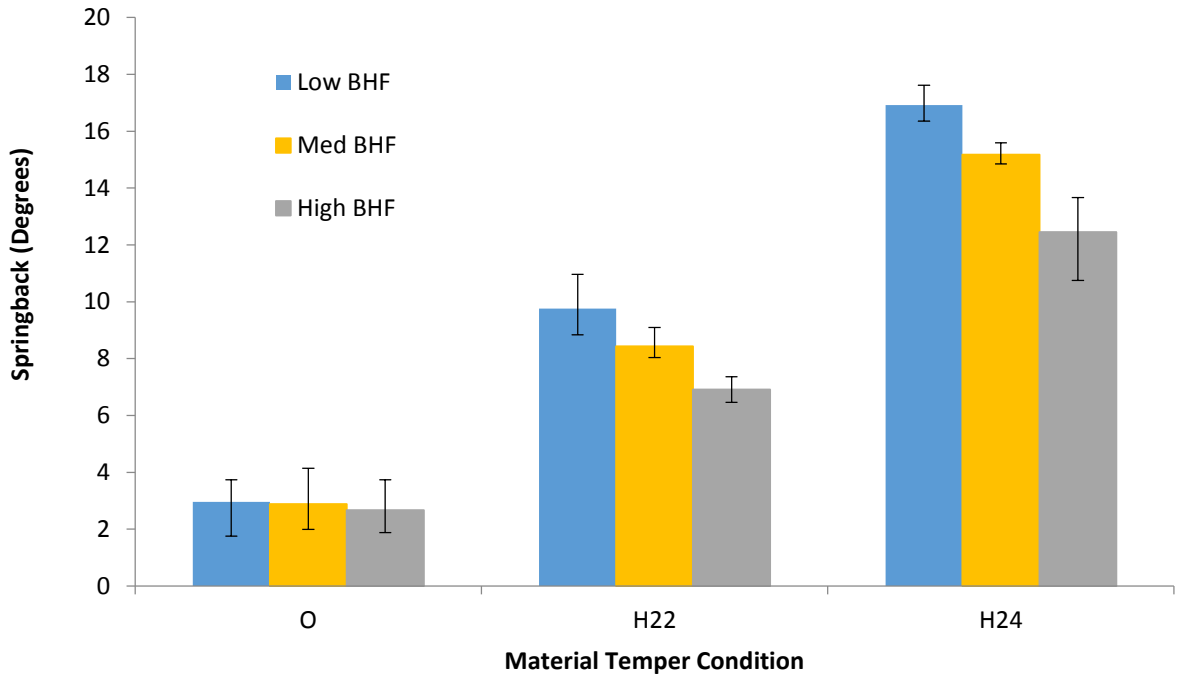


**Figure 42: Springback comparison for all three tempers with low (171.3N) and high (1174N) blank holding force at RT.**

Figure 43 shows the plot of resulting springback using the two lubricants. Both lubrication conditions showed a decrease in springback. However, the variation in springback values was greater when Fuchs was used as a lubricant. This can be attributed to the nature of the application method used for the experiment. Fuchs lubricant was applied by hand using a brush. Although care was taken to apply the lubricant consistently, there will clearly be variation from blank to blank. In contrast, the Teflon was provided in spray canister and was easily applied to the blank. This method produced a relatively smooth lubricant layer on the blank. An important aspect of the chosen lubricants is the residue left on the surface of the samples after forming. This is a concern because the residual layer may adversely affect the brazing performance. Figure 44 shows the blanks with Fuchs and Teflon lubricant. White flakes were clearly visible on the samples that were prepared with the Fuchs lubricant whereas the Teflon layer had smooth finish. To prevent large build-up of lubricant particles, the die surfaces were cleaned with a cloth in between forming of samples prepared with Fuchs lubricant. The dies were cleaned with ethanol before forming samples prepared with spray Teflon. The influence of these lubricants on brazeability is the focus of on-going work.

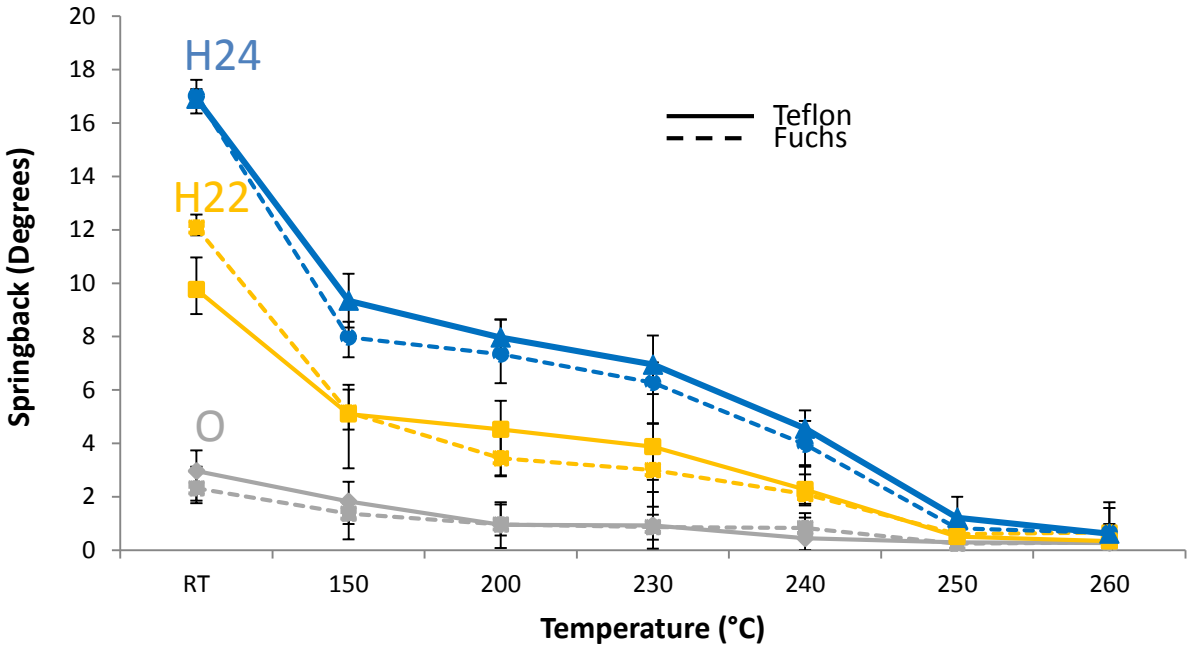


**Figure 43: Springback comparison between two lubricants, Fuchs and Teflon using 171.3N blank holder force.**

**Figure 44: Surface of samples prepared with Fuchs (left) and Teflon (right) lubricant.**

# 4.0 Numerical Models of U-shape Forming & Springback

This section describes efforts to model the forming and springback behaviour of aluminum brazing sheet under warm conditions. The simulations were performed using the commercial finite element code LS-Dyna software Version 971 revision 5.

As seen in the gathered tensile experiment results, the mechanical behaviour of aluminum alloy sheet exhibits significant thermal softening and strain rate dependency at elevated temperatures. Therefore, a material model that accounts for temperature and strain-rate dependency is needed to accurately model the forming response. Another issue that arises is due to the negative sloping trend in the flow stress curves in the experimental data, which causes the LS-Dyna explicit dynamic solver to display convergence issues.

To work around this issue, the material response was estimated using a Voce hardening law, which approximates the behaviour at elevated temperature with an assumption that the flow stress saturates after a certain plastic strain level [39]. The following sections show the results from fitting the Voce constitutive model to the measured tensile data and subsequent results from simulation of the U-channel forming and springback. The forming simulations assume isotropic sheet behaviour. Future work will consider development of a material model that better describes the mechanical behaviour, including anisotropic effects at elevated temperatures and the actual negative hardening behaviour at large strains at elevated temperature. For the models shown here, the Von Mises yield surface was used.

## 4.1 Constitutive Equation & Fit

The original Voce hardening law does not take into account strain rate sensitivity. Therefore, a modified version of the Voce model was used (herein referred to as "Modified-Voce"), which includes a combination of a logarithmic and an exponential strain rate term [40]. The constitutive equation is as follows:

Original Voce Model: $$\sigma_v(\varepsilon_P) = \left[\sigma_{sat} + (\sigma_y - \sigma_{sat})e^{\left(-\frac{\varepsilon_p}{\varepsilon_r}\right)}\right]$$

Modified Voce Model: $$\sigma_{vm}(\varepsilon_p, \dot{\varepsilon}) = \sigma_v(\varepsilon_p)\, x(\dot{\varepsilon})$$

Strain-Rate Term: $$x(\dot{\varepsilon}) = [A \ln(\dot{\varepsilon}) + (1 + \dot{\varepsilon})^B]$$

Where, $\sigma_{sat}$ is the saturation stress, $\sigma_y$ is the yield stress, $\varepsilon_r$ is the relaxation strain, $\varepsilon_p$ is the plastic strain, $\dot{\varepsilon}$ is the strain rate A and B are strain rate parameters.

The experimental uniaxial stress-strain data was used to fit the constitutive parameters of the Modified Voce material model for each temper at room temperature, 150, 200, and 250°C. These parameter values for O-, H22-, and H24-temper are listed in Table 6, Table 7 and Table 8, respective. Non-linear regression analysis was performed using the statistical analysis software MYSTAT12. [41]

**Table 6: Modified Voce material model parameters for O-temper.**

| | Room Temperature | 150°C | 200°C | 250°C |
|---|---|---|---|---|
| $\sigma_{sat}$ (MPa) | 175 | 138 | 115 | 83 |
| $\sigma_y$ (MPa) | 58 | 65 | 65 | 50 |
| $\varepsilon_r$ | 0.059 | 0.075 | 0.065 | 0.15 |
| A | 0.005 | 0.015 | 0.07 | 0.056 |
| B | 0.4 | 5 | 4 | 10 |

**Table 7: Modified Voce material model parameters for H22-temper.**

| | Room Temperature | 150°C | 200°C | 250°C |
|---|---|---|---|---|
| $\sigma_{sat}$ (MPa) | 183 | 143 | 116.75 | 85.75 |
| $\sigma_y$ (MPa) | 150 | 135 | 116 | 85.15 |
| $\varepsilon_r$ | 0.04 | 0.043 | 0.008 | 0.107 |
| A | 0.00001 | 0.008 | 0.015 | 0.002 |
| B | 0.624 | 2.437 | 4 | 10.243 |

**Table 8: Modified Voce material model parameters for H24-temper.**

| | Room Temperature | 150°C | 200°C | 250°C |
|---|---|---|---|---|
| $\sigma_{sat}$ (MPa) | 250 | 173.33 | 144 | 104 |
| $\sigma_y$ (MPa) | 209.51 | 175 | 143.5 | 101.6 |
| $\varepsilon_r$ | 0.076 | 0.07 | 0.13 | 0.25 |
| A | 0.003 | 0.007 | 0.018 | 0.006 |
| B | 0.01 | 3.81 | 5.96 | 13.785 |

The predicted tensile stress-strain response and experimental data are plotted in Figure 45 through Figure 50 for O-, H22- and H24-tempers at both strain rates.

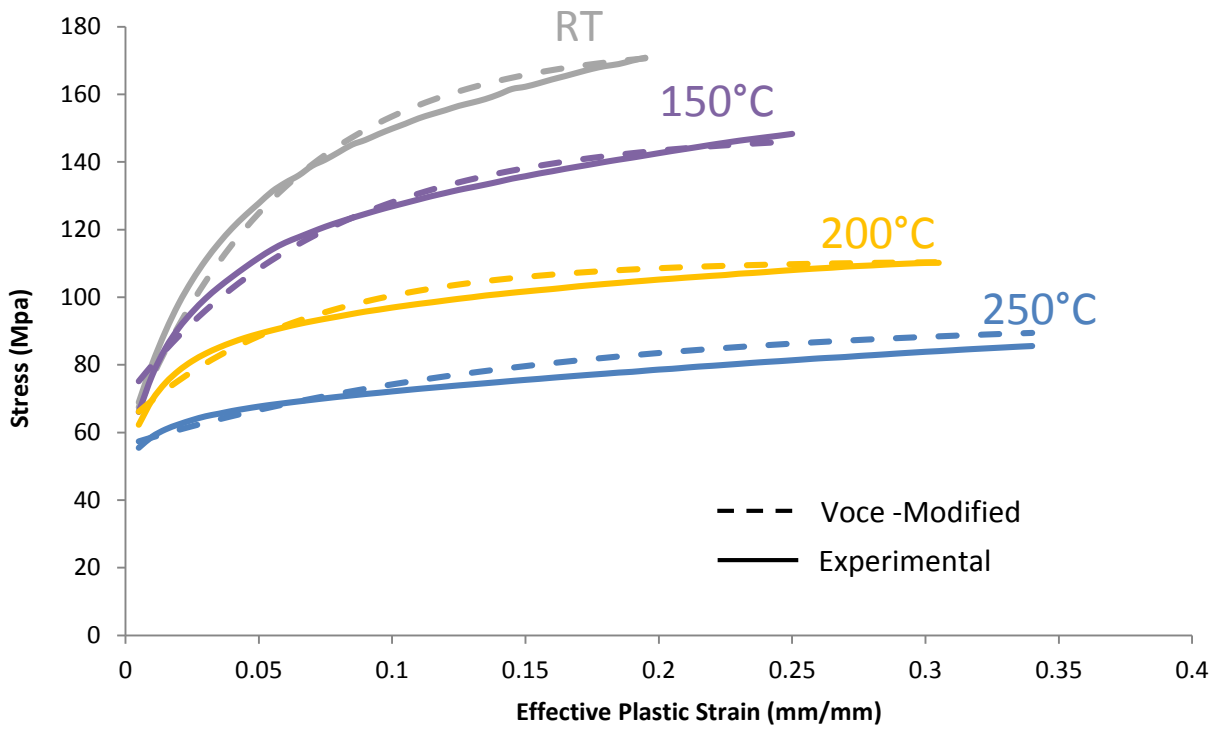


**Figure 45: Predicted flow curve response vs experimental data for O-Temper at room temperature, 150, 200, and 250°C, and at a strain rate of 0.02/s.**

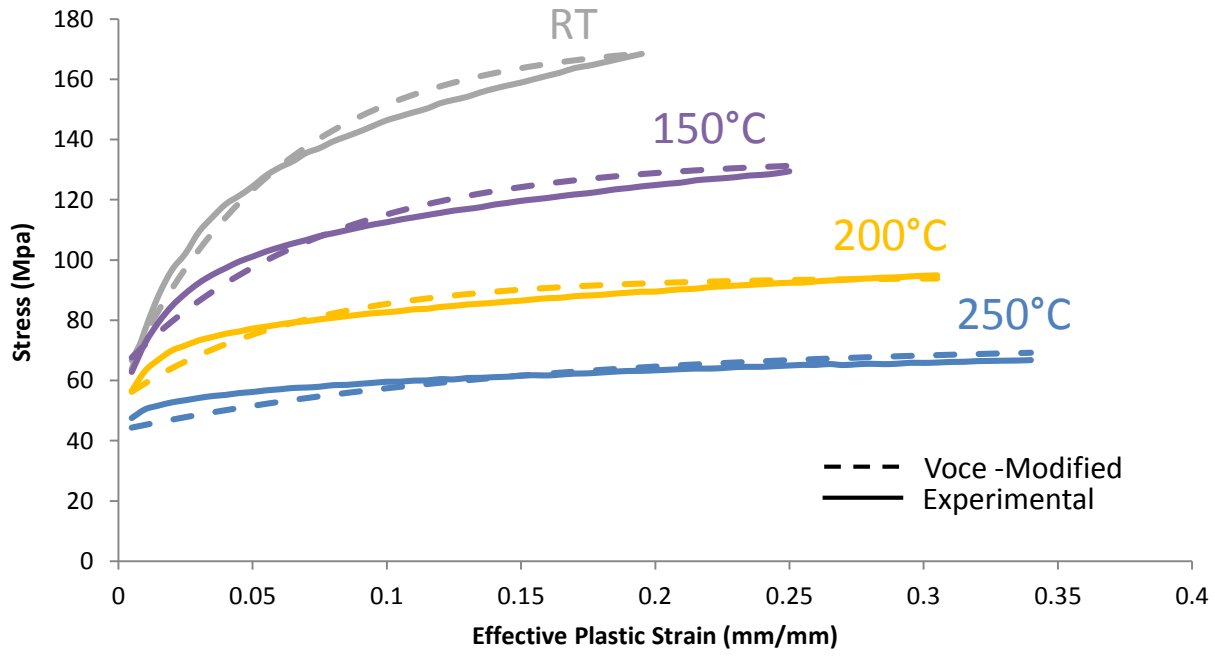


**Figure 46: Predicted flow curve response vs experimental data for O-Temper at room temperature, 150, 200, and 250°C, and at a strain rate of 0.002/s.**

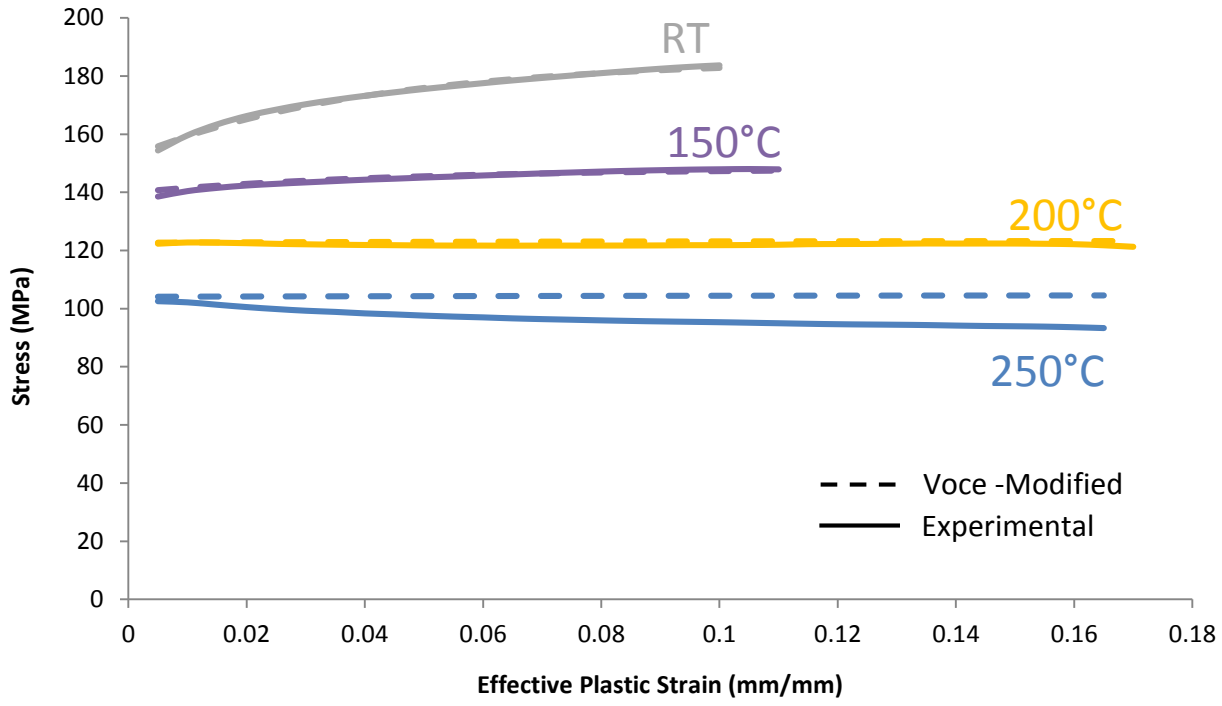


**Figure 47: Predicted flow curve response vs experimental data for H22-Temper at room temperature, 150, 200, and 250°C, and at a strain rate of 0.02/s.**

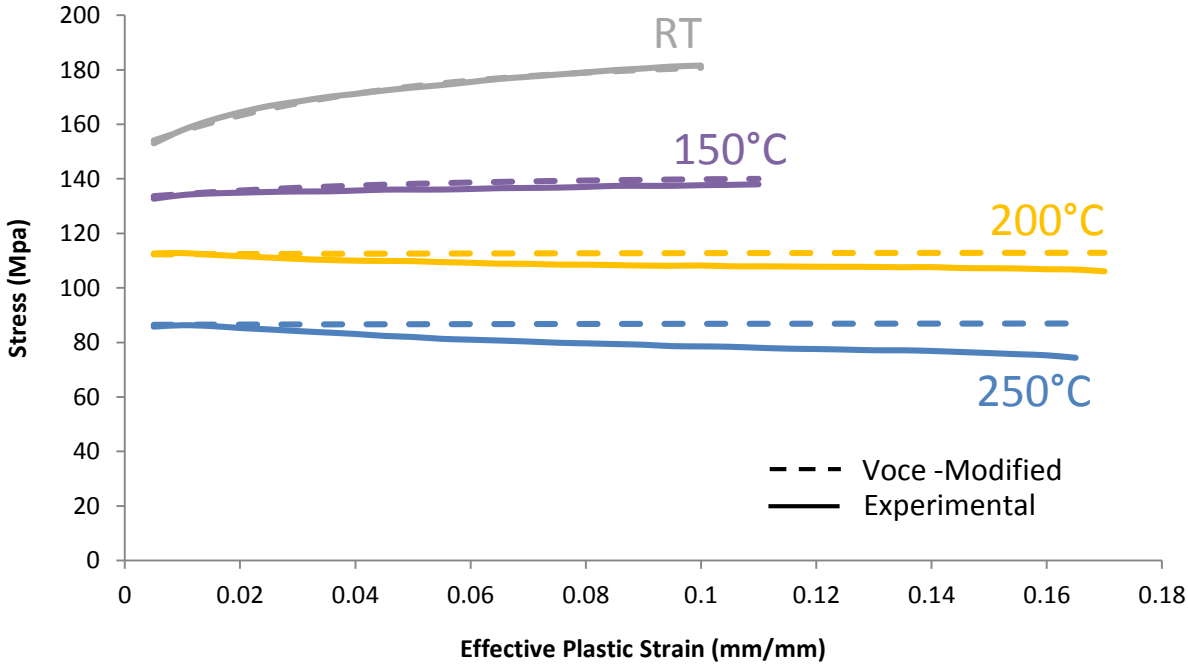


**Figure 48: Predicted flow curve response vs experimental data for H22-Temper at room temperature, 150, 200, and 250°C, and at a strain rate of 0.002/s.**

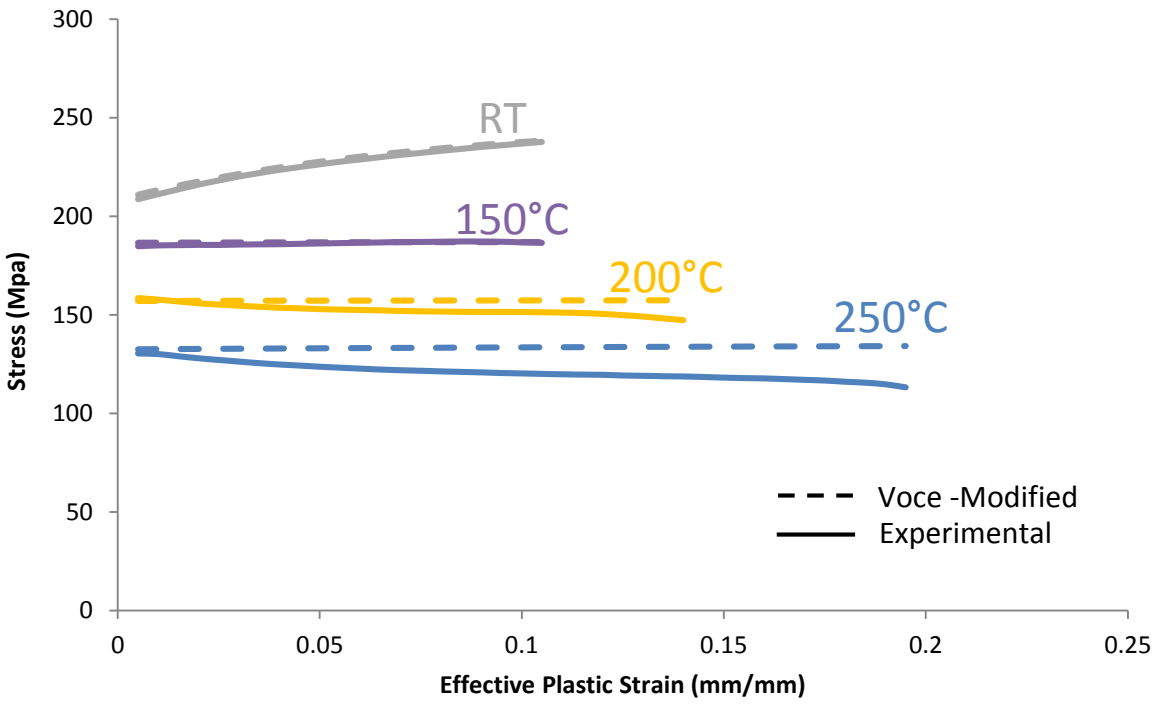


**Figure 49: Predicted flow curve response vs experimental data for H24-Temper at room temperature, 150, 200, and 250°C, and at a strain rate of 0.02/s.**

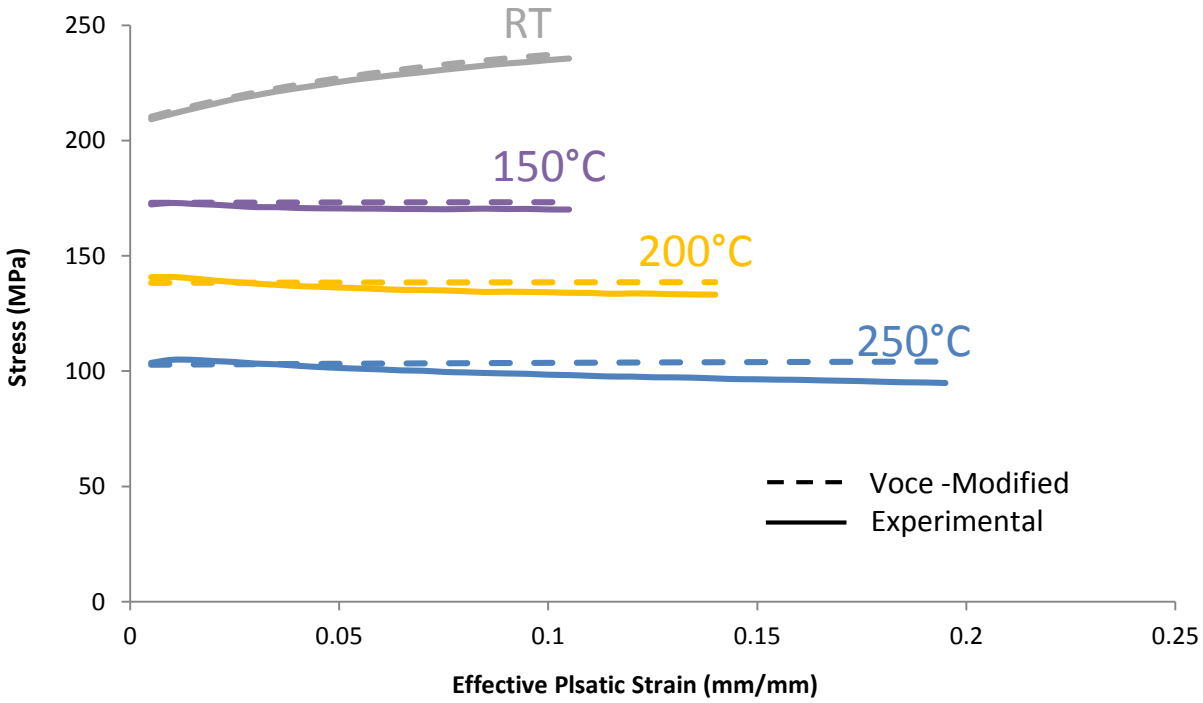


**Figure 50: Predicted flow curve response vs experimental data for H24-Temper at room temperature, 150, 200, and 250°C, and at a strain rate of 0.002/s.**

There was moderate agreement with the stress-strain response predicted by the Modified-Voce model and the experimental data. The variation between the model and experimental stress-strain was higher for strain-hardened tempers at temperatures greater than 200°C, since the Modified-Voce model does not admit the negative hardening behaviour observed in the experimental data. The maximum variation was 18% between the stress values at maximum strain, for the H24-temper at 250°C. The stress-strain response predicted by the Modified-Voce constitutive model was used in the forming simulations discussed in the subsequent sections. The strain rate in the model results exceeded the highest (0.02/s) strain rate used in characterization study. Therefore, the material model reverted to the higher strain-rate data to predict material behaviour. The springback was simulated assuming an elastic material response after forming.

## 4.2 Modelling of Forming and Springback

This section presents details for implementation of the Modified-Voce constitutive model to simulate forming aluminum brazing sheets. The forming and springback simulations are divided into two separate models, where the output of the forming simulation serves as an input to the springback simulation. The output of the forming simulation is a 'dynain' file which contains the formed U-shape geometry and the associated stress state of the elements at the end of the simulation.

### 4.2.1 Forming Model Set-up

The forming model consists of four components, the die, punch, binder and the blank. The model geometry is illustrated in Figure 51. The geometry was extracted from the 3D CAD model of the tooling components used in the refined springback study. The forming simulations were conducted using the explicit dynamic method.

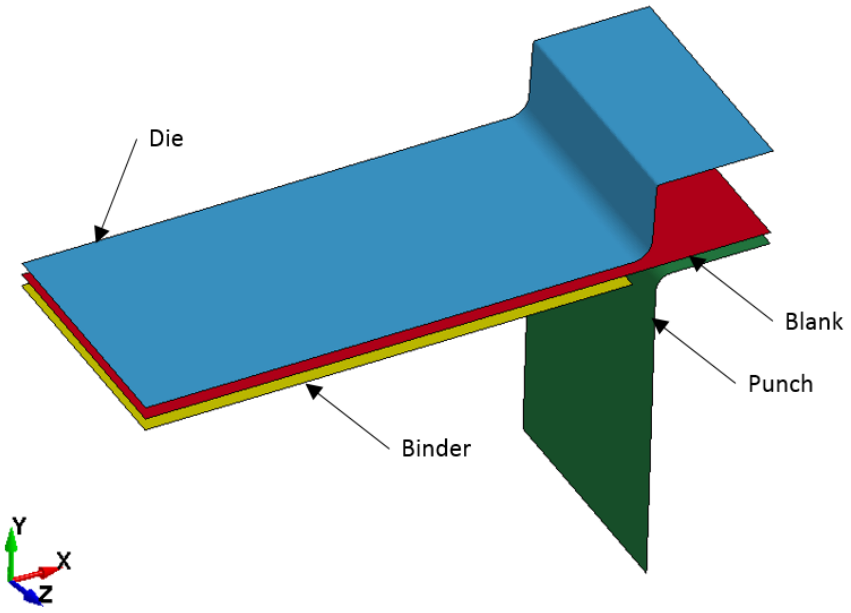


**Figure 51: U-shape forming model geometry configuration.**

The mesh was created in Hypermesh. Four-node quad shell elements were used for all components. The Belytschko-Tsay element formulation was used for the shell elements [42]. Li et al (2002) reported that accurate springback analysis requires up to 51 through-thickness integration points but 15-25 points are sufficient [29]. However, the number also depends on the material model, forming process, friction coefficient, loading and geometry. The number of through-thickness integration points adopted for the blank was twenty-one. A Gauss integration scheme was used for all deformable shell elements. The tooling was treated as rigid. The mesh configuration of the forming model is shown in Figure 52.

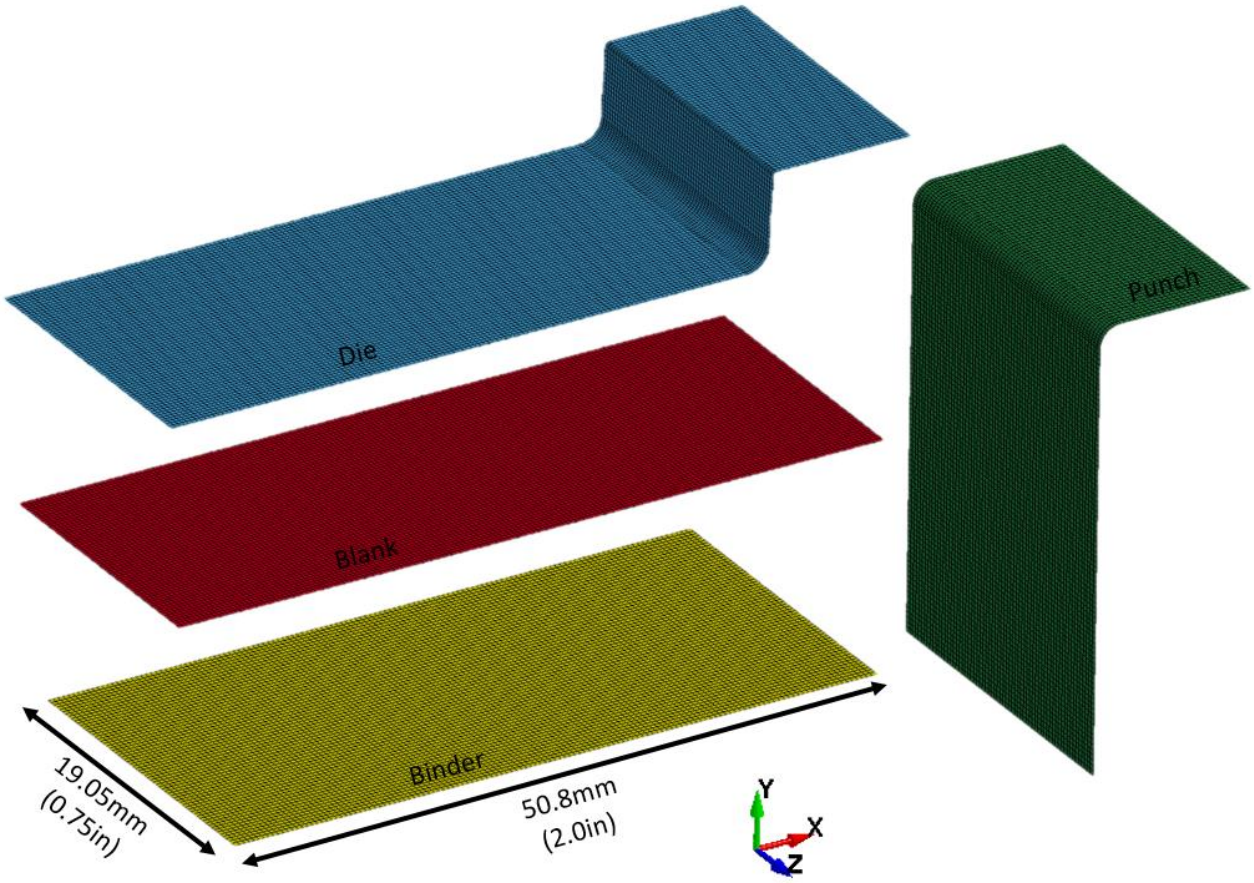


**Figure 52: U-shape model mesh configuration.**

The element size was 0.30 X 0.30mm for the blank and much of the tooling surfaces. The element size for the tooling near the radii was reduced to 0.30 X 0.16mm to fully capture the curvature.

Surface to surface contact was specified between the interacting surfaces. The contact algorithm utilizes a penalty method which prevents nodes of the blank (slave) from penetrating the tooling (master) surface segments. This contact algorithm is called the “penalty method” [42].

Previous studies done at University of Waterloo reported a friction coefficient of 0.043 for surfaces lubricated with Teflon sheets [23]. This model uses the same friction coefficient and assumes that the coefficient remains constant at elevated temperature. Future work is planned to characterize change in friction coefficient at higher temperature for various warm forming lubricants.

The binder and punch velocity was time-scaled to decrease run-time of the simulations. The punch and binder motion with respect to the simulation time is illustrated in Figure 53.

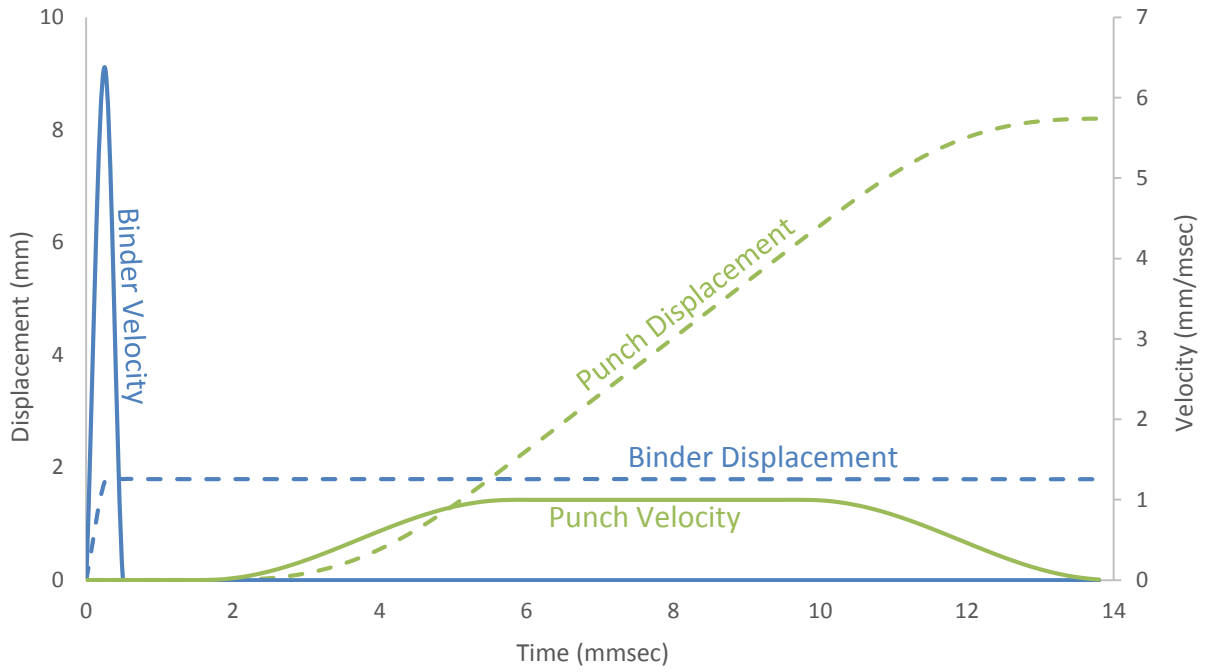


**Figure 53: Binder and punch displacement curves for the U-channel forming model.**

Initially, the binder is activated to clamp the blank. A force of 42.8 N was applied to keep the binder in position during forming. Subsequently, the punch motion is activated to draw the blank in to the die cavity. The die was constrained in all degrees of freedom. Symmetry boundary conditions were applied to the edge nodes at the central plane of the blank. These boundary conditions are shown in Figure 54. The edge nodes at the YX-plane were constrained in translation motion in the Z-direction and rotational motion around the X- and Y-axes. The edge nodes at the YZ-plane were contained in the X-direction and rotational motion around the Y- and Z-axes.

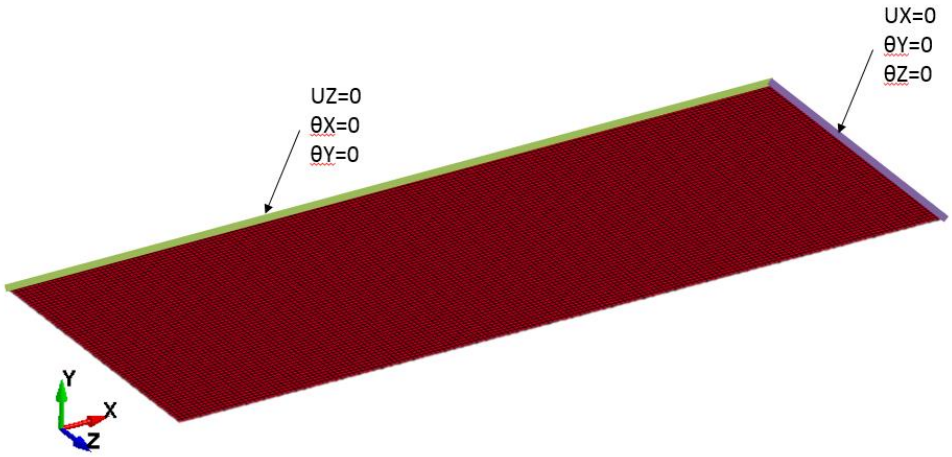


**Figure 54: Symmetry boundary conditions specified for the blank.**

The tooling components, which do not undergo permanent deformation were characterized as rigid. As mentioned before, the material behaviour for the blank was characterized by the stress-strain response predicted by the Modified-Voce model. The Piecewise Linear Plasticity material model (*MAT_024) was selected to model material response. Each temperature condition had its own unique material definition for all three material tempers. The material properties used for each temper at each test condition are tabulated in Table 9, Table 10, and Table 11. The yield stress values were calculated from the measured data from the material characterization study.

**Table 9: Material property values used in the O-temper material cards.**

| | Density ($g/mm^3$) | Poisson's Ratio | Yield Strength (MPa) | Elastic Modulus (MPa) |
|---|---|---|---|---|
| Room Temperature | 2.74E-3 | 0.33 | 67 | 35700 |
| 150°C | | | 63 | 25000 |
| 200°C | | | 60 | 22500 |
| 250°C | | | 57 | 14000 |

**Table 10: Material property values used in the H22-temper material cards.**

| | Density ($g/mm^3$) | Poisson's Ratio | Yield Strength (MPa) | Elastic Modulus (MPa) |
|---|---|---|---|---|
| Room Temperature | 2.74E-3 | 0.33 | 150 | 70500 |
| 150°C | | | 135 | 57700 |
| 200°C | | | 116 | 35000 |
| 250°C | | | 85 | 33500 |

**Table 11: Material property values used in the H24-temper material cards.**

| | Density ($g/mm^3$) | Poisson's Ratio | Yield Strength (MPa) | Elastic Modulus (MPa) |
|---|---|---|---|---|
| Room Temperature | 2.74E-3 | 0.33 | 210 | 78000 |
| 150°C | | | 175 | 56500 |
| 200°C | | | 145 | 48900 |
| 250°C | | | 101 | 42500 |

### 4.2.2 Springback Model Set-up

The springback simulations were performed using the static implicit time integration scheme in LS-Dyna to enforce static equilibrium and avoid dynamic oscillations commonly present in explicit dynamic time integration. Model information is passed between the forming model and the springback analysis via a "dynain" file generated at the end of forming simulations. This file contains deformed geometry (mesh) and predicted stress for each integration point within the blank that is used to initialize the springback analysis. For the springback analysis, the tooling mesh and contact boundary conditions were removed, mimicking removal of the part from the tooling after forming. The original symmetry boundary condition were still imposed on the blank. Boundary condition was added that constrained rigid body translation of the blank in all six global degrees of freedom. Figure 55 shows the boundary conditions added to the blank. The elastic material (*MAT_001) model was used to simulate the behaviour of the blank material using material properties mentioned in the previous section.

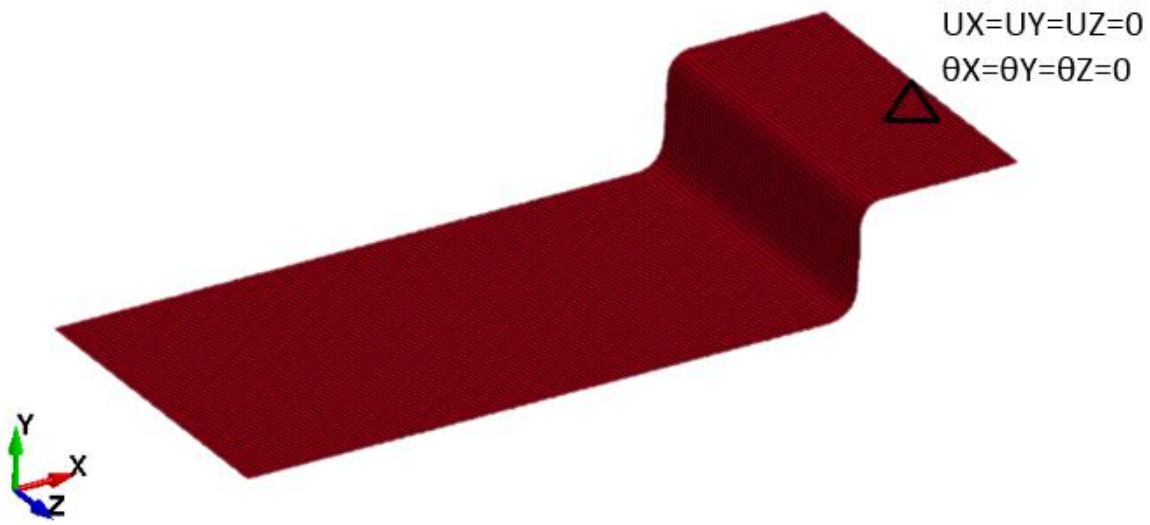


**Figure 55: Boundary conditions for the springback simulation.**

### 4.2.3 Forming Model Results

Due to the number of simulations performed, only a representative set of results from the forming and springback models are shown. The springback simulation results are shown in Section 4.2.4.

Figure 57 through Figure 62 show contour plots of major and minor in-plane stress in the formed U-channel part for the O-, H22-, and H24-tempers at room temperature and 250°C. The “outer” and “inner” shell surface refer to the outermost through-thickness integration points, as labelled in Figure 56. At “Bend 1” the stress on the outer surface are compressive while on the inner surface the stress is tensile. The opposite applied for “Bend 2”.

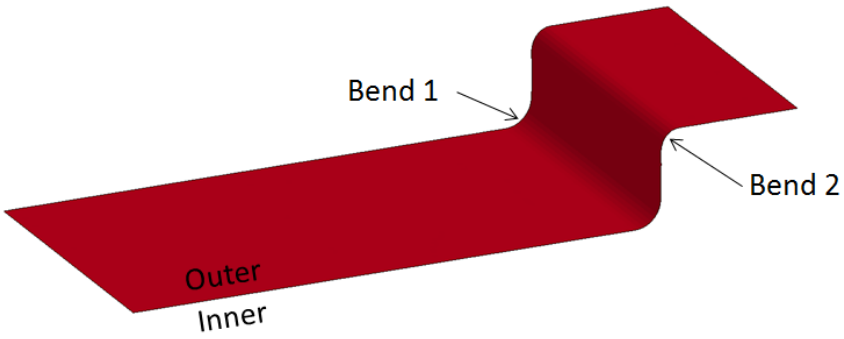


**Figure 56: Orientation of outer and inner shell surfaces of the blank indicating position of surface integration points.**

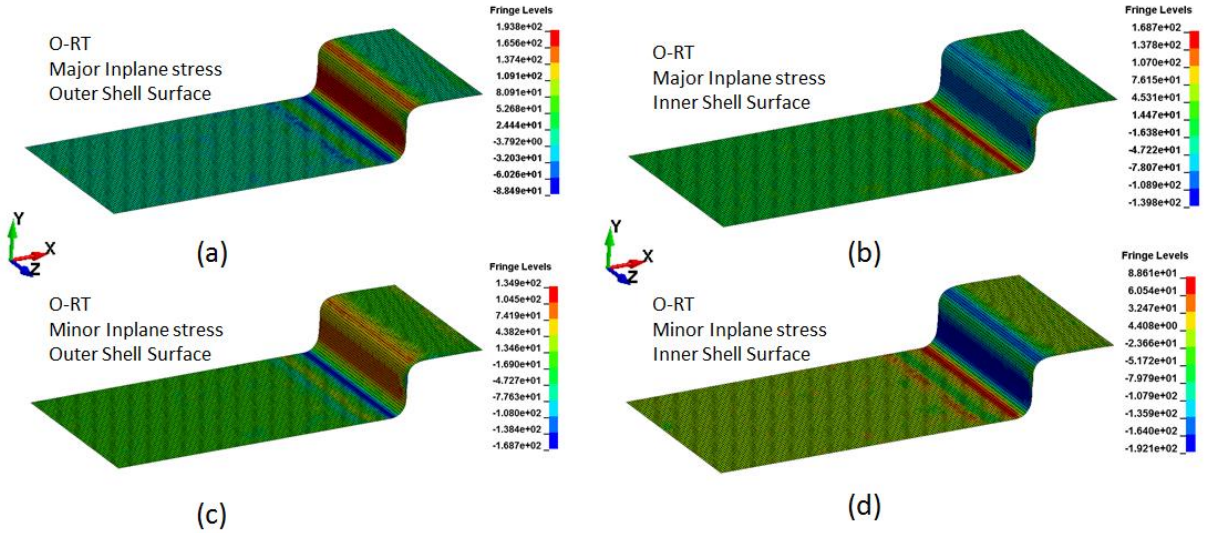


**Figure 57: Contour plots of O-temper U-channel formed at room temperature (stress in MPa). (a) Major in-plane stress at the outer shell surface. (b) Major in-plane stress at the inner shell surface. (c) Minor in-plane stress at the outer shell surface. (d) Minor in-plane stress at the inner shell surface.**

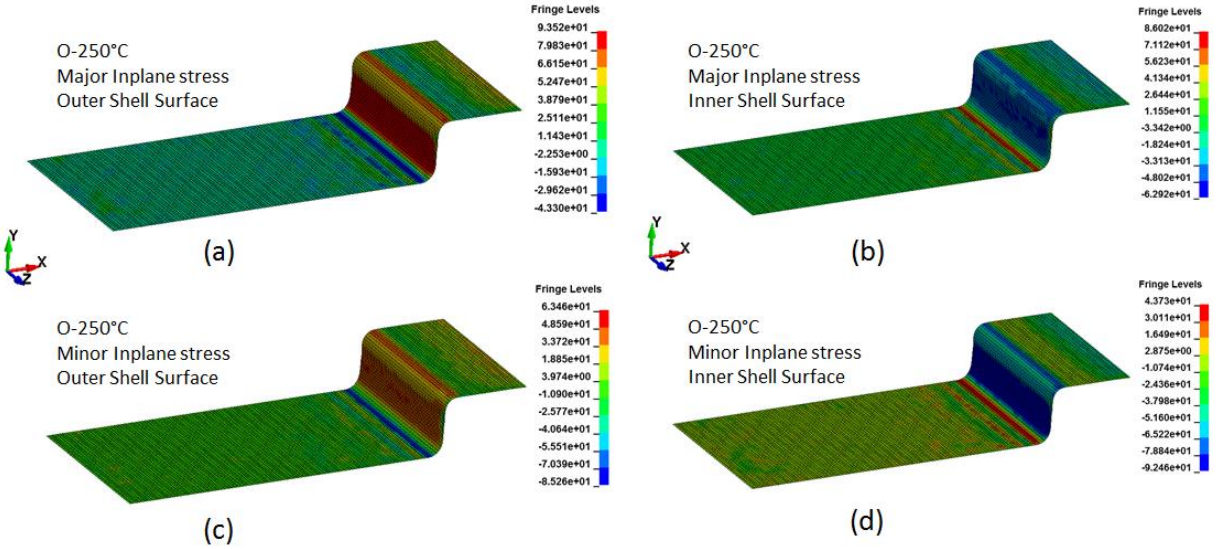


**Figure 58: Contour plots of O-temper U-channel formed at 250°C (stress in MPa). (a) Major in-plane stress at the outer shell surface. (b) Major in-plane stress at the inner shell surface. (c) Minor in-plane stress at the outer shell surface. (d) Minor in-plane stress at the inner shell surface.**

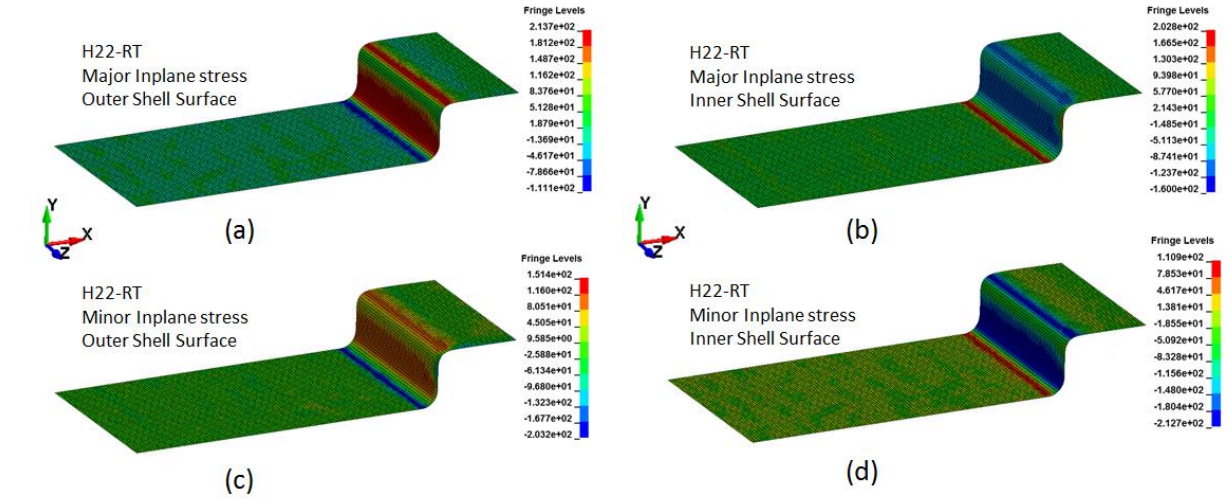


**Figure 59: Contour plots of H22-temper U-channel formed at room temperature (stress in MPa). (a) Major in-plane stress at the outer shell surface. (b) Major in-plane stress at the inner shell surface. (c) Minor in-plane stress at the outer shell surface. (d) Minor in-plane stress at the inner shell surface.**

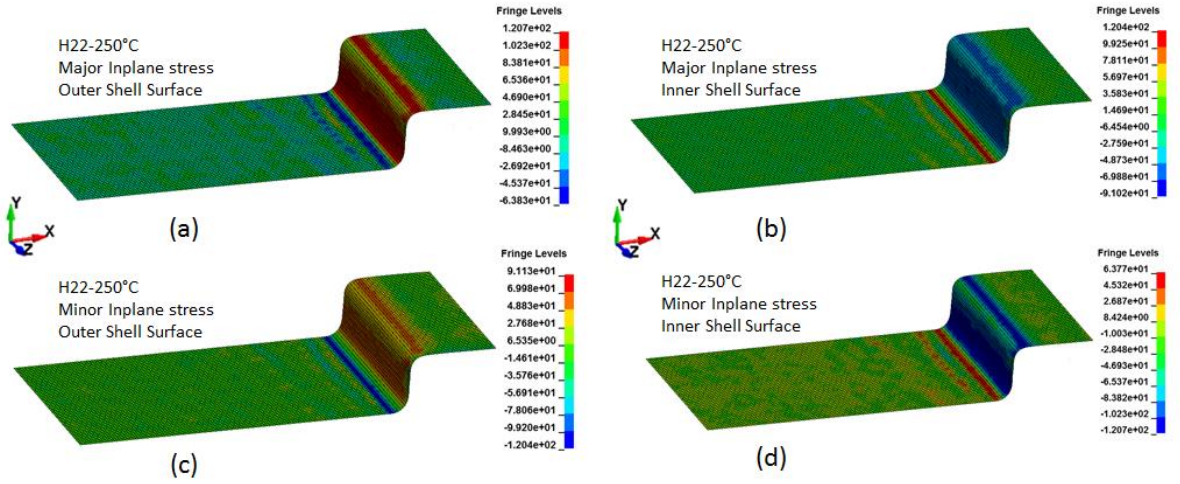


**Figure 60: Contour plots of H22-temper U-channel formed at 250°C (stress in MPa). (a) Major in-plane stress at the outer shell surface. (b) Major in-plane stress at the inner shell surface. (c) Minor in-plane stress at the outer shell surface. (d) Minor in-plane stress at the inner shell surface.**

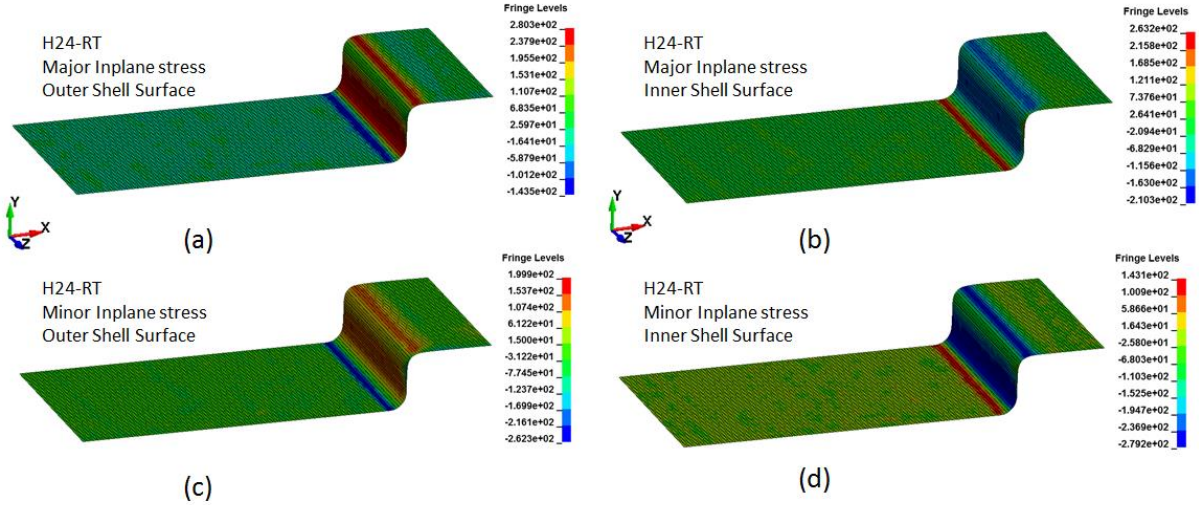


**Figure 61: Contour plots of H24-temper U-channel formed at room temperature (stress in MPa). (a) Major in-plane stress at the outer shell surface. (b) Major in-plane stress at the inner shell surface. (c) Minor in-plane stress at the outer shell surface. (d) Minor in-plane stress at the inner shell surface.**

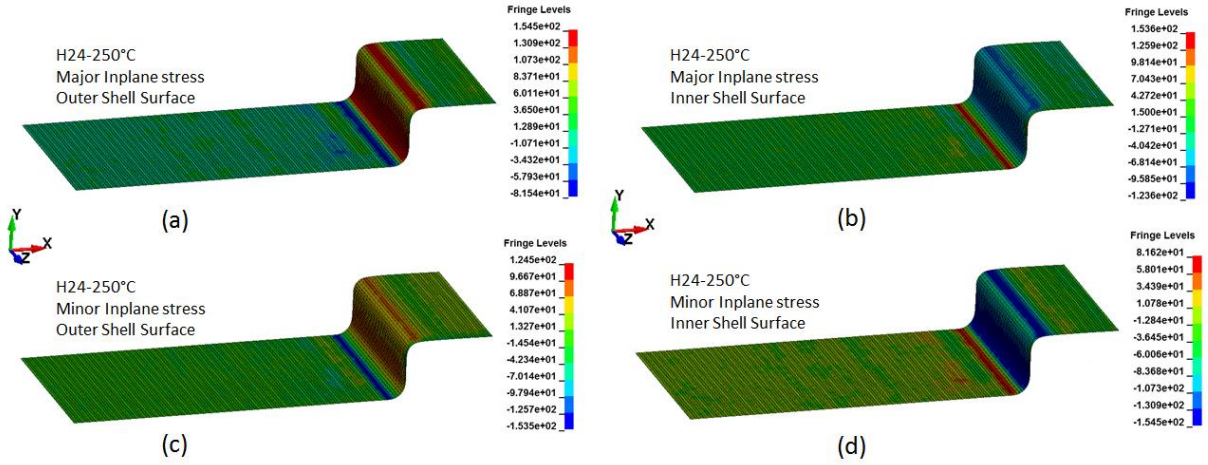


**Figure 62: Contour plots of H24-temper U-channel formed at 250°C (stress in MPa). (a) Major in-plane stress at the outer shell surface. (b) Major in-plane stress at the inner shell surface. (c) Minor in-plane stress at the outer shell surface. (d) Minor in-plane stress at the inner shell surface.**

It can be seen in the contour plots that stress values in the formed samples for all three tempers is lower at 250°C, relative to the samples formed at room temperature. The effect of elevated temperature on forming stresses in the blank is further illustrated Figure 63. The plot contains maximum value for major in-plane stress on the inner surface for all three tempers at room temperature and 250°C. This value corresponds to the major in-plane stress in the Bend 1 region.

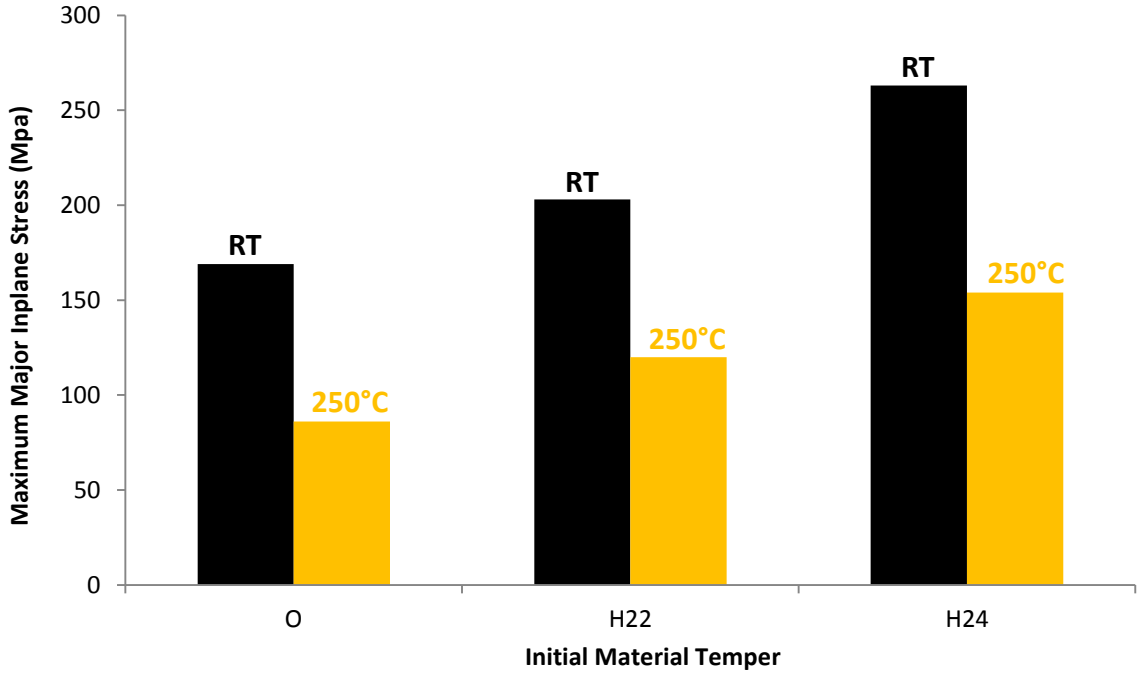


**Figure 63: Maximum major in-plane stress values at room temperature and 250°C for all three temper conditions.**

The stress values were 49.1, 40.9, and 41.4% lower at 250°C compared to room temperature for the O-, H22-, and H24-tempers, respectively. Furthermore, the stress profiles were also analyzed along the flange and the bend region. The profiles are plotted in Figure 64 through Figure 66 for U-channel parts formed at room temperature and 250°C for O-, H22-, and H24-tempers. The profiles shown below are from a single path starting from flange edge to the center plane of the U-channel.

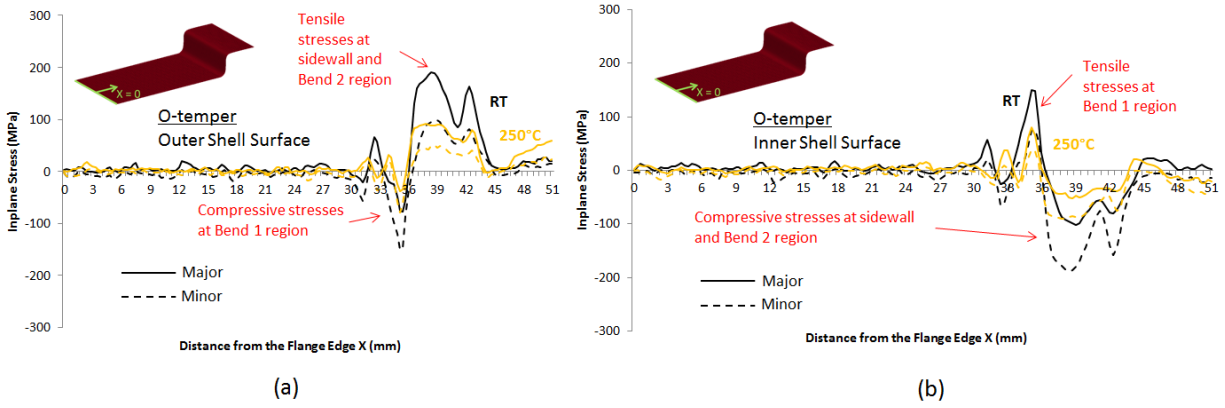


**Figure 64: Major and minor in-plane stress profiles for U-channels formed with O-temper at room temperature and 250°C. (a) Outer shell surface. (b) Inner shell surface.**

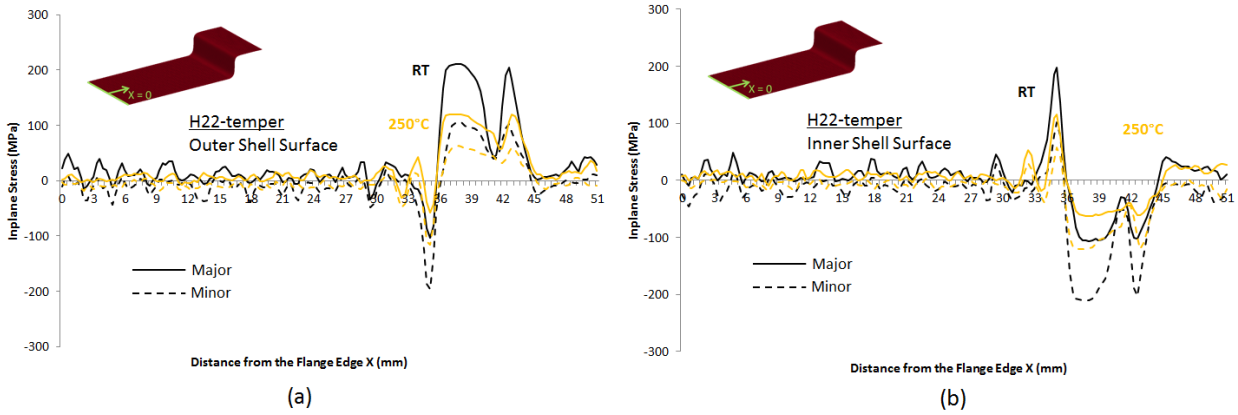


**Figure 65: Major and minor in-plane stress profiles for U-channels formed with H22-temper at room temperature and 250°C. (a) Outer shell surface. (b) Inner shell surface.**

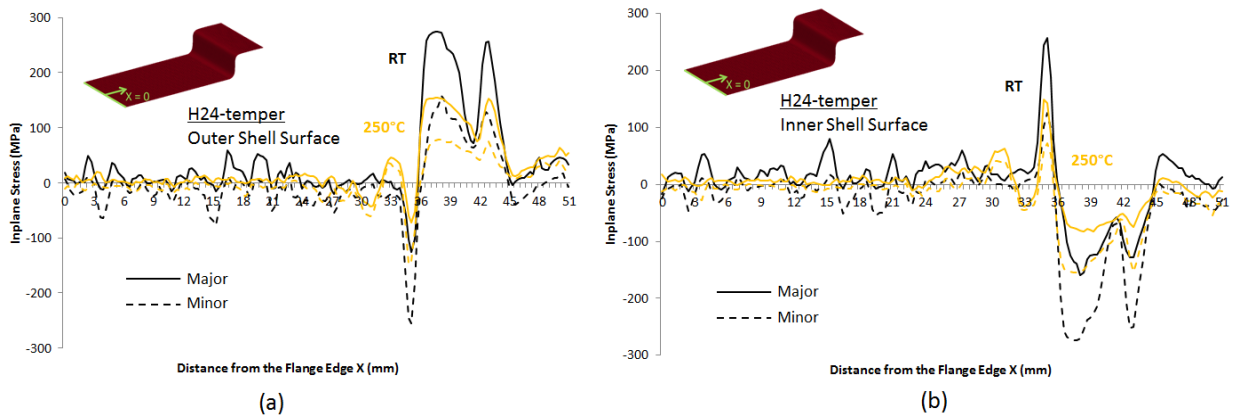


**Figure 66: Major and minor in-plane stress profiles for U-channels formed with H24-temper at room temperature and 250°C. (a) Outer shell surface. (b) Inner shell surface.**

The stress profiles show the transition between the tensile and compressive stresses on each surface at Bend 1, sidewall and Bend 2 regions. Also, the forming stresses are higher in the strain hardened tempers compared to the fully annealed condition for room temperature and warm forming temperature. However, the peak stress values are lower for 250°C compared to room temperature forming for all three temper conditions.

### 4.2.4 Springback Model Results

To compare springback behaviour as a function of forming conditions, the positional coordinates of nodes at the edge were extracted from the output and plotted. The predicted springback behaviour of each temper at room temperature and at 250°C are compared in Figure 67 and Figure 68, respectively. The label "REF" is the tooling profile or the ideal U-shape part that exhibit zero springback.

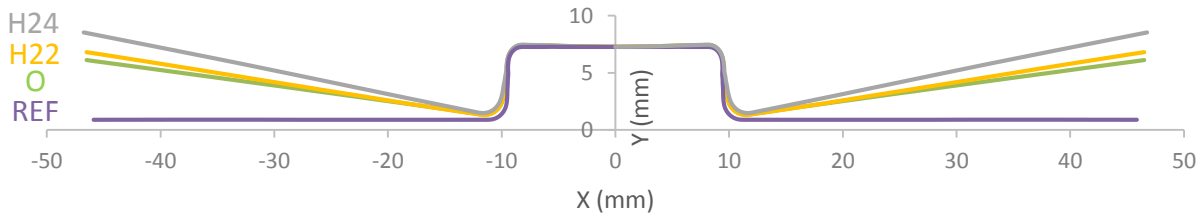


**Figure 67: Plot of predicted springback profiles for O-, H22- and H24-temper formed at room temperature.**

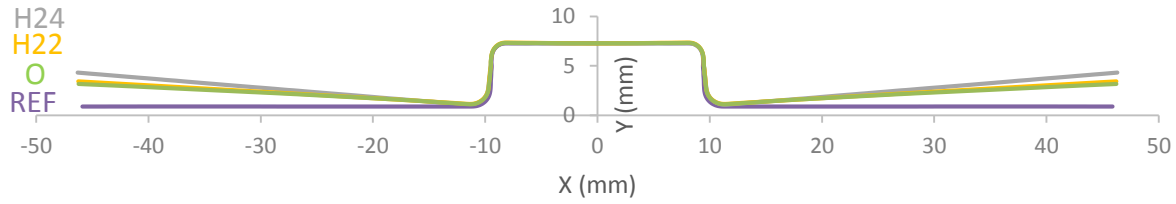


**Figure 68: Plot of predicted springback profiles for O-, H22- and H24-temper formed at 250°C.**

The predicted trend in springback behaviour of the O-, H22- and H24-tempers was similar to the experimental results. The predicted springback of the H24-temper was the highest, followed by the H22- and O-temper. The change in springback of behaviour with respect to increasing temperature as predicted by the model is shown in Figure 69 through Figure 71, for all three tempers.

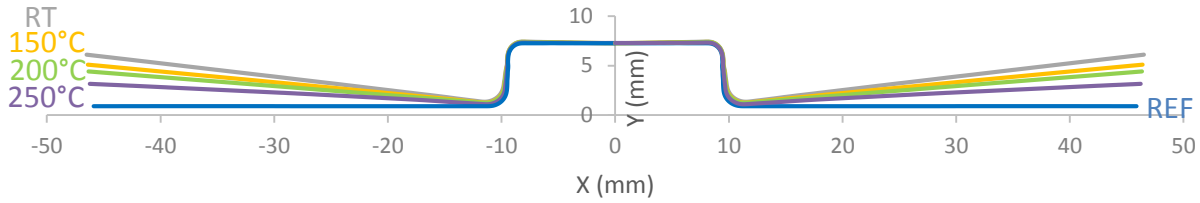


**Figure 69: Predicted springback profiles for O-temper samples formed at room temperature, 150, 200 and 250°C.**

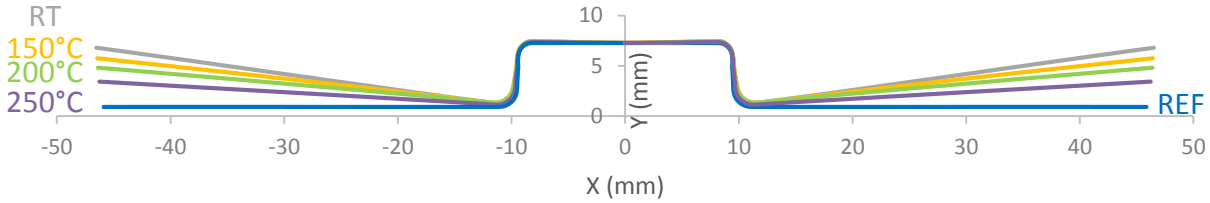


**Figure 70: Predicted springback profiles for H22-temper samples formed at room temperature, 150, 200 and 250°C.**

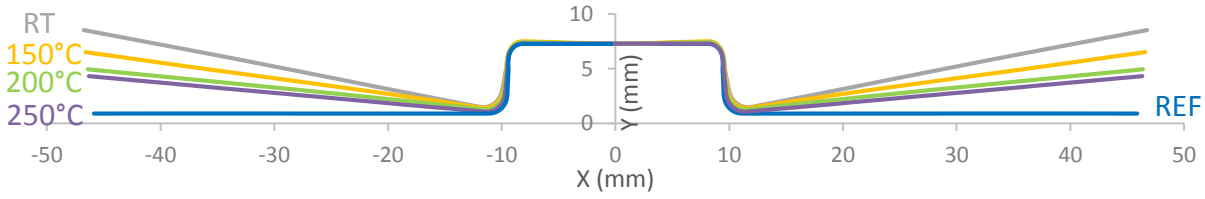


**Figure 71: Predicted springback profiles for H24-temper samples formed at room temperature, 150, 200 and 250°C.**

The relative trend in predicted springback profiles was similar to that of the experimental results for all three tempers. As the forming temperature increased, each temper exhibited lower springback. To compare predicted values with the experimental data, the predicted springback profiles were further analyzed to quantify reduction in geometric deviation due to springback with increased forming

temperature. The experiments only considered sidewall angle deviation but the other major geometric deviation is the change in flange angle. However, the improvement in flange angle deviation can be predicted using the model. The procedure for quantifying the sidewall angle and flange angle from the predicted springback profiles is illustrated in Figure 72.

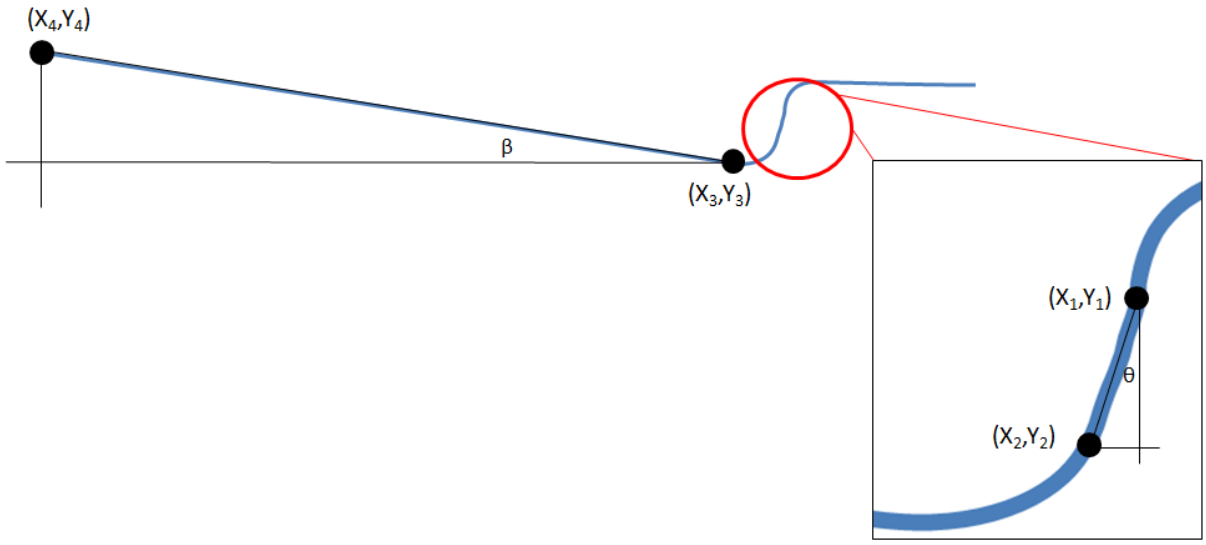


**Figure 72: Schematic of extracting sidewall angle (θ-2.5°) and flange angle (β) from the predicted springback profiles.**

Figure 72 shows the points of interest on the U-channel profile that were measured from which the side wall angle and the flange angle can be determined. The following formulae outline how the values were calculated.

Sidewall angle:

$$d_s = \sqrt{(x_2 - x_1)^2 + (y_2 - y_1)^2}$$

$$\Delta y_s = y_2 - y_1$$

$$\theta = \cos^{-1}\left(\frac{\Delta y_s}{d_s}\right)\frac{180^{\circ}}{\pi} - 2.5$$

$$Sidewall\ angle\ deviation = \theta - 2.5^{\circ}$$

Flange angle:

$$d_f = \sqrt{(x_4 - x_3)^2 + (y_4 - y_3)^2}$$

$$\Delta y_f = y_4 - y_3$$

$$Flange\ angle\ \beta = \sin^{-1}\left(\frac{\Delta y_f}{d_f}\right)\frac{180^{\circ}}{\pi}$$

This analysis was performed for all outputs. The predicted sidewall angle deviation is compared with the experimental results in Figure 73. Figure 74 shows the predicted trend in flange angle.

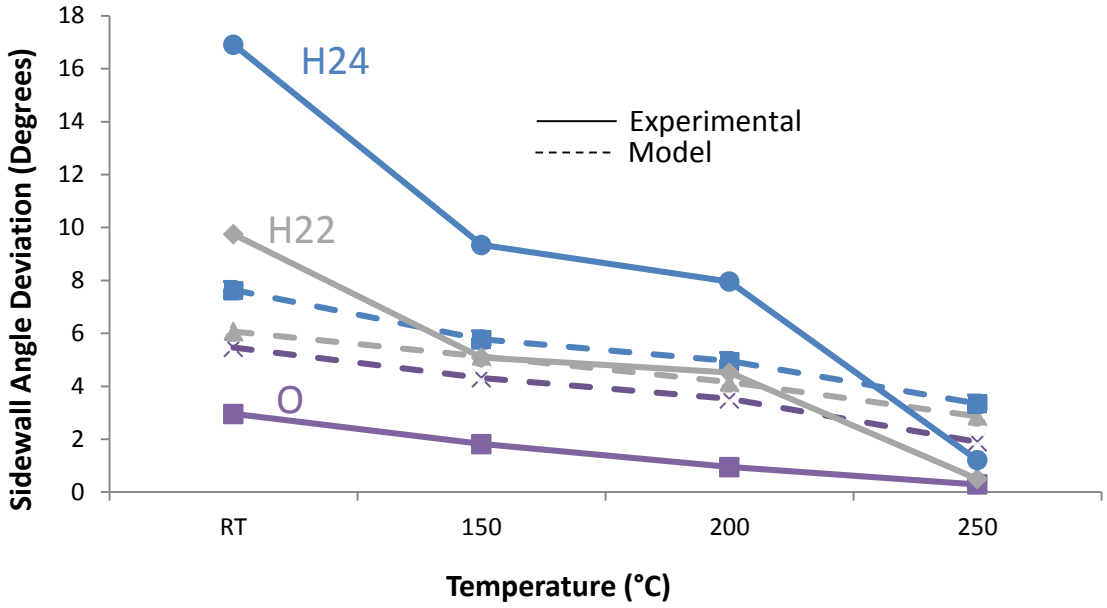


**Figure 73: Predicted sidewall angle deviation of O-, H22- and H24-temper for samples formed at room temperature, 150, 200 and 250°C.**

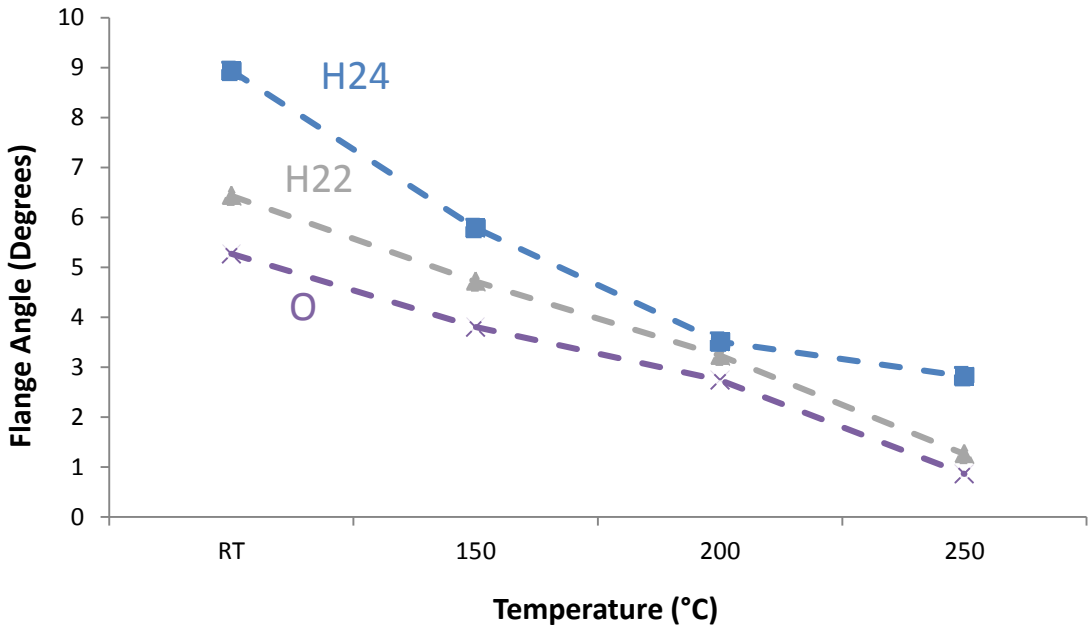


**Figure 74: Predicted flange angle of O-, H22- and H24-temper for samples formed at room temperature, 150, 200 and 250°C.**

The model predicts gradual improvement in springback behaviour with increasing forming temperature for all three material tempers. The sidewall angle deviation and flange angle decreased with increase in forming temperature. Also, the relative trend between the strain hardened tempers and the fully annealed condition was also as expected. The strain hardened tempers exhibited greater geometric deviation compared the fully annealed condition.

However, the magnitude of the sidewall angle deviation was significantly different from what was measured in the springback study. There could be a few reasons for this discrepancy, which are discussed further in the following section.

### 4.2.5 Discussion

The model qualitatively captures an improvement in springback behaviour of aluminum brazing sheets. The discrepancy between the experimental and predicted sidewall angle deviation values could be attributed to a number of numerical parameters and model inputs.

As mentioned before, in order to ascertain accurate springback behaviour, the model must consider all process steps that may affect residual stresses in the part. Although, this was an isothermal warm forming process, the current model neglects heat transfer to the surroundings in the forming model, which may not be representative of the actual temperature distribution in the components. Furthermore, the

constitutive fit of the modified-Voce model did not account for the reduction in strength seen in H-tempers with increasing plastic strain at higher temperature. Therefore the model does not show the same degree of improvement in springback with temperature increase as seen in the experimental data, particularly for the strain-hardened tempers. To investigate this discrepancy, the constitutive fit was scaled to reduce the strength of the H-temper alloys at high effective plastic strain values, thereby partially capturing the strain softening effect. A scaling factor of 0.95 was applied to the 250°C stress-strain curves for the H22- and H24-temper materials. Figure 75 and Figure 76 illustrate the difference in the scaled and as originally fit material responses for H24- and H22-tempers at 250°C. The corresponding predicted sidewall angle deviations using the scaled constitutive fit are shown in Figure 77.

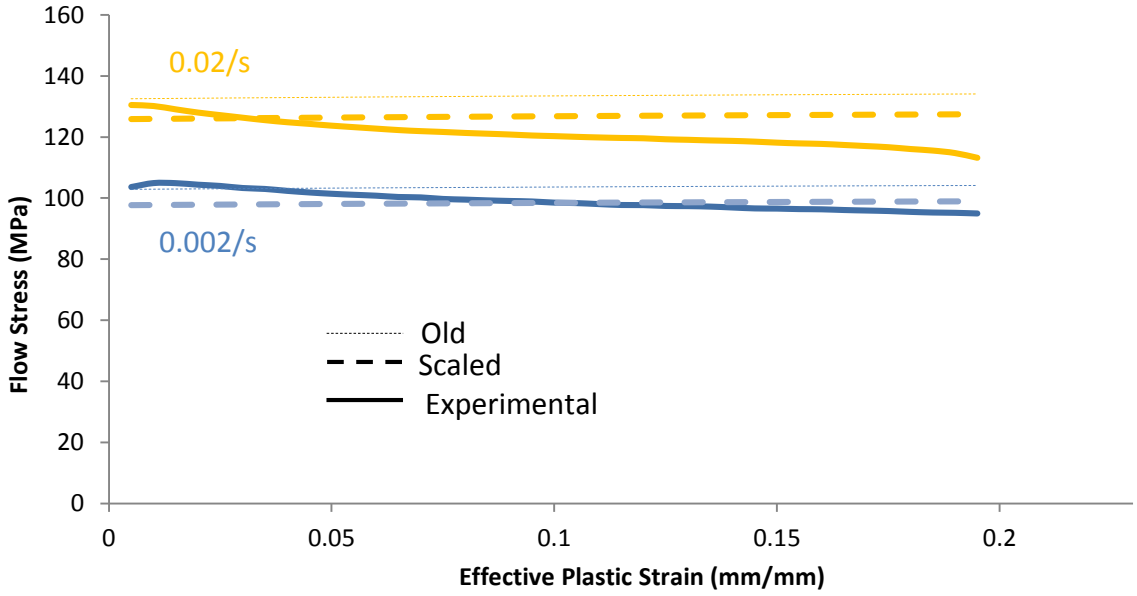


**Figure 75: Comparison of scaled constitutive fit with original and experimental values for H24-temper at 250°C.**

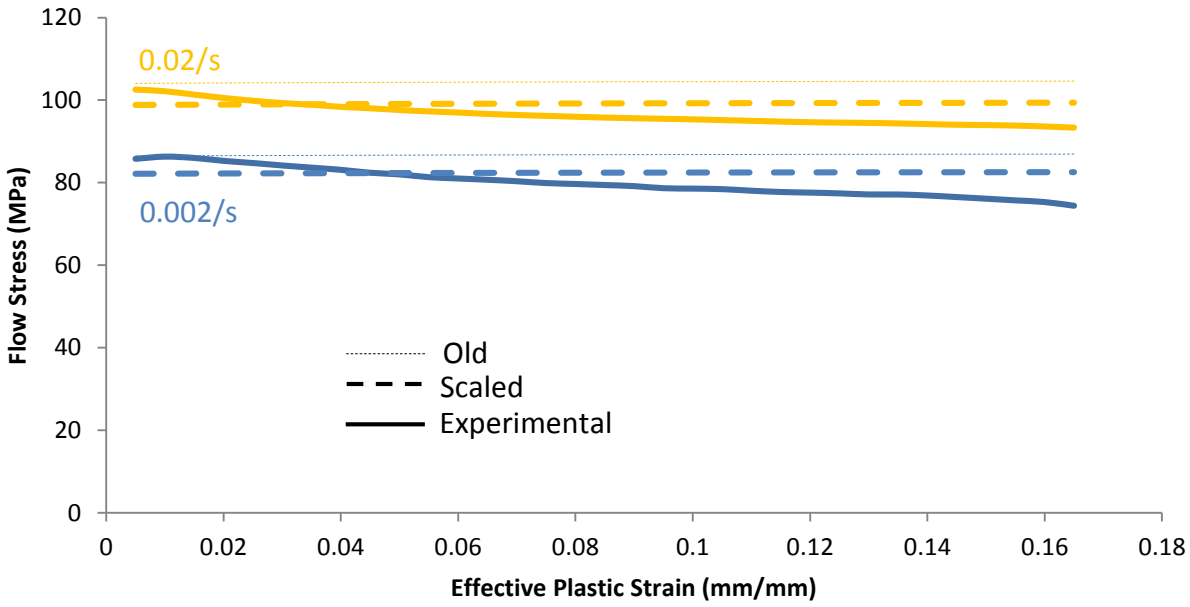


**Figure 76: Comparison of scaled constitutive fit with original and experimental values for H22-temper at 250°C.**

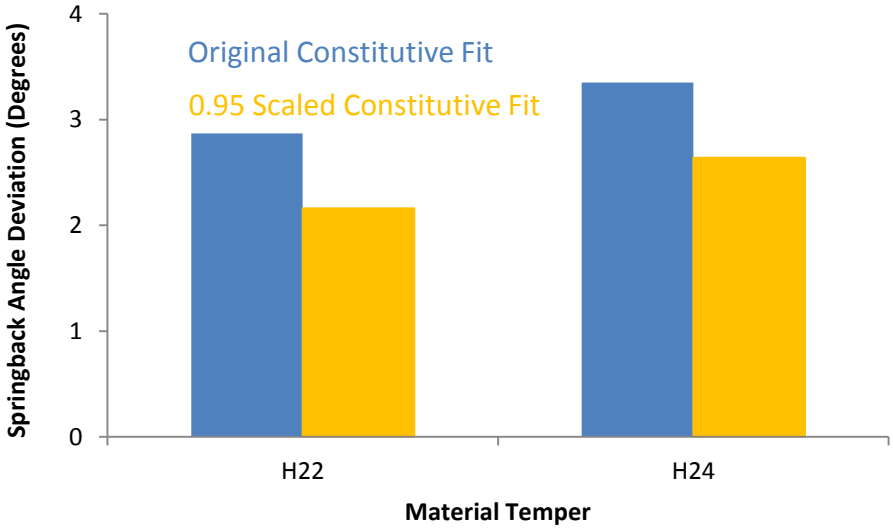


**Figure 77: Sensitivity of the predicted Sensitivity of predicted sidewall angle deviation to the constitutive fit.**

At 95% lower modelled strength, the predicted sidewall angle deviation also decreased measurably for H22 and H24 tempers at a forming temperature of 250°C. Although the magnitude of the angle is small to begin with, the sensitivity of the predicted springback to constitutive fit is apparent in the results. Therefore, an appropriate material model is needed that considers thermal softening and strain rate dependency at elevated temperatures.

To further consider the sensitivity of the springback predictions to physical and numerical parameters, the effect of adopted friction coefficient was examined [29] [43]. The friction coefficient used in the simulations reported above was taken from published data for .08 mm thick Teflon film. The samples in the springback experiments were prepared using spray Teflon, which may exhibit different friction characteristics that are unknown at this point. Also, the adopted number of through-thickness integration points can also have an impact on the springback prediction, for example.

The sensitivity of the model results to friction coefficient was evaluated. The plot shown in Figure 78 illustrates the difference in predicted sidewall angle deviation when the friction coefficient is increased from 0.043 to 0.15 for all three material temper conditions formed at room temperature.

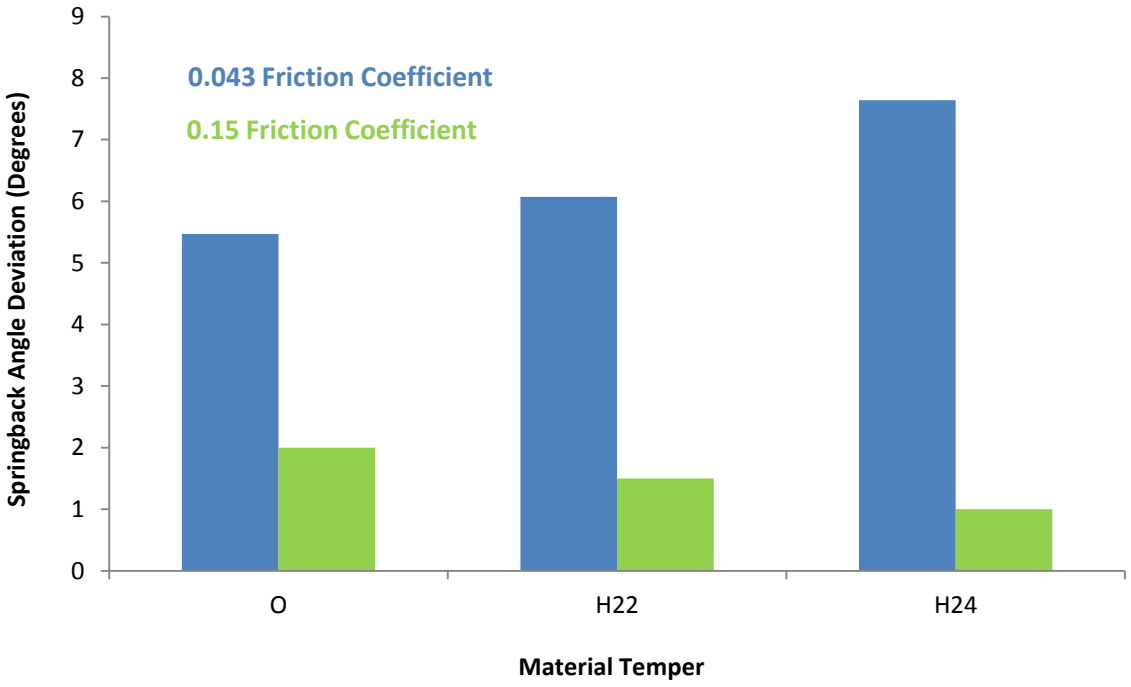


**Figure 78: Sensitivity of predicted sidewall angle deviation to the friction coefficient used in the forming model of O-, H22-, and H24-tempers at room temperature.**

The sidewall angle deviation was significantly lower for higher friction coefficient, demonstrating that the prediction of springback is highly sensitive to the adopted friction coefficient value. Higher friction increases the membrane component of stress during forming of the sheet, thereby reducing the operative moment and resulting springback [17]. To create a more accurate model, future work is suggested in the following section.

# 5.0 Discussion, Conclusion & Recommendations

## 5.1 Discussion

The tensile tests showed thermal softening and increased strain-rate sensitivity at elevated temperatures in the O-, H22-, and H24-tempers. The reduced flow stress at elevated temperature is not permanent, at least for forming up to 250°C, and the room temperature strength is recovered after warm forming.

The springback experiment results showed that springback reduced steadily for all three tempers as the forming temperature was increased from room temperature to 250°C. The effect of temperature on springback was relatively low for the O-temper condition, but significant for the H22- and H24-tempers. The results indicate that with warm forming, the room temperature springback in H24-temper parts can be reduced to a magnitude comparable to forming O-temper material at room temperature. This result can be observed in Figure 44. The principal advantages of warm forming are improved formability and lower springback which opens up opportunities for use of higher-strength tempers in current applications and the ability to form more complex geometries with the O-temper. The costs associated with increased tooling complexity to perform warm forming should be considered based on the application.

## 5.2 Conclusion

The following conclusions can be made based on the results of this research:

1. Forming temperature exerts a dramatic influence on springback for the tempers considered. The reduction in springback for all tempers was in the range 91-95% when forming at 250°C versus room temperature.

2. The H24-temper, the hardest of the three tempers, exhibited the highest springback, followed by the H22- and the O-tempers. At room temperature, the average sidewall angle deviation in H24-, H22- and O-temper was 17, 11, and 3°, respectively. While at 250°C, the average sidewall angle deviation was reduced down to 1.21, 0.50, and 0.29°, respectively.

3. Limited springback reduction was observed with increased temperature for the O-temper condition (91%); however, the room temperature springback was already low to start with.

4. Springback behaviour did not change significantly with respect to type of lubricant used during forming. However, both lubricants used (Fuchs and Teflon spray) offer low (similar) friction coefficients whereas a higher friction level will likely result in lower springback, as predicted by the numerical models.

5. Residual particles were clearly visible on samples after forming with the Fuchs lubricant. This residual layer may have a negative impact on brazeability performance. Similar issues may result from the Teflon spray.

6. Tensile experiments were performed to characterize material behaviour at elevated temperatures. The results showed a thermal softening at warm forming temperatures, allowing for improved formability and lower springback, as observed in the springback studies. The room temperature strength is recovered after warm forming.

7. Numerical models were created to simulate the warm forming and springback response of brazing sheet material. The Modified-Voce constitutive equation was used to model the material behaviour. The models predicted gradual decrease in springback with increasing temperature, in qualitative accord with the experiments; however, significant differences were observed between the predicted and measured springback.

8. The sensitivity of the predicted springback to selected parameters in the numerical model was investigated. The model is highly sensitive to the constitutive fit and friction coefficient.

## 5.3 Recommendations

Recommendations for future work are as follows:

1. Experiments should be performed considering actual battery cooler plate geometries to assess potential formability and springback improvements at warm forming temperatures.

2. For the numerical model, the material characterization study should be expanded to include additional strain rates, as well as use of advanced imaging systems to capture lateral strain for calculating plastic strain ratios (r-values).

3. A more complex material model which takes into account the observed negative hardening of the harder tempers at elevated temperatures should be considered to better predict material

4. A wider range of lubricants should be considered and the friction coefficient at elevated temperatures should be determined in order to verify the influence of lubricant selection (friction coefficient) on springback in the models.

5. The effect of the warm forming lubricants considered in this study on brazeability should be assessed.

# References


[1] A. Pesaran, S. Burch and M. Keyser, "An approach for designing thermal management systems for electric and hybrid vehicle battery packs," *Vehicle Thermal Management Systems Conference and Exhibition,* May 1999.

[2] J. Hirsch, "Aluminum in Innovative Light-Weight Car Design," *Materials Transactions,* vol. 52, no. 5, pp. 818-824, 1 May 2011.

[3] R. Cobden, "Aluminum: Physical properties, characteristics and alloys," European Aluminum Association, 1994.

[4] H. Hayashi and T. Nakagawa, "Recent trends in sheet metals and their formability in manufacturing automotive panels," *Journal of Materials Processing Technology,* vol. 46, pp. 455-487, 1994.

[5] C. Sonsino, "Light-weight design chances using high-strength steels," *Materials Science & Engineering Technology,* vol. 38, no. 1, pp. 9-22, 2007.

[6] A. Jarrett and Y. Kim, "Design Optimization of Electric Vehicle Battery Cooling Plates for Thermal Perfomance," *Journal of Power Sources,* vol. 196, no. 23, pp. 10359-10368, 11 June 2011.

[7] D. Weber, S. Spencer and P. Spacher, "Battery Cooling Plate Design with Discrete Channels". United States Patent 7,851,080, 14 12 2010.

[8] C. Sigli, H. Terryn, I. Graeve, H. Shercliff and M. Ryckeboer, "Brazing Processes," aluMATTER, [Online]. Available: http://aluminium.matter.org.uk.

[9] "Aluminum Brazing Sheets," UACJ, 2016. [Online]. Available: http://www.uacj.co.jp.

[10] S. Winkler, *Personal Communication,* Dana Corporation, 2015.

[11] S. Hecker, "Formability of Aluminum Alloy Sheets," *Journal of Engineering Materials and Technology,* vol. 97, no. 1, pp. 66-73, 1975.

[12] M. Kleiner, M. Geiger and A. Klaus, "Manufacturing of Lightweight Components by Metal Forming," *CIRP Annals - Manufacturing Technology,* vol. 52, no. 2, pp. 521-542, 2003.

[13] S. Benson, "Bending Basics: The hows and whys of springback and springforward," *The Fabricator,* 9 July 2014.

[14] M. Gotzinger, K. S, M. Cardew-Hall and P. Hodgson, "A Methodology for Springback Prediction," *Automotive & Transportation Technology Congress & Exhibition Proceedings,* 2001.

[15] S. Jan and J. Miroslav, "Springback prediction in sheet metal forming processes," *Journal of Technology of Plasticity,* vol. 37, no. 1, 2012.

[16] I. Burchitz, "Springback: improvement of its predictabliity," 2005.

[17] T. Altan and A. Tekkaya, Sheet Metal Forming: Processes and Applications, ASM International, 2012.

[18] P. Cain, "Warm Forming Aluminum Magnesium Products," The Fabricator, 1 August 2009. [Online].

[19] S. Toros, F. Ozturk and I. Kacar, "Review of warm forming of aluminum–magnesium alloys," *Journal of Materials Processing Technology,* vol. 207, pp. 1-12, 2008.

[20] S. Zhang, K. Zhang, Y. Xu, Z. Wang, Y. Xu and Z. Wang, "Deep-drawing of magnesium alloy sheets at warm temperatures," *Journal of Material Processing Technology,* vol. 185, no. 1-3, pp. 147-151, 2007.

[21] K. Takata, "Warm Forming of Aluminum Alloys," *Nippon Steel Technical Report,* vol. 103, May 2012.

[22] R. Schubert, "Warm Forming - Principles, Applications, Case Study," *SME,* 2003.

[23] R. Bagheriasl, "Formability of Aluminum Alloy Sheet at Elevated Temperatures," University of Waterloo, Waterloo, 2012.

[24] J. McKinley, "Warm Forming of Aluminum Brazing Sheets - Experiments and Numerical Simulations," Univerisity of Waterloo, Waterloo, 2010.

[25] F. Shehata, M. Painter and R. Pearce, "Warm Forming of Aluminum/Magnesium Alloy Sheet," *Journal of Mechanical Working Technology,* vol. 2, pp. 279-290, 1978.

[26] D. Li and A. Ghosh, "Biaxial warm forming behaviour of aluminum sheet alloys," *Journal of Material Process Technology,* vol. 145, pp. 281-293, 2004.

[27] H. Wang, Y. Luo, P. Friedman, M. Chen and L. Gao, "Warm Forming Behaviour of High Strength Aluminum Alloy AA7075," *Transactions of Nonferrous Metals Society of China,* vol. 22, pp. 1-7, 2012.

[28] S. Kurukuri, A. Van Den Boogard, A. Miroux and B. Holmedal, "Warm forming simuation of Al-Mg Sheet," *Journal of Materials Processing Technology,* vol. 209, no. 15-16, pp. 5636-5645, 2009.

[29] K. Li, W. Carden and W. R, "Simulation of Springback," *Internatinal Journal of Mechanical Sciences,* vol. 44, pp. 103-122, 2002.

[30] H. Livatyali and T. Alan, "Prediction and Elimination of Springback in Straight Flanging using computer aided design methods: Part 1 - Experimental Investigations," *Journal of Materials Processing Technology,* vol. 117, pp. 262-268, 2001.

[31] Y. Ling, H. Lee and B. Cheok, "Finite Element Analysis of Springback in L-bending of Sheet Metal," *Journal of Materials Processing Technology,* vol. 168, pp. 296-302, 2005.

[32] R. Greze, P. Manach, S. Laurent and L. Menezes, "Influence of the temperature on residual stresses and springback effect in an aluminum alloy," *International Journal of Mechanical Sciences,* vol. 52, pp. 1094-1100, 2010.

[33] Y. Moon, S. Kang, J. Cho and T. Kim, "Effect of tool temperature on the reduction of the springback of aluminum sheets," *Journal of Materials Processing Technology,* vol. 132, pp. 365-368, 2003.

[34] H. Kim, S. Choi, K. L. Lee and H. Kim, "Experimental determination of forming limit diagram and springback characteristics of AZ31B Mg alloy sheets at elevated temperatures," *Materials Transactions,* vol. 49, no. 5, pp. 1112-1119, 2008.

[35] D. Nguyen, Y. S, J. D, T. Banh and Y. Kim, "A study on material modeling to predict spring-back in v-bending of AZ31 magnesium alloy sheet at various temperatures," *Journal of Advanced Manufacturing Technology,* vol. 62, pp. 5551-562, 2012.

[36] M. Benoit, *Personal Communication,* University of Waterloo, 2015.

[37] H. Jin, *Personal Communication,* CANMET Materials, 2015.

[38] C. F, Elements of Metallurgy and Engineering Alloys, Ohio: ASM International Materials Park, 2008.

[39] E. Voce, "The relationship between stress and strain for homogenous deformation," *Journal of the Institute of Metals,* vol. 74, no. 11, pp. 537-562, 1948.

[40] T. Rahmaan, A. Bardelcik, J. Imbert, C. Butcher and M. Worswick, "Effect of strain rate on flow stress and anisotropy of DP600, TRIP780, AA5182-O sheet metal alloys," *International Journal of Impact Engineering,* vol. 88, pp. 72-90, 2016.

[41] L. Wilkinson, *MYSTAT 12,* San Jose, California: SYSTAT, 1982.

[42] "LS-DYNA Theory Manual," Livermore Software Technology Corporation (LSTC), Livermore, 2016.

[43] K. Li, L. Geng and R. Wagoner, "Simulation of Springback with the Draw/Bend Test," *IEEE,* vol. 0, pp. 91-104, 1999.

[44] M. Lee, S. Kim, R. Wagoner, K. Chung and H. Kim, "Constitutive Modelling for Anisotropic/Asymmeteric Hardening Behaviour of Magnesium Alloy Sheets," *International Journal of Plasticity,* vol. 25, pp. 70-104, 2009.

[45] W. Carden, L. Geng, D. Matlock and R. Wagoner, "Measurement of Springback," *International Journal of Mechanical Sciences,* vol. 44, pp. 79-101, 2002.

[46] R. Wagoner and M. Li, "Simulation of Springback: Through-thickness integration," *Internation Journal of Plasticity,* vol. 23, pp. 345-360, 2007.

# Appendix A – Tooling Detailed Drawings

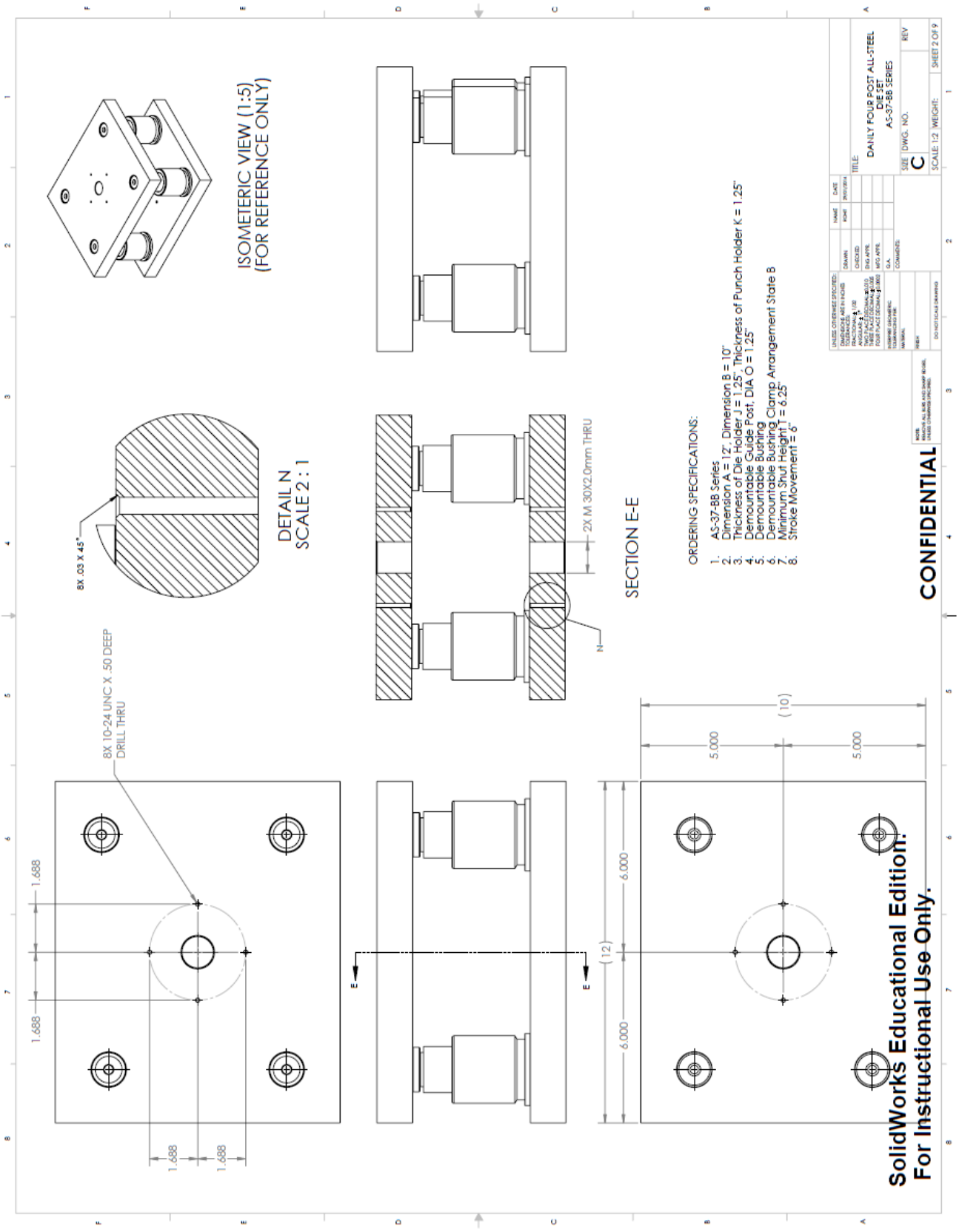


**Figure 79: Detailed drawings of the standard four-pillar die set used in the springback studies.**

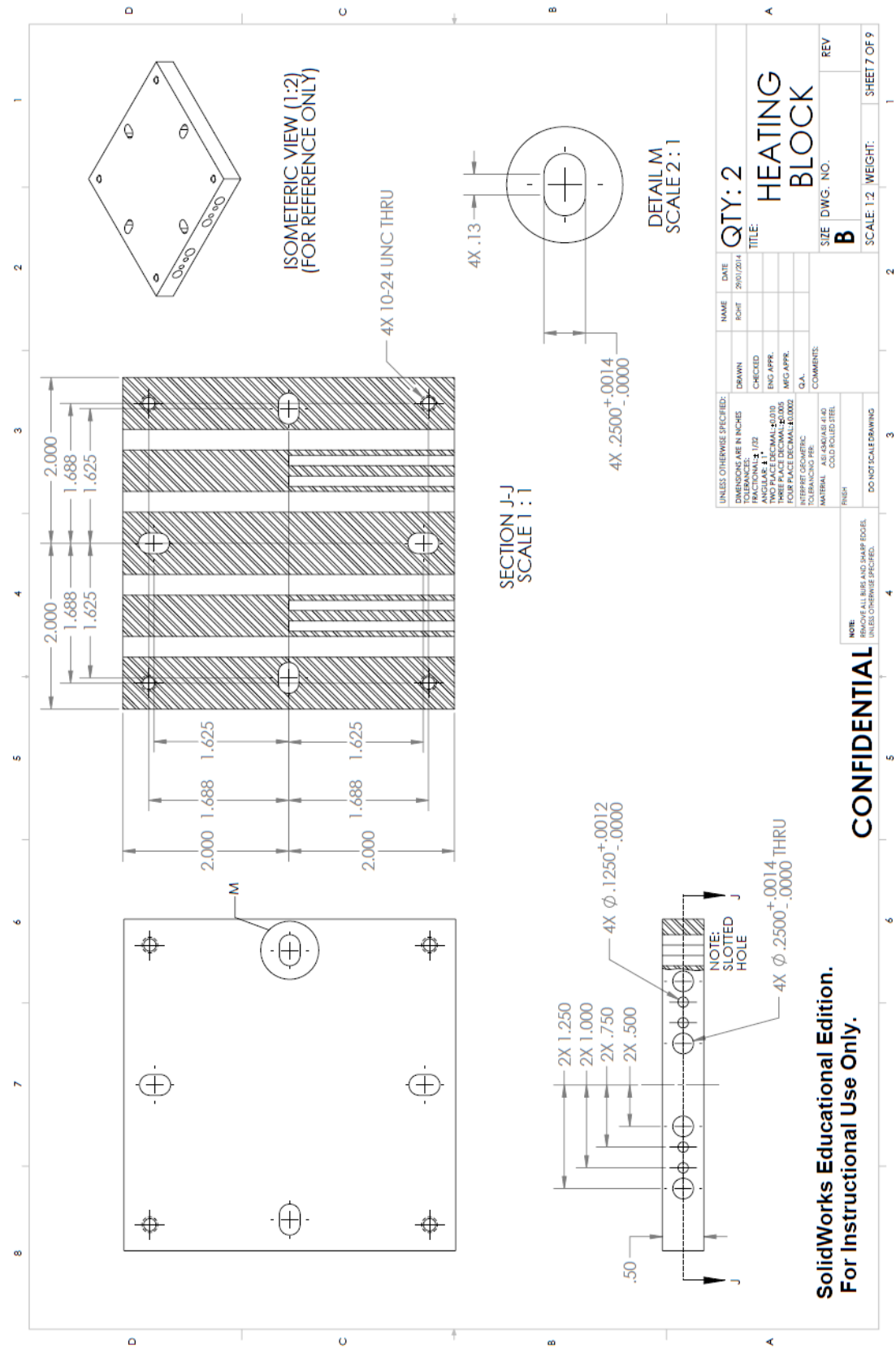


**Figure 80: Detailed drawing of the heating block used in the benchmark study.**

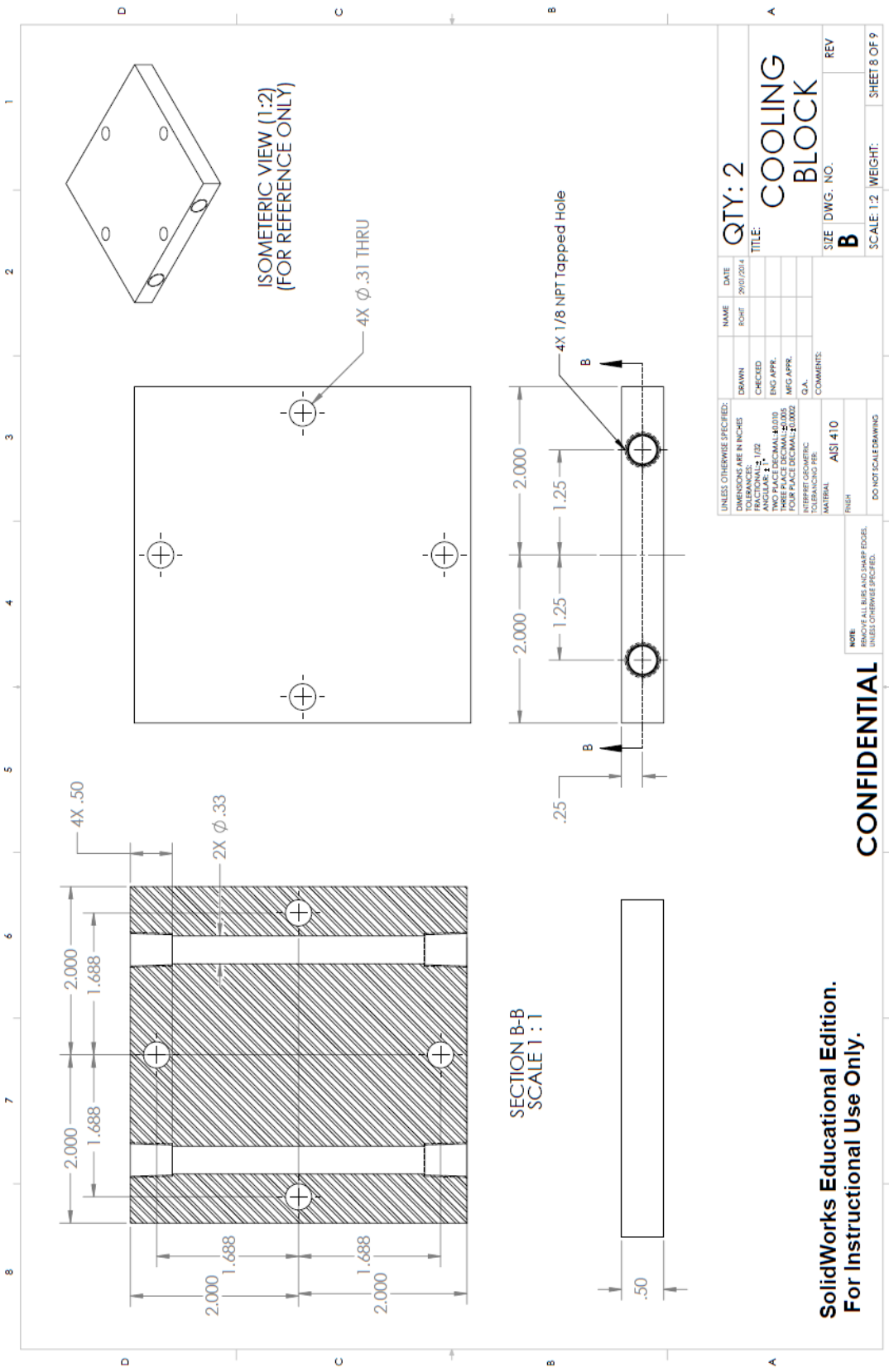


**Figure 81: Detailed drawing of the cooling block used in the benchmark study.**

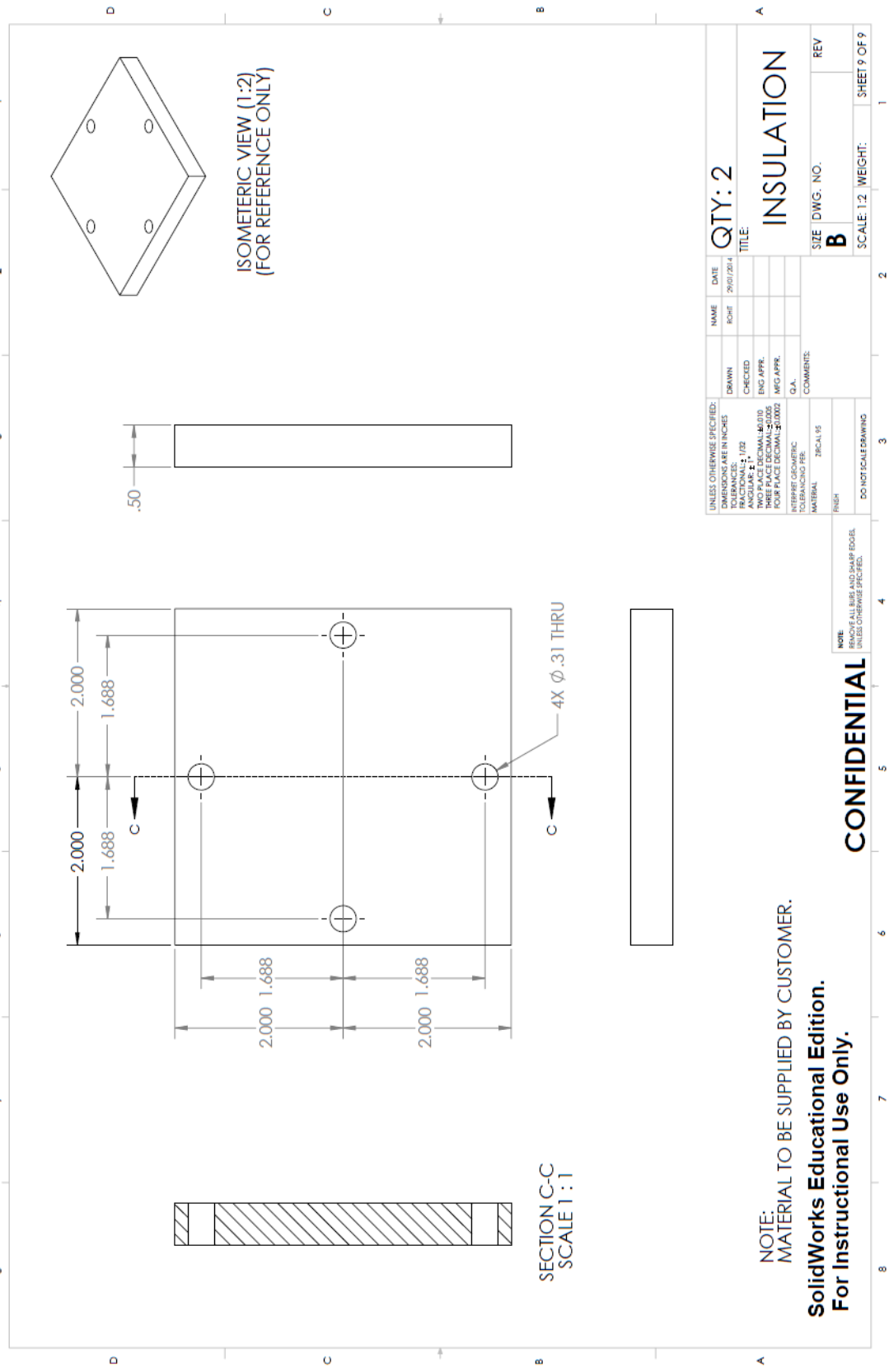


**Figure 82: Detailed drawing of the cooling block used in the benchmark study.**

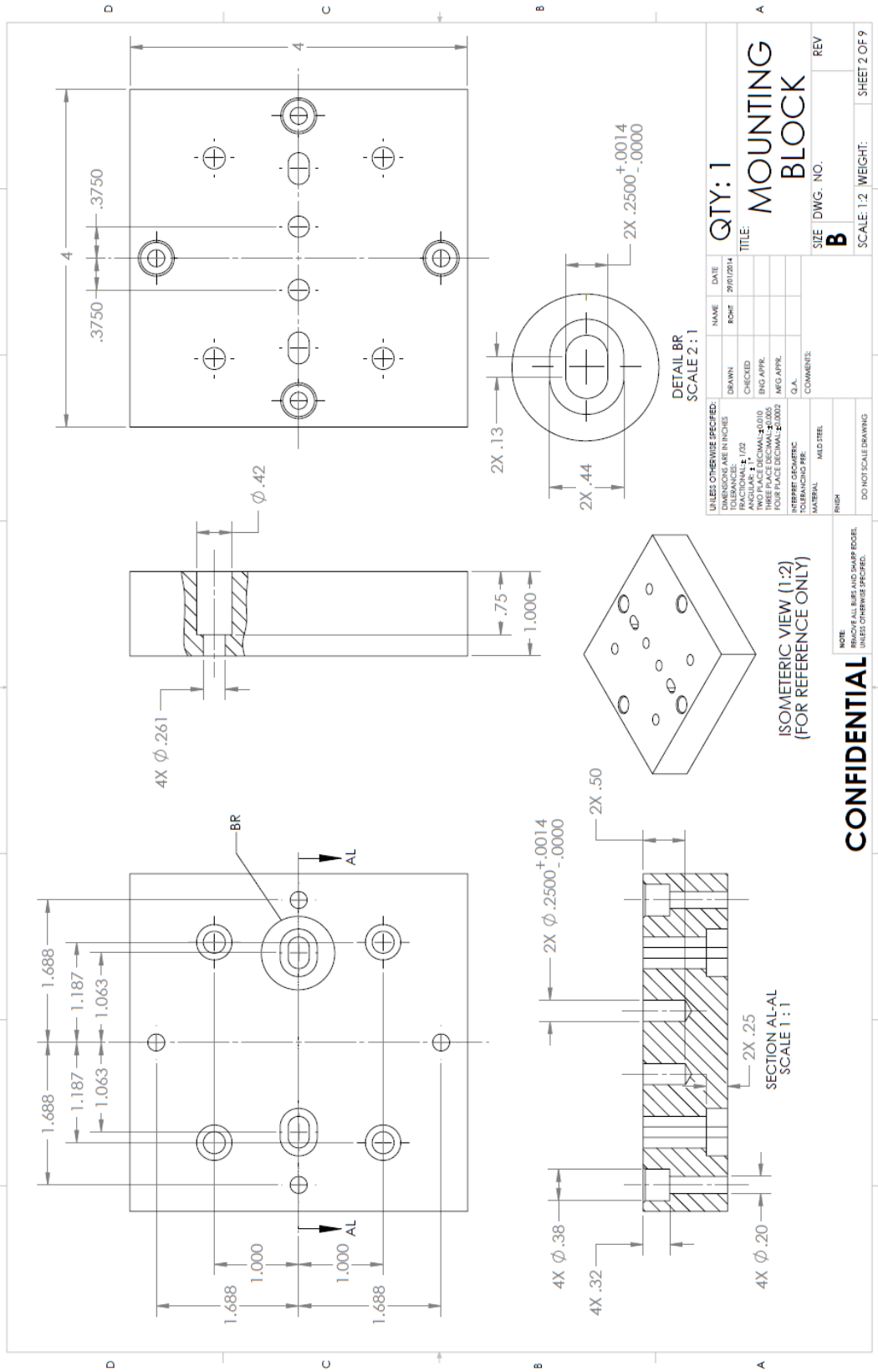


**Figure 83: Detailed drawing of the mounting block used in the comprehensive springback study.**

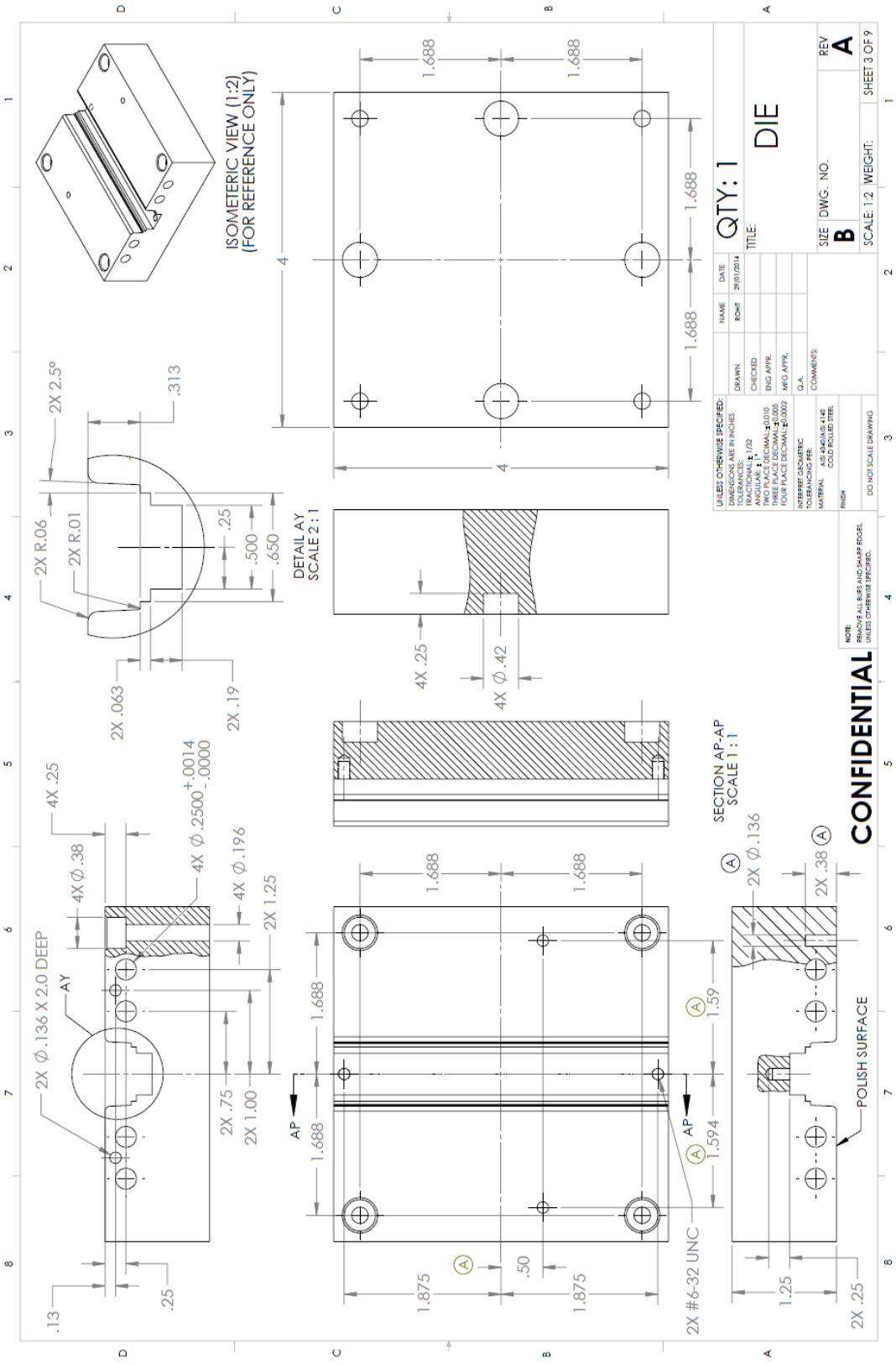


**Figure 84: Detailed drawing of the die used in the comprehensive springback study.**

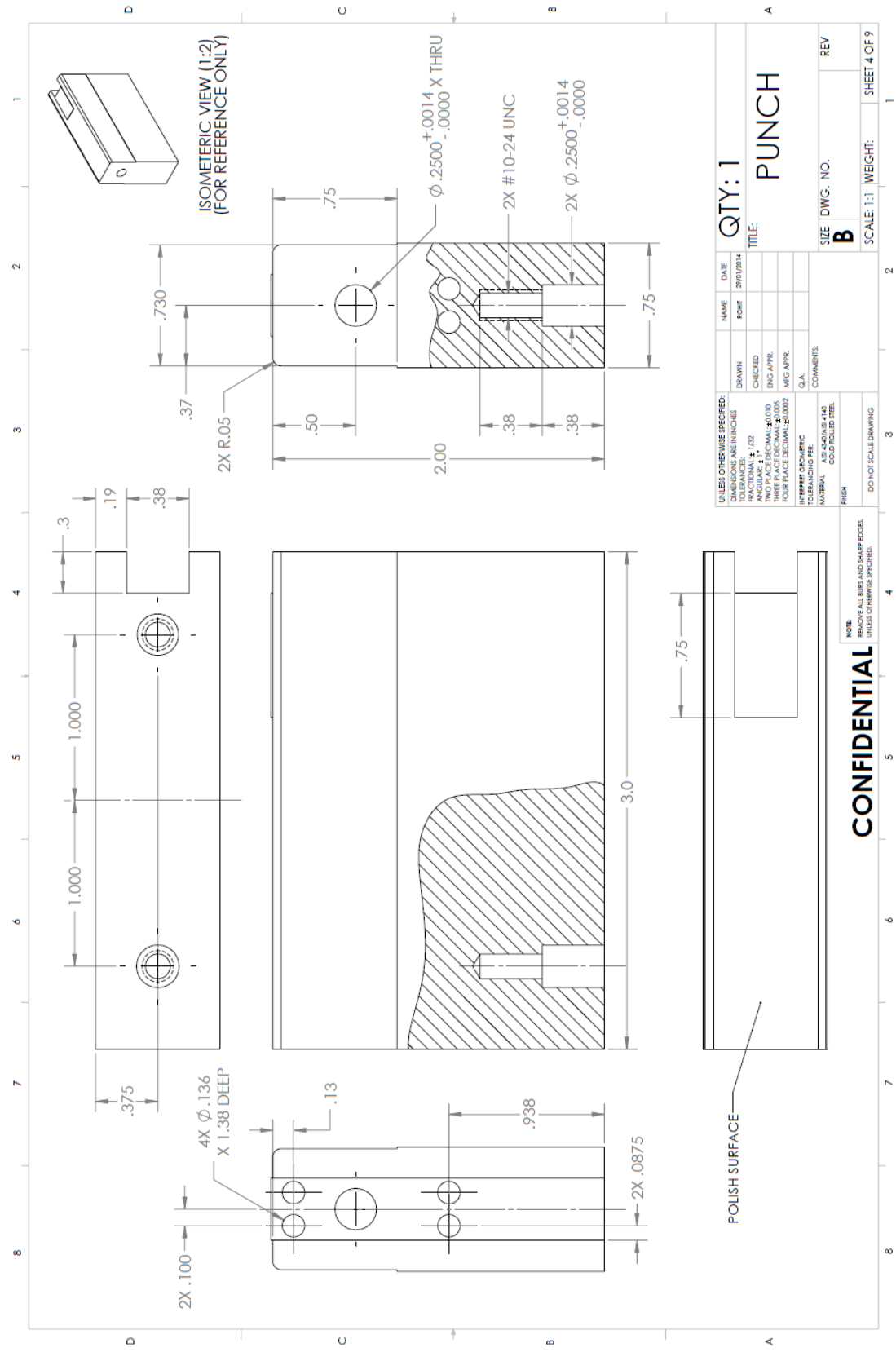


**Figure 85: Detailed drawing of the punch used in the comprehensive springback study.**

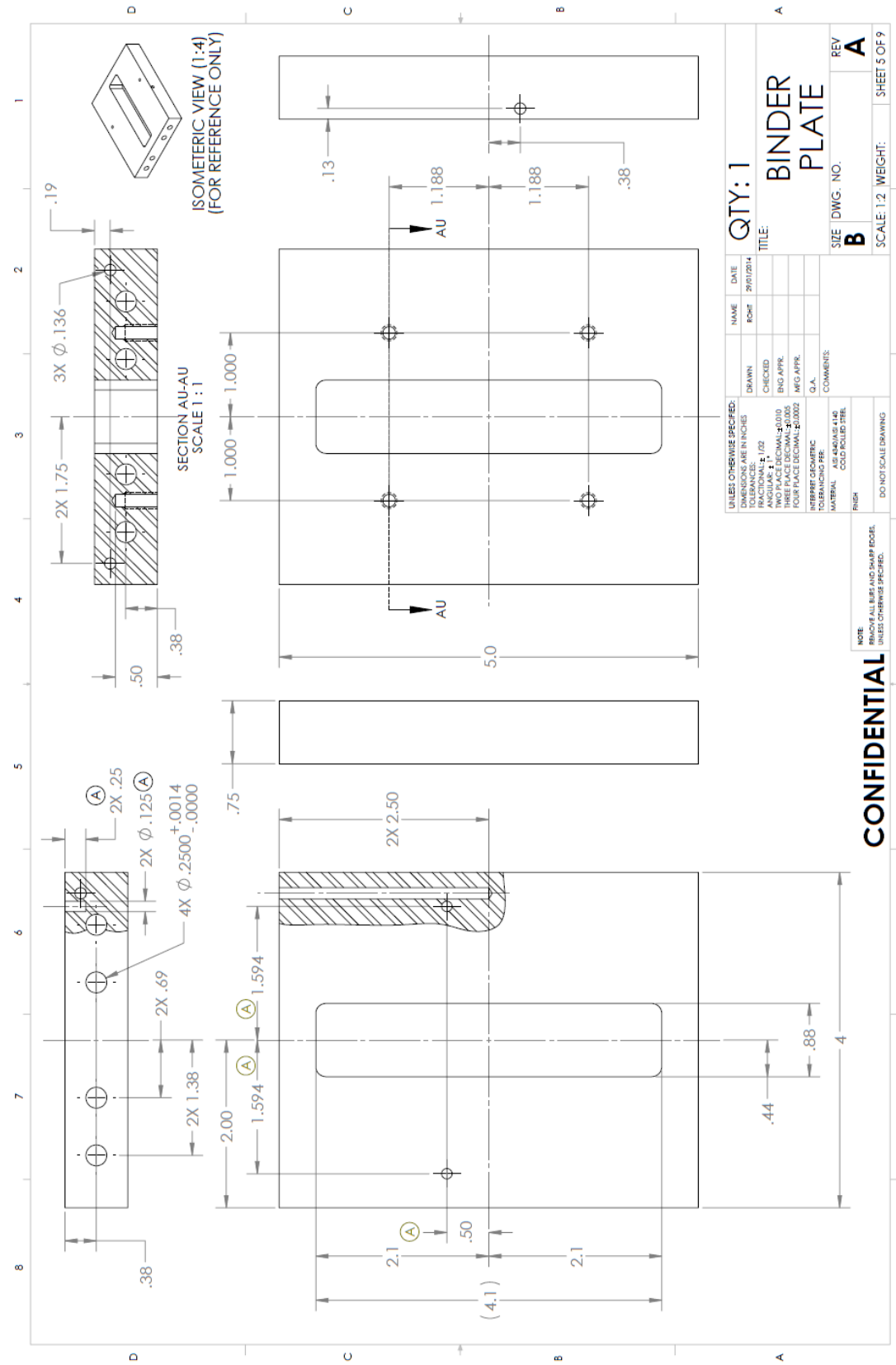


**Figure 86: Detailed drawing of the binder plate used in the comprehensive springback study.**

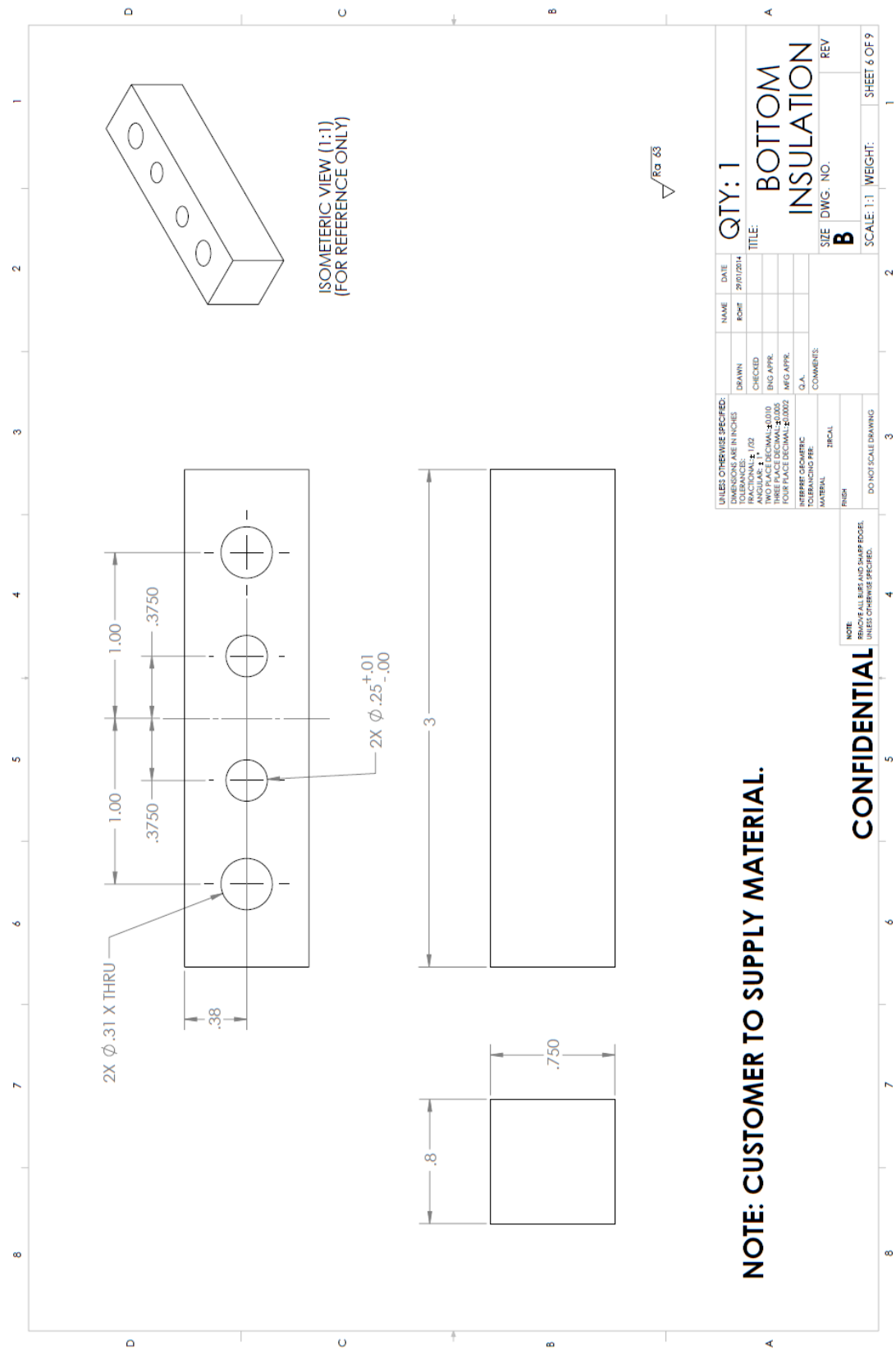


**Figure 87: Detailed drawing of the insulation block used in the comprehensive springback study.**